



NTNU – Trondheim
Norwegian University of
Science and Technology

Analysis of Harmonic Conditions in Subsea Electrical Power Systems for Oil and Gas Installations

Øyvind Garvik

Master of Energy and Environmental Engineering

Submission date: June 2015

Supervisor: Hans Kristian Høidalen, ELKRAFT

Co-supervisor: Nicola Chiesa, Statoil ASA
Øyvind Holm Snefjellå, Statoil ASA

Norwegian University of Science and Technology
Department of Electric Power Engineering

Problem Description

The background for this master's thesis is the author's specialization project, fall 2014. The thesis' aims are to analyze and investigate harmonic and resonance conditions occurring in electrical subsea power systems, characterized by long step-out cables, for offshore oil and gas installations. Two separate network topologies will be modeled, simulated and thoroughly analyzed utilizing the simulation software DIgSILENT PowerFactory 15.1. Due to subsea power electronic components, harmonic currents are injected into the power system.

Several variants of the network topologies will be simulated, where key parameters (i.e. cable lengths) are varied, and further analyzed. In addition, both worst-case and lower-level THD (total harmonic distortion) scenarios will be identified and analyzed. The goals of the thesis are to reveal possible problematic cases, limitations or general characteristics in the design and operation of such subsea power systems, with respect to harmonic content. Further, mitigation and measures concerning reduction of possible harmonic problems will be discussed.

Assignment given: 15. January 2015

Supervisor: Prof. Hans Kristian Høidalen, Dept. of Electrical Power Engineering, NTNU

Co-supervisors: Nicola Chiesa and Øyvind Holm Sneffjellå, Statoil ASA

Preface


This master's thesis has been written in the 10th semester, and is the final stage of the master's program Energy and Environmental Engineering, Electrical Power Engineering at the Norwegian University of Technology and Science (NTNU). The work is done as a continuation of the specialization project, fall 2014, with the title "Oil and Gas Subsea Transmission and Distribution Networks". As for the specialization project, Statoil ASA has been a valuable and supportive partner and co-supervisor during the work.

First, I want to thank my supervisor at NTNU, Professor Hans Kristian Høidalen at the Department of Electrical Power Engineering, for his guidance and great help with this thesis. Also, a big thank you to my co-supervisors Nicola Chiesa and Øyvind Holm Snefjellå at Statoil ASA, for their support and constructive feedback. The cooperation has assured realistic electrical systems and scenarios, relevant challenges and personal motivation.

I also want to thank my dear sister Hege Garvik Arefjord for her support with the English editing and proofreading.

Finally, I want to thank all my good friends at NTNU, especially the other students at my study hall the last year. You have made these five years fantastic.

Trondheim, June 2015



Abstract

Models of two separate network topologies are developed in cooperation with Statoil ASA to assure realistic construction of the networks along with relevant scenarios. The networks are implemented, simulated and thoroughly analyzed, utilizing the simulation software DIgSILENT PowerFactory 15.1. Simulation scripts have been developed utilizing the DIgSILENT Programming Language. These scripts are used to scan through a wide range of cable lengths to reveal possible trends, patterns or relations in the network topologies' harmonic behavior. Further, two case studies are investigated for each of the network topologies, where the first is a worst-case scenario, and the second is a lower-level THD variant. For the latter case, possible means to assure acceptable THD levels are discussed.

From the simulation results, problematic cable lengths and system limitations are revealed for both network topologies. The severity and potential hazardousness of the separate harmonic components are identified. In addition, limitations with respect to rectifier type utilized in the subsea variable speed drives, which are the harmonic current sources in the networks, are identified.

The two network topologies under consideration have some major constructional differences. How these differences affects the harmonic currents and their manifestation as harmonic voltages, are investigated. It has been found that the presence of a subsea step-down transformer has a substantial effect on how the harmonic currents behave. In addition, each cable's influence on the system's harmonic behavior is very influenced by the presence (or absence) of such a subsea transformer. *With* a subsea step-down transformer, more or less "local" resonances leads to powerful harmonic current amplifications in the subsea distribution system. The harmonic currents spreads throughout the system, causing increased harmonic voltages. *Without* a subsea step-down transformer, resonances in the long step-out cable is most problematic, when it comes to harmonic content. Possible resonances are then determined by the most dominant (i.e. the longest) cable. Further, this gives limitations to possible simplifications to be done when modeling and studying harmonics in similar subsea power systems. Generally, a long step-out cable and very short subsea distribution cables are beneficial when it comes to minimizing harmonic voltage content. In addition, naturally formed low-pass filters have substantial damping effects on the harmonics.

It has been found that the utilized theoretical harmonic current spectrum of 12-pulse rectifiers most likely is a *too* conservative simplification. The quantitative credibility of the simulation results are therefore questionable. However, the qualitative analysis of the thesis should present valuable results and observations.

Most of the results presented in the following do focus on the total harmonic distortion (THD) of the system voltages, network impedances and harmonic current- and voltage spectra. Throughout the analysis, it is aimed to explain the connection between these results, as well as the physical phenomena they are caused by.

Sammendrag

To separate nettverkstopologier har blitt konstruert i samarbeid med Statoil ASA for å sikre realistiske nettverkskonfigurasjoner, i tillegg til relevante scenarier og problemstillinger. De to nettverkene har blitt modellert, simulert og analysert ved hjelp av simuleringsverktøyet DIgSILENT PowerFactory 15.1. Videre har simuleringskript blitt utviklet i programmeringsspråket DIgSILENT Programming Language. Skriptene benyttes til å skanne igjennom svært mange varianter av de implementerte nettverkstopologiene, hvor nettverkens kabellengder endres for hver variant. Dermed kan overordnede tendenser og mønstre i de harmoniske spenningenes oppførsel oppdages. Videre er to spesifikke varianter identifisert og grundig analysert for hver av nettverkstopologiene. Den første er en variant hvor tilstanden av harmoniske er verst tenkelig. Den andre varianten har vesentlig lavere innhold av harmoniske strømmer og spenninger. For den siste blir også eventuelle tiltak for å bedre den harmoniske situasjonen diskutert.

Fra simuleringsresultatene har problematiske kabellengder og begrensninger i systemet blitt identifisert, for begge nettverkstopologier. I tillegg har begrensninger med tanke på valg av likerettertype i systemets undersjøiske frekvensomformere blitt avdekket.

De to aktuelle nettverkstopologiene har visse grunnleggende forskjeller i deres konstruksjon. Hvordan disse ulikhetene spiller inn på harmoniske strømmers oppførsel, og hvordan disse manifesterer seg som harmoniske spenninger, er kartlagt. Det har vist seg at tilstedeværelse av en undersjøisk distribusjonstransformator har avgjørende effekt på hvordan harmoniske strømmer og spenninger oppfører seg i kraftsystemet. I tillegg påvirkes påvirkningskraften hver enkelte kabel har på systemets harmoniske spenninger betraktelig, ved tilstedeværelse av en slik transformator. *Med* en undersjøisk distribusjonstransformator tilstede, er mer eller mindre ”lokale” resonanser og harmoniske strømforsterkninger i de undersjøiske distribusjonskablene den største utfordringen med tanke på harmoniske spenninger. *Uten* en undersjøisk distribusjonstransformator er resonans i den lange forsyningskabelen mellom plattform/kilde og det undersjøiske distribusjonssystemet den største utfordringen. Videre setter dette klare begrensninger på eventuelle forenklinger i modelleringer av slike nettverk. Generelt gir en lang forsyningskabel og korte distribusjonskabler de beste forholdene med tanke på spenningsharmoniske. I tillegg gir naturlig forekommende lav-pass filtre svært god demping av harmoniske.

Det har vist seg at det teoretiske harmoniske strømspektrumet benyttet i modellering av likeretterne i denne oppgaven, er en i overkant konservativ forenkling. Dette har ført til at det kan settes spørsmål ved simuleringsresultatenes kredibilitet fra et kvantitativt synspunkt. Kvalitativt, skal i midlertid resultatene være av verdi.

Resultatene presentert i denne oppgaven omhandler for det meste forvrenging av spenningenes bølgeform (THD), nettverksimpedanser og harmoniske strøm- og spenningspektra. Gjennomgående forsøkes det å forklare sammenhengen mellom disse, i tillegg til de fysiske mekanismene som ligger bak.

Contents

Problem Description	i
Preface	iii
Abstract	iv
Sammendrag	v
List of Figures	viii
List of Tables	xi
List of Abbreviations	xii
1 Introduction	1
1.1 The Subsea Power System	1
1.2 Scope of Work	2
1.3 Context	2
1.4 Outline of the Thesis	3
2 Network Topologies	4
2.1 <i>Long Step-out</i> Topology	4
2.2 <i>Short Step-out</i> Topology	6
3 Theoretical Background	7
3.1 Harmonic Current Generation	7
3.1.1 6-Pulse Bridge Rectifier	7
3.1.2 12 - and 24 - Pulse Bridge Rectifier	11
3.1.3 Static Var Compensator (SVC) Harmonics	14
3.2 Network Impedance and Resonance	15
3.2.1 Series- and Parallel Resonance	15
3.2.2 Network Impedance Characteristics	16
3.3 Harmonic Current Amplification	17
3.4 Frequency Selective Circuits	20
3.4.1 RL Low-Pass Filter	20
3.4.2 RC Low-Pass Filter	20
3.4.3 LCL Low-Pass Filter	21
3.5 Potential Problems Caused by Harmonics	22
3.6 Harmonic Mitigation	23
3.6.1 Rectifier Choice	23
3.6.2 Transformer Phase-Shift	23
3.6.3 Active- and Passive Harmonic Filtering	23
3.7 International Standards Concerning Harmonics	24

4	Network Component Simplification and Modeling	26
4.1	Transformer Modeling	26
4.2	Cable Modeling	27
4.2.1	Distributed Parameters Model	28
4.2.2	Frequency-Dependent Resistances	29
4.2.3	Cable Impedance	31
4.3	VSD Modeling	32
4.3.1	Rectifier Model	32
4.4	Load Modeling	34
4.5	Topside Grid Modeling	34
4.6	Static Var Compensator Modeling	35
4.7	<i>Long Step-out</i> Implementation in PowerFactory	36
4.7.1	Voltage Control (Topside Transformer Tap-Changer)	37
4.7.2	Reactive Power Control (Topside SVC)	38
4.8	<i>Short Step-out</i> Implementation in PowerFactory	39
4.8.1	Voltage Control (Topside Transformer Tap-Changer)	40
4.8.2	Reactive Power Control (Topside SVC)	40
4.9	System Design Criteria	40
5	Simulation Software, Strategy and Methodology	41
5.1	Simulation Software - DIgSILENT PowerFactory 15.1	41
5.1.1	Load Flow	41
5.1.2	Harmonic Load Flow	42
5.1.3	Frequency Sweep	42
5.1.4	DIgSILENT Programming Language (DPL)	42
5.2	Simulation Strategy	43
5.2.1	<i>Long Step-out</i> Series Scan Settings	43
5.2.2	<i>Short Step-out</i> Series Scan Settings	44
5.2.3	PowerFactory DPL Script (Pseudo-Code)	45
6	<i>Long Step-out</i> Harmonics and Resonance Analysis	46
6.1	<i>Long Step-out</i> Series Scan	48
6.2	<i>Long Step-out</i> Harmonic and Resonance Behavior	53
6.3	Case Study 1: <i>Long Step-out</i> Worst-Case THD Scenario	57
6.4	Case Study 2: <i>Long Step-out</i> Lower THD Scenario	62
6.5	General Observations for the <i>Long Step-out</i>	65
7	<i>Short Step-out</i> Harmonics and Resonance Analysis	68
7.1	<i>Short Step-out</i> Series Scan	70
7.2	<i>Short Step-out</i> Harmonic and Resonance Behavior	73
7.3	Case Study 3: <i>Short Step-out</i> Worst-Case THD Scenario	77
7.4	Case Study 4: <i>Short Step-out</i> Lower THD Scenario	82
7.5	General Observations for the <i>Short Step-out</i>	86
8	Discussion	89
9	Conclusion	92

References	95
A General	97
A.1 Frequency-Dependent Cable Resistances	97
B Network Component Parameters	98
B.1 <i>Long Step-out</i> Topology	98
B.1.1 Cable Parameters	98
B.1.2 Transformer Parameters	99
B.1.3 Load Parameters	99
B.1.4 Rectifier Parameters	99
B.1.5 SVC Parameters	100
B.1.6 Topside Grid Parameters	100
B.2 <i>Short Step-out</i> Topology	100
B.2.1 Cable Parameters	100
B.2.2 Transformer Parameters	101
B.2.3 Load Parameters	101
B.2.4 Rectifier Parameters	101
B.2.5 SVC Parameters	102
B.2.6 Topside Grid Parameters	102
C Harmonic and Resonance Analysis - Extras	103
C.1 <i>Long Step-out</i>	103
C.1.1 Case Study 1	103
C.1.2 General Observations for the <i>Long Step-out</i>	105
C.2 <i>Short Step-out</i>	109
C.2.1 Case Study 3	109
C.2.2 General Observations for the <i>Short Step-out</i>	110
D DPL Scripts	114
D.1 <i>Long Step-out</i> Topology DPL Script	114
D.2 <i>Short Step-out</i> DPL Script	121

List of Figures

2.1 Principal construction of the <i>Long Step-out</i> topology	4
2.2 Principal construction of the <i>Short Step-out</i> topology	6
3.1 6-pulse diode bridge rectifier	8
3.2 Voltage and current at AC-terminals of an ideal 6-pulse rectifier	9
3.3 Harmonic current spectrum of 6-pulse rectifier	9
3.4 AC current of a 6-pulse rectifier from EMT-simulation test	10
3.5 Series-connected 12-pulse bridge rectifier	11
3.6 Input- and output voltage for Rectifier 1 and 2	12
3.7 Output DC-voltage of an ideal 12-pulse rectifier	13
3.8 Harmonic current spectrum of a 12-pulse rectifier	13
3.9 Model of a thyristor-controlled reactor (TCR)	14
3.10 Series RLC circuit, [1]	15

3.11	Parallel RLC circuit, [1]	16
3.12	Network impedance characteristic of parallel RLC circuit in Figure 3.11	17
3.13	Simplified source-cable-network circuit	18
3.14	Simplified cable circuit with harmonic current amplification	18
3.15	Possible current amplification in a 30 km long, $U_m = 36kV$, 185 mm ² subsea power cable	19
3.16	Series RL low-pass filter	20
3.17	Series RC low-pass filter	20
3.18	LCL low-pass filter	21
3.19	IEC 61000-2-4 Class 2 harmonic voltage spectrum	25
4.1	Positive- and negative sequence model of two-winding transformer, in Ohms	26
4.2	Positive- and negative sequence model of three-winding transformer, in per unit	27
4.3	Distributed parameters model for cable modeling in PowerFactory	28
4.4	Equivalent circuit for long cable model with distributed parameters [1]	29
4.5	Impedance of cable section with a distributed parameters model	31
4.6	Single-line representation of a 12-pulse rectifier implemented in PowerFactory	33
4.7	DC- and AC voltages of PowerFactory 12-pulse rectifier model	33
4.8	Single-phase DC current source load model	34
4.9	Positive-sequence model of grid element	35
4.10	General model of Static Var Compensator (SVC) system	35
4.11	PowerFactory implementation and naming of the <i>Long Step-out</i>	36
4.12	Schematic representation of tap-changer control system	37
4.13	Schematic representation of reactive power control system	38
4.14	PowerFactory implementation and naming of the <i>Short Step-out</i>	39
6.1	Main busbars and cables of <i>Long Step-out</i>	46
6.2	Short-circuit current ratio at subsea busbars	47
6.3	<i>Long Step-out</i> Series Scan; <i>Topside Main</i> THD levels	48
6.4	<i>Long Step-out</i> Series Scan; <i>Topside HV</i> and <i>Switchboard B</i> THD levels	50
6.5	<i>Long Step-out</i> Series Scan; <i>Switchboard A</i> THD levels	51
6.6	<i>Long Step-out</i> contour plots of <i>Topside Main</i> and <i>Switchboard A</i> THD levels	53
6.7	<i>Long Step-out</i> contour plots of <i>Switchboard A</i> , <i>Switchboard B</i> and <i>Topside Main</i> THD levels	54
6.8	Development of <i>Switchboard B</i> network impedance characteristic	54
6.9	<i>Long Step-out</i> contour plots of <i>Switchboard A</i> and <i>Switchboard B</i> THD levels	56
6.10	Explanatory sketch for Figure 6.11 and 6.12	57
6.11	Case Study 1: Harmonic currents in <i>Load Cable 1</i> with network impedance characteristic seen from <i>Switchboard A</i>	58
6.12	Case Study 1: Harmonic currents in <i>Load Cable 2</i> with network impedance characteristic seen from <i>Switchboard A</i>	58
6.13	Case Study 1: Harmonic voltage spectrum and network impedance characteristic seen from <i>Switchboard A</i>	59
6.14	Explanatory sketch for Figure 6.15	59
6.15	Case Study 1: Harmonic currents in <i>Step-out Cable</i> with network impedance characteristic seen from <i>Topside HV</i>	60
6.16	Case Study 1: Harmonic voltage spectrum and network impedance characteristic seen from <i>Topside Main</i>	61

6.17	Case Study 2: Harmonic voltages and network impedance characteristic seen from <i>Switchboard A</i>	62
6.18	Explanatory sketch for Figure 6.19	63
6.19	Case Study 2: Harmonic currents in <i>Step-out Cable</i>	63
6.20	Case Study 2: Harmonic voltages and network impedance characteristic seen from <i>Topside Main</i>	64
6.21	Topside busbars' THD levels with injected 11 th and 13 th harmonic currents, only	66
6.22	Subsea busbars' THD levels with injected 11 th and 13 th harmonic currents, only	67
7.1	Main busbars and cables of the <i>Short Step-out</i>	68
7.2	Short-circuit current ratio at subsea busbars	69
7.3	<i>Short Step-out</i> Series Scan; <i>Topside Main</i> and <i>Topside HV</i> THD levels	71
7.4	<i>Short Step-out</i> Series Scan; <i>Switchboard A</i> and <i>Switchboard B</i> THD levels	72
7.5	THD at <i>Topside Main</i> with varying <i>Step-out Cable</i> length	73
7.6	Network impedance characteristics at <i>Topside Main</i> with a <i>Step-out Cable</i> length of 1 km and 60 km	74
7.7	Development of harmonic order and amplitude of parallel resonances in the network impedance characteristic of <i>Topside Main</i>	74
7.8	<i>Short Step-out</i> contour plots of <i>Topside Main</i> THD levels when remaining cables are kept short and long	76
7.9	Explanatory sketch for Figure 7.10	77
7.10	Case Study 3: Harmonic currents in <i>Load Cable 1</i> with network impedance characteristic seen from <i>Switchboard A</i>	78
7.11	Explanatory sketch for Figure 7.12	78
7.12	Case Study 3: Harmonic currents in <i>Supply Cable</i> with network impedance characteristic seen from <i>Switchboard A</i>	79
7.13	Case Study 3: Harmonic voltages and network impedance characteristic seen from <i>Switchboard A</i>	79
7.14	Case Study 3: Harmonic voltages and network impedance characteristic seen from <i>Topside Main</i>	80
7.15	Harmonic current amplification for varying <i>T5_step-up</i> transformer short-circuit impedance	81
7.16	Explanatory sketch for Figure 7.17	82
7.17	Case Study 4: Harmonic currents in <i>Load Cable 1</i> through <i>Load Cable 4</i> with network impedance characteristic seen from <i>Switchboard A</i>	83
7.18	Case Study 4: Harmonic voltage spectrum and network impedance characteristic seen from <i>Switchboard A</i>	83
7.19	Explanatory sketch for Figure 7.20	84
7.20	Case Study 4: Harmonic currents in <i>Step-out Cable</i> with network impedance characteristic seen from <i>Topside HV</i>	84
7.21	Case Study 4: Harmonic voltage spectrum and network impedance characteristic seen from <i>Topside Main</i>	85
7.22	Topside busbars' THD levels caused by the 11 th and 13 th harmonic current, only	87
7.23	Subsea busbars' THD levels caused by the 11 th and 13 th harmonic current, only	88

8.1	Comparison of theoretical- and EMT-test's harmonic current spectra	89
A.1	Frequency-dependency of cable conductor resistances	97
C.1	Case Study 1: Explanatory sketch for Figure C.2	103
C.2	Case Study 1: Harmonic current spectra of <i>Supply Cable B</i> , network impedance characteristic at <i>Switchboard B</i>	103
C.3	Case Study 1: Harmonic voltage spectrum and network impedance characteristic at <i>Switchboard B</i>	104
C.4	Busbars' THD levels caused by 23 th and 25 th harmonics, only	105
C.5	Busbars' THD levels caused by 35 th and 37 th harmonics, only	106
C.6	Busbars' THD levels caused by 47 th and 49 th harmonics only	107
C.7	Cable length variation order for Figure C.4, C.5 and C.6	108
C.8	Case Study 3: Harmonic voltage spectrum and network impedance characteristic at <i>Switchboard B</i>	109
C.9	Case Study 3: Harmonic voltage spectrum and network impedance characteristic at <i>Topside HV</i>	109
C.10	Busbars' THD levels caused by 23 rd and 25 th harmonic currents, only	110
C.11	Busbars' THD levels caused by 35 th and 37 th harmonic currents, only	111
C.12	Busbars' THD levels caused by 47 th and 49 th harmonic currents, only	112
C.13	Cable length variation order for Figure C.10, C.11 and C.12	113

List of Tables

3.1	IEC 61000-2-4 Class 2 harmonic voltage limits, [2]	25
4.1	<i>Long Step-out</i> cable lengths	37
4.2	<i>Short Step-out</i> cable lengths	40
5.1	Cable length variations for <i>Long Step-out</i> , initial Series Scan	44
5.2	Cable length variations for <i>Short Step-out</i> , initial Series Scan	44
6.1	<i>Long Step-out</i> cable lengths	47
6.2	Cable lengths for Case Study 1	57
6.3	Cable lengths for Case Study 2	62
7.1	<i>Short Step-out</i> cable lengths	69
7.2	Cable lengths for Case Study 3	77
7.3	Cable lengths for Case Study 4	82
8.1	THD levels in Case Study 1 and 2 with the EMT-test's harmonic current spectra	90
B.1	<i>Long Step-out</i> cable parameters	98
B.2	<i>Long Step-out</i> cable operational voltages	98
B.3	<i>Long Step-out</i> transformer parameters	99
B.4	<i>Long Step-out</i> load parameters	99
B.5	<i>Long Step-out</i> rectifier parameters	99
B.6	<i>Long Step-out</i> SVC specifications	100
B.7	<i>Long Step-out</i> topside grid specifications	100
B.8	<i>Short Step-out</i> cable parameters	100
B.9	<i>Short Step-out</i> cable operational voltages	100
B.10	<i>Short Step-out</i> transformer parameters	101
B.11	<i>Short Step-out</i> load parameters	101
B.12	<i>Short Step-out</i> rectifier parameters	101

B.13 <i>Short Step-out</i> SVC specifications	102
B.14 <i>Short Step-out</i> topside grid specifications	102

List of Abbreviations

<i>CSI</i>	Current Source Inverter
<i>DPL</i>	DIgSILENT Programming Language
<i>ESP</i>	Electrical Submersible Pump
<i>FPSO</i>	Floating Production, Storage and Offloading Unit
<i>IEC</i>	International Electrotechnical Commission
<i>IEEE</i>	Institute of Electrical and Electronics Engineers
<i>NEK</i>	Norsk Elektroteknisk Komité
<i>PCC</i>	Point of Common Coupling
<i>PWM</i>	Pulse-width Modulation
<i>SVC</i>	Static Var Compensator
<i>TCR</i>	Thyristor-Controlled Reactor
<i>THD</i>	Total Harmonic Distortion
<i>VSD</i>	Variable Speed Drive
<i>VSI</i>	Voltage Source Inverter
<i>XLPE</i>	Cross-linked polyethylene

1 Introduction

1.1 The Subsea Power System

With offshore oil and gas resources located in deeper waters and farther from shore, subsea processing facilities are becoming increasingly relevant for the petroleum industry. For both economic and technical reasons, increasingly more of the processing equipment are placed on the seabed. To be able to operate and control such subsea installations, a reliable electrical power system is required. Designed as a radial cable network with potentially very long cable lengths, these systems introduces several technical challenges. Depending on the geographical location, surrounding infrastructure and the types of subsea loads, the severity of each technical challenge changes, and leads to unique tailor-made solution for each system.

The construction of the next generation's subsea power system is dominated by a (long) step-out cable which connects the topside system (e.g. the power system of an offshore platform) to a subsea distribution system. Through subsea switchgear modules, the power is distributed to the various loads. Pumps, providing steady flows of condensate, oil or water with mechanical power ratings ranging from a few kW to a few MW, are still the most widespread subsea load type. To assure steady and efficient transportation of petroleum gas, subsea gas compressors may also be installed on the seabed. With mechanical power ratings of up to 12 MW, this machinery becomes both large and very power consuming. Other loads such as electrical heating for pipelines, control system and magnetic bearings do exist, but will not be discussed in this thesis.

Electrical motors drive the subsea pumps and gas compressors. To be able to operate these machines in a safe and flexible way, Variable Speed Drives (VSDs) are required. This allows the operator to adjust the speed (and thus the fluid flow) after his own desire. A VSD is a frequency converter consisting of a bridge rectifier, a DC-link and normally a PWM-inverter (pulse-width modulated). The bridge rectifier causes harmonic currents to be injected into the cable network. Further, this could lead to unacceptable levels of voltage waveform distortion (THD) due to resonance phenomena. All subsea pumps in operation today have their VSDs mounted topside. For each subsea load, a separate power cable is required from topside to subsea. A goal for future systems is to place the VSDs subsea, which increases the flexibility of the system. Even though no such system is in normal operation today, full size pilot installations have been constructed and tested[3]. This thesis will only discuss subsea-mounted VSDs.

The development of subsea power systems have several challenges which are not found in onshore systems. Up until recently, there have been a lack of international standards concerning both subsea power equipment and system requirements. Only guidelines, specific qualifications and modified standards originally for onshore applications, have been accessible. Initiated by Statoil in 2010, a joint industry project was started with the title Subsea Electrical Power Standardization (SEPS) [4]. Statoil, Chevron, ExxonMobil and Shell, among others, are currently working to establish international standards for the subsea power industry. In addition to the lack of relevant standards, a subsea power system has extreme reliability requirements. Due to the inaccessibility for maintenance and very high outage cost, complete backup systems or -components are not unusual.

1.2 Scope of Work

This thesis aims to investigate and analyze harmonic and resonance conditions in subsea power systems for oil and gas installations. Two separate and realistic network topologies, a *Long Step-out* cable topology and a *Short Step-out* cable topology will be modeled, simulated and studied in detail. By the use of the simulation software DIgSILENT PowerFactory 15.1, several simulations will be conducted where key network parameters (i.e. cable lengths) are varied, to get the best possible understanding of the harmonic behavior of the systems.

The harmonic and resonance study will be concentrated around the harmonic currents injected by subsea VSDs, and how these current do behave in the radial cable network. Possible resonance problems will be studied in detail. Only the distortion of the voltage waveform (THD) will be weighted in the evaluation of the results. Other unwanted effects caused by the harmonics, such as excessive heating, will therefore not be part of the evaluation of the results. Relevant international standards concerning voltage quality will be utilized when evaluating the results. Due to the scope of the applied standard, only harmonics ranging from harmonic order 1 to 50 (50 - 2500 Hz) will be considered.

The goal of this thesis is to get a total understanding of the harmonic and resonance conditions in such power systems. The aim is to reveal possible limitations in the construction and operation of such subsea power systems, in addition to investigation of worst-case scenarios. With a solid understanding of the harmonic behavior, harmonic mitigation and avoiding designing pitfalls becomes easier.

For flexibility and visual purposes, MathWorks MATLAB will be utilized for post-processing of the PowerFactory simulation results.

1.3 Context

Several studies concerning harmonic and resonance conditions in subsea power cable distribution systems have been done. Liang and Jackson [5] studied the resonance and harmonic conditions in an offshore subsea power system of interconnected platforms. With a radial network construction and VSD driven loads, the system analyzed by Liang and Jackson has several similarities to the power systems to be analyzed in this thesis. They concluded that a complete harmonic and resonance analysis is absolutely necessary for power systems, consisting of subsea cables. In addition, several measures to mitigate the harmonic content might be necessary to assure acceptable system performance.

Chien and Bucknall [6] demonstrated the influence of subsea cables' resonance capabilities on the system's harmonic conditions. In addition, not only the harmonic sources themselves but also the interactions between the electrical components, are crucial for an understanding of the harmonic behavior of subsea power systems.

Emphasized by Råd [7], the identification of resonance frequencies in power systems consisting of long subsea power cables, is crucial to assure correct and acceptable operation of motor loads supplied by long subsea power cables.

Most of the previous studies done on this subject, are focused on power systems where the

VSDs are placed topside (including [7]). A long cable supplies the subsea electrical motor, directly. Step-up and step-down transformers might be needed for long cable lengths. The harmonic content in the cable system is therefore determined by the high-frequency switching of the PWM-inverter, and *not* by the bridge rectifier. As discussed earlier, the next generation's subsea power systems will aim to place the VSDs subsea. Since the concept of subsea VSDs still are relatively new, most of the studies done on this field are internal studies commissioned by the petroleum industry, and therefore not openly accessible.

1.4 Outline of the Thesis

Section 2 *Network Topologies* presents the principal construction of the two network topologies studied in this thesis, and briefly discusses their current relevance. Section 3 *Theoretical Background* offers an overview of the physical theory behind observed harmonic and resonance phenomena. In addition, harmonic mitigation techniques and relevant international standards concerning harmonic content in power systems, are discussed. Further, Section 4 *Network Component Simplification and Modeling* describes the modeling of the electrical components and the implementation in DIgSILENT PowerFactory. In Section 5 *Simulation Software, Strategy and Methodology* the method and simulation strategy are discussed. Section 6 *Long Step-out Harmonics and Resonance Analysis* and 7 *Short Step-out Harmonics and Resonance Analysis* presents the analysis and results of the investigated networks. Section 8 presents a discussion of the findings. In Section 9, conclusions are drawn in addition to a presentation of possible further works.

2 Network Topologies

The two network topologies to be analyzed in this thesis are constructed in cooperation with Statoil ASA. Their constructional characteristics and possible roles in real subsea systems, are discussed in the following sections. Both topologies are constructed with subsea VSDs, therefore representing the next generation of subsea power systems. Placing the VSDs subsea facilitates further expansion of the power system. Additionally, only one step-out cable (connecting topside system to subsea system) would then be needed, instead of having one for each subsea load. However, this approach is still mostly on the research and development stage with very little field experience [8]. This is clearly reflected in the available literature on the subject, which is dominated by studies on systems with topside mounted VSDs.

Some technical limitations are posed on the construction of subsea power systems. Currently, the voltage levels are limited to 145 kV and 36 kV for dry-mate and wet-mate connectors, respectively. Since wet-mate connectors are likely to be used in the subsea distribution system (for flexibility purposes), the voltage is currently limited to 36 kV.

Only AC transmission systems with a fundamental frequency of 50 Hz, will be considered in this thesis. For longer lengths or higher power-ratings, low-frequency AC systems or DC systems should be considered to keep losses and voltages under control.

2.1 Long Step-out Topology

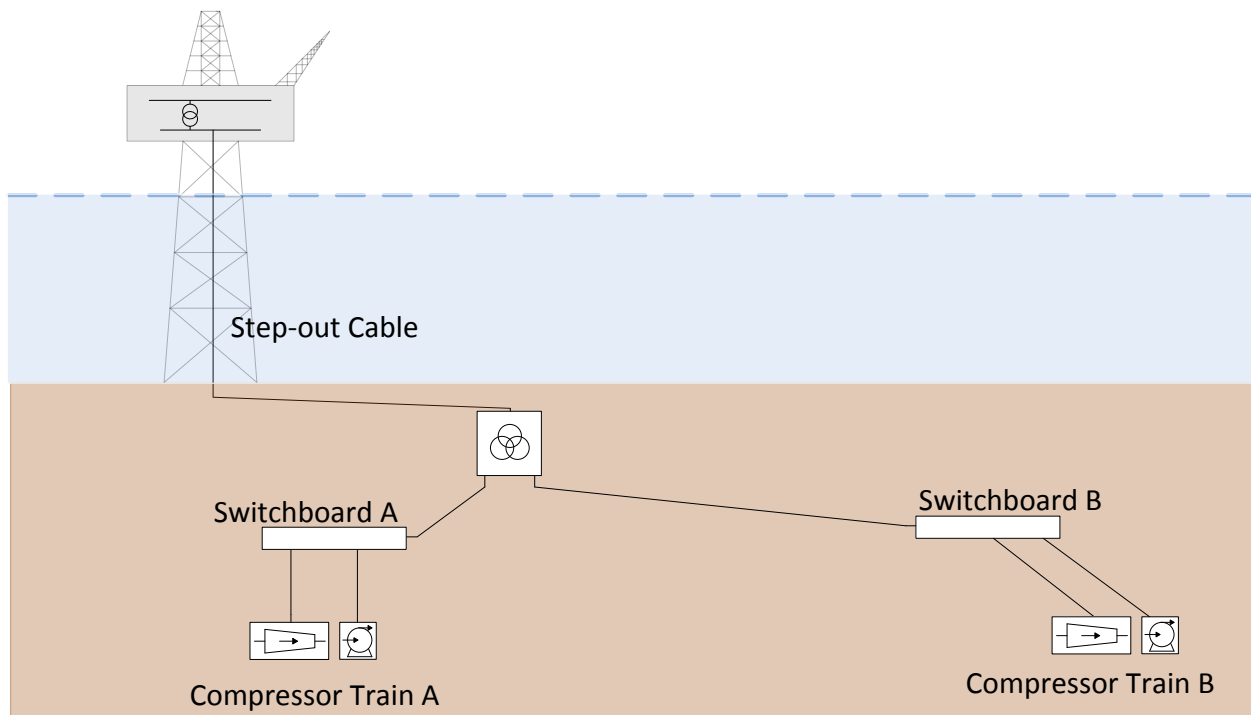


Figure 2.1: Principal construction of the *Long Step-out* topology

Offshore gas wells are often located far from the user or the receiving terminal. To compensate for the pressure drop in the pipeline, subsea gas compressor can be used to boost the gas pressure. Increased recovery and accelerated production are some of

the benefits with the use of subsea gas compression. Several booster stations might be needed along the pipeline to assure the desired gas flow. Onshore booster stations are well-established technology while subsea gas boosting is not in operation today.

Raw gas from the offshore reservoir contains not only gas but also water, moist and petroleum bi-products. Pressurizing the fluids and the gases simultaneously in the same machinery have proven to be very difficult, even though hybrid pumping systems emerges in the market. Today, the solution is to use a separator which separates the gases, fluids and possible solids. The gas can then be pressurized by a gas compressor, while the fluids are pressurized by a condensate pump. After pressurization, the fluid and gas can be transported in one common pipeline. A construction consisting of a gas compressor, a condensate pump and the required processing equipment, is referred to as a *compressor train*, and is normally mounted on a steel template. The gas compressor and condensate pump are therefore always placed close together.

The *Long Step-out* topology, modeled and analyzed in this thesis, represents the electrical power system supplying two subsea compressor trains, from the power system of an offshore oil platform. Figure 2.1 shows the principal construction of the topology, which from now on will be referred to as simply the *Long Step-out*. The electrical system is characterized by a very long step-out cable (50 - 200 km) connecting the topside platform grid to the subsea distribution system. Due to the very long step-out cable, a topside step-up transformer and a subsea step-down transformer are required, as shown in the figure.

The main power system on an oil platform is normally an 11 kV system, fed by gas turbine generators. For the *Long Step-out*, the voltage is further transformed to 75 kV by the topside step-up transformer. On the ocean floor, the long step-out cable is connected to a three-winding step-down transformer. Here, the voltage is transformed to 30 kV for both the secondary and tertiary winding. Supply cables from the secondary and tertiary windings further supplies *Switchboard A* and *Switchboard B*. Two load cables connected to *Switchboard A* supplies the gas compressor load and the condensate pump load in *Compressor Train A*. Likewise, two load cables connected to *Switchboard B* supplies the gas compressor load and the condensate pump load in *Compressor Train B*.

The two compressor trains are identical in their load configuration with one 12 MW (shaft power) gas compressor and a 500 kW (shaft power) condensate pump, each. Both the compressors and the pumps are driven by electrical motors which in turn are driven by VSDs.

Section 4 describes the modeling of all electrical components in the *Long Step-out*, in addition to relevant model simplifications. Further, Section 4.7 describes the complete network topology implementation in DIgSILENT PowerFactory.

During 2015, the Åsgard Subsea Gas Compression system is planned to be set into operation. Two compressor trains, each with an 11.5 MW compressor, are placed at 300 meters depth with a step-out power cable length of 43 km. The electrical power is supplied from the FPSO Åsgard A (Floating Production, Storage and Offloading Unit). The Åsgard Subsea Gas Compression system will utilize topside VSDs.

2.2 *Short Step-out* Topology

Some oil wells, often called low-energy wells, do not have sufficient well pressure to sustain the wanted oil flow or production rate. To assure longer operational lifetime and increased production efficiency, pumps can be utilized. Electrical Submersible Pumps (ESPs) can be installed inside the wellbore to pump up the crude. The power rating of such pumps normally lies from a few hundred kW to a few MWs. Combining the use of oil pumps in the wellbore with water injection pumps on the outskirts of the reservoir could increase the lifespan and productivity drastically. Ocean water is actively pumped into the reservoir, increasing the well pressure and creating an artificial flow towards the wellhead. The power ratings of the water injection pumps lies in the same range as the oil pumps. Figure 2.2 shows the principle construction of the *Short Step-out* topology, from now on referred to as only the *Short Step-out*. Due to lower total power rating and shorter step-out cable length, a subsea step-down transformer is not required.

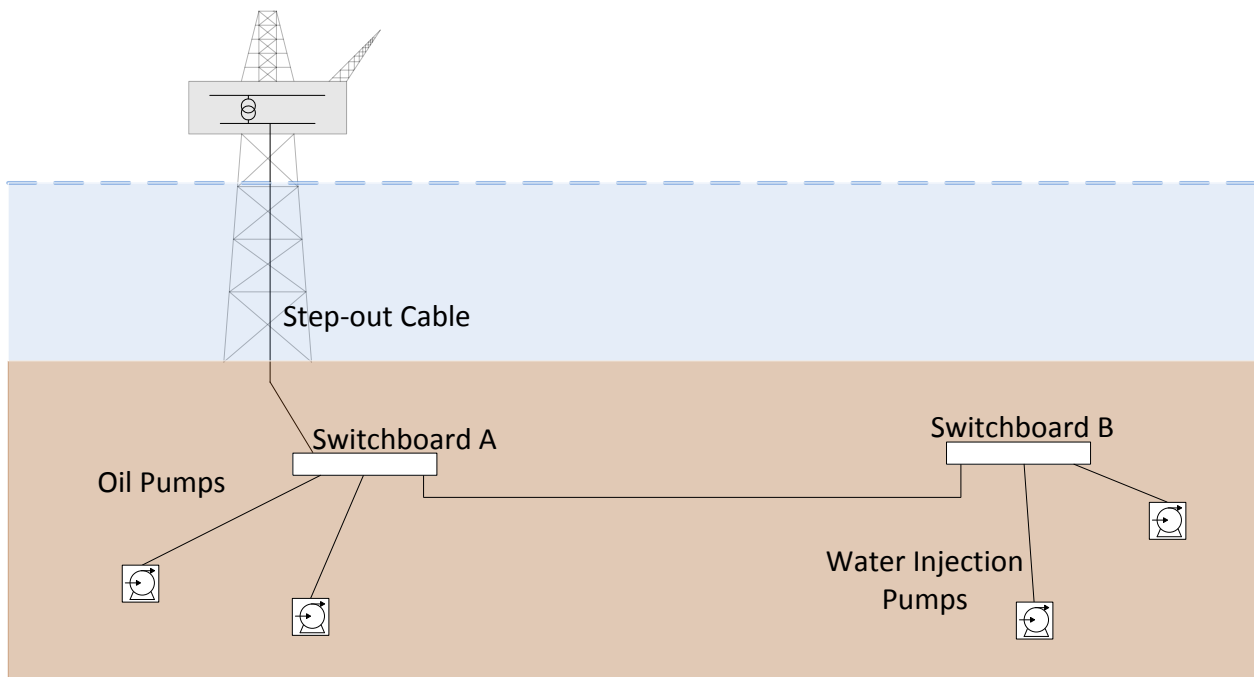


Figure 2.2: Principal construction of the *Short Step-out* topology

The topside 11 kV voltage supply is transformed to 30 kV and a step-out cable supplies the electrical power to the subsea busbar *Switchboard A*. *Switchboard A* further supplies two oil pumps through power cables (note that the cables supplying the oil pumps do not necessarily have equal lengths). A power cable connected to *Switchboard A*, further supplies *Switchboard B*, which in turn supplies two water injection pumps. Both the oil- and water injection pumps modeled in this thesis, have a shaft power ratings of 3 MW. Section 4 describes the component modeling and simplifications applied. Section 4.8 describes how the *Short Step-out* is implemented in PowerFactory, based on this section, and Section 4. Subsea pump installations are more known and established technology than subsea gas compression. The Peregrino Field (operated by Statoil) off the coast of Brazil, is one of the fields utilizing ESPs to increase oil recovery. The Tordis Field (also operated by Statoil) on the Norwegian Continental Shelf is one of the fields utilizing water injection for pressure support.

3 Theoretical Background

To fully understand the behavior of harmonics in an electrical power system, it is important to understand the mechanisms that generates the harmonics, the properties of the power system for different frequencies and how these interact with each other. This section will discuss the theoretical background concerning harmonic current generation, relevant resonance phenomena, network impedances and how these together determines the harmonic content in a power system. International standards defining voltage quality requirements will be discussed. Even though harmonic mitigation are not the main focus of this thesis, some techniques will be briefly discussed, along with possible unwanted effects caused by harmonics.

3.1 Harmonic Current Generation

The harmonic currents present in the electrical systems considered in this thesis, are mainly caused by the subsea VSDs. As mentioned earlier, a VSD consist of a rectifier, a DC-link and an inverter. This construction has two separate harmonic sources; the rectifier and the inverter. The high-frequency switching of the inverter would cause harmonics. However, when viewed from the supply-side of the VSD, these harmonic have to cross the DC-link with its smoothening capacitor filter. Simulation tests in PowerFactory have shown that the contribution of inverter-caused harmonics are negligible compared to the harmonics generated by the rectifier, when observed from the supply-side of the VSD (with the modeling utilized in this thesis). In reality, there would also be a small harmonic contribution from the load-frequency. The harmonic currents caused by the rectifiers will therefore be the only harmonic contribution from the VSDs, considered in this thesis. The modeling and PowerFactory implementation of the VSDs are discussed in Section 4.3.1, while the following section will describe the mechanisms behind the harmonic currents generation of the rectifiers.

To assure reactive power- and voltage control in the power systems, Static Var Compensators (SVC) are installed topside in both topologies. These are Thyristor-Controlled Reactors (TCR). Due to the switching of the thyristors, harmonics are generated. The magnitudes of these harmonics are relatively small compared to the rectifier harmonics, however, to obtain a network model as accurate as possible, the SVC harmonic source will be included. Section 3.1.3 briefly discusses the harmonics caused by the SVC.

3.1.1 6-Pulse Bridge Rectifier

Figure 3.1 displays the construction of a 6-pulse diode bridge rectifier where A, B and C are the three-phase input system. Thyristors may be used instead of diodes, but this requires gate-driving circuits, which in turn increases the complexity. Only diode rectifiers will be discussed here.

Let us assume that the AC-side of the rectifier has zero inductance, the diodes are ideal, and a three-phase AC voltage is applied to the A, B and C terminals. When phase A has the highest potential, diode D1 will be forward biased while diode D2 and D3 will be reversed biased. Likewise, when phase B has the highest potential, diode D2 will be forward biased and diode D1 and D3 will be reversed biased. The same applies for phase C and diode D3. The potential of the positive DC-terminal is therefore equal to the AC-phase with the *highest* potential. Likewise, the potential of the negative DC-terminal

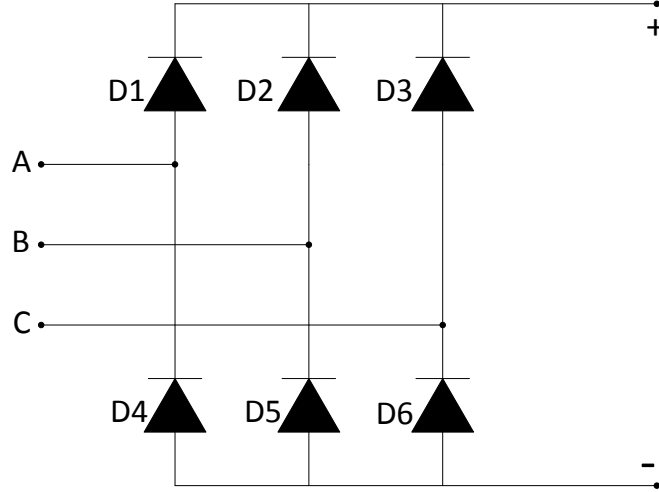


Figure 3.1: 6-pulse diode bridge rectifier

will always be equal to the AC-phase with the *lowest* potential. The DC-voltage can be written as

$$v_d = v_{Pn} - v_{Nn} \quad (3.1)$$

where v_{Pn} and v_{Nn} are the potential at the positive and negative DC-terminals respectively, which are determined by the phase with highest and lowest potential, as described above. With a perfect sinusoidal three-phase voltage, it can be shown that the voltage v_d gets a pulsating waveform with amplitude $\sqrt{2}V_{LL}$, where V_{LL} is the line-line AC-voltage [9]. Each pulse can be described as

$$v_d = \sqrt{2}V_{LL}\cos(\omega t) \quad \text{where} \quad -\frac{1}{6}\pi < \omega t < \frac{1}{6}\pi \quad (3.2)$$

During one period of line frequency, the DC-voltage experiences six pulses, thereby the name *6-pulse rectifier*. To find the average DC-voltage, V_{dc} , we can integrate Equation 3.2 over the duration of one pulse and divide by the duration.

$$V_{dc} = \frac{1}{\pi/3} \int_{-\pi/6}^{\pi/6} \sqrt{2}V_{LL}\cos(\omega t)d\omega t = \frac{3}{\pi}\sqrt{2}V_{LL} \approx 1.35V_{LL} \quad (3.3)$$

This shows that the average DC-voltage of a three-phase diode bridge rectifier is 1.35 times the line-line AC-voltage. Assuming a constant DC load-current and still no AC-side inductance, we can plot one of the AC-phase's voltage- and current waveform (Figure 3.2).

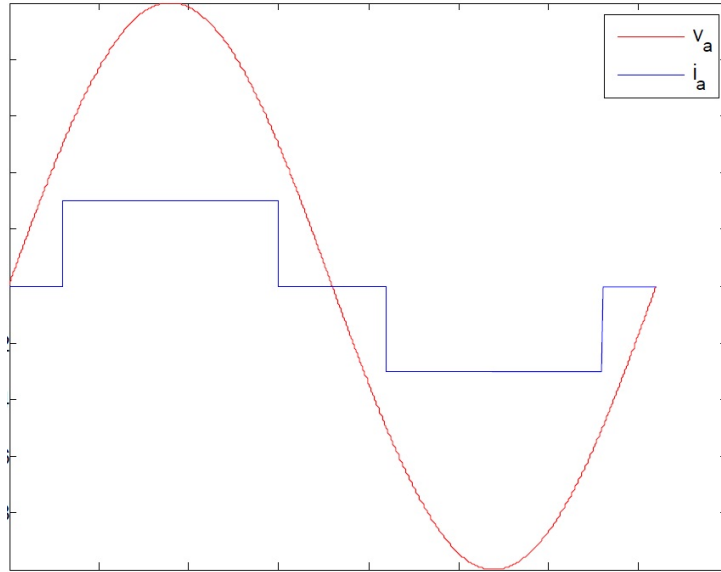


Figure 3.2: Voltage and current at AC-terminals of an ideal 6-pulse rectifier

It is clear that the current is not sinusoidal. By conducting Fourier analysis on the current i_a , we find that the harmonic current amplitudes can be written as

$$I_{sh} = \frac{I_{s1}}{h} \quad (3.4)$$

where I_{s1} is the amplitude of the fundamental frequency component (50 Hz) and h is the harmonic order. Due to a balanced, symmetrical three-phase system, the 3rd harmonics and their multiples are canceled, which leaves the harmonic orders to be given by

$$h_{6p} = 6k \pm 1 \quad \text{where } k = 1, 2, 3... \quad (3.5)$$

Figure 3.3 presents the resulting harmonic current spectrum injected by a 6-pulse rectifier.

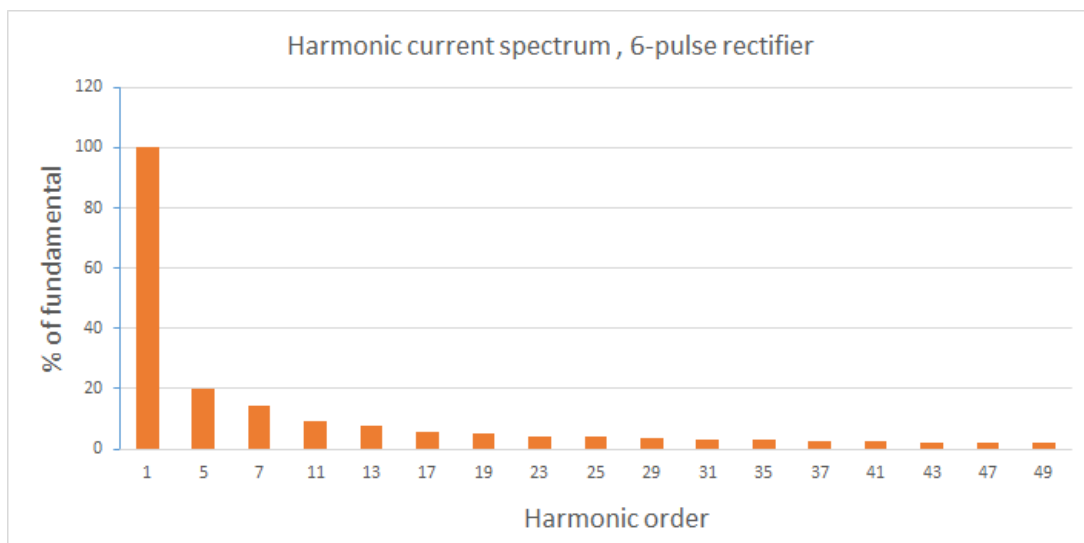


Figure 3.3: Harmonic current spectrum of 6-pulse rectifier

The VSDs discussed in this thesis have smoothing capacitors at their rectifier’s DC-bus. Due to the very large capacitance, the voltage is close to constant and the load viewed from the DC-bus act more like a voltage source. This is usually referred to as a voltage source inverter (VSI) approach. The DC-side current source approach utilized above, is mostly relevant when deriving the harmonics generated by the rectifier. Alternatively, the shunt-connected smoothing capacitor could be replaced with a large series-connected inductance, resulting in a nearly constant DC-current. This construction is usually called current source inverter (CSI).

In the deriving of the harmonic current spectrum for the 6-pulse rectifier above, an assumption of zero AC-side inductance was made. This assumption is only acceptable when deriving the theoretical harmonic current spectrum. Due to a non-zero AC-side inductance, the current commutations between the rectifier diodes will not be instantaneous. The non-instantaneous current commutation between the conducting diodes will lead to lower harmonics than suggested by the theoretical spectrum derived above. Figure 3.4 shows the current of one of the AC-phases of a 6-pulse diode. The plot is a result of an EMT (electromagnetic transient)-simulation test of a 6-pulse rectifier. A smoothing capacitor (2 mF) has been added to the DC-bus in the EMT-simulation. A current source load is connected to the DC-bus.

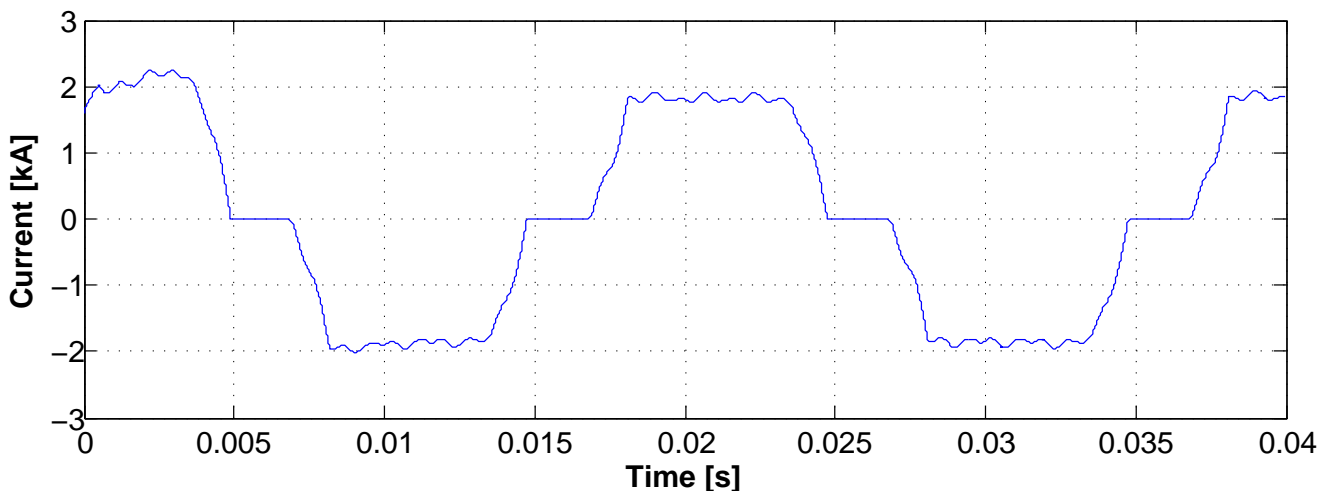


Figure 3.4: AC current of a 6-pulse rectifier from EMT-simulation test

When comparing the current plot in Figure 3.4 to the ideal current i_a , in Figure 3.2, it is clear that the ideal current is not equal to the more realistic current from the EMT-test. Also stated by DIgSILENT themselves, the theoretical spectrum will normally result in higher harmonics than what would be realistic for a power system. Still, the theoretical spectra should give a reasonably good basis for harmonic analysis. The harmonic current spectra utilized in this thesis, are therefore a conservative simplification, which should be kept in mind when analyzing the results.

As can be seen form Figure 3.3, a 6-pulse rectifier generates large amounts of harmonic currents. To reduce the injection of harmonic currents, several 6-pulse rectifiers are often operated together, which leads to canceling of certain harmonics.

3.1.2 12 - and 24 - Pulse Bridge Rectifier

A 12-pulse rectifier can be achieved by connecting two 6-pulse rectifiers either in parallel (to divide the current between the two) or in series (to divide the voltage between the two). A series connection is the most relevant for a subsea VSD. Parallel connected 12-pulse rectifiers will for this reason not be discussed. However, the principle of harmonic current generation is the same as for a series connected rectifier. Figure 3.5 shows the construction of a 12-pulse series connected rectifier.

Here, a 6-phase input is required instead of a normal three-phase input. Usually, this is accomplished by the use of a three-winding transformer where the secondary winding supplies phases A, B and C, while the tertiary winding supplies D, E and F. By introducing a phase-shift between the secondary and tertiary windings of 30 electrical degrees, the two three-phase sets (ABC and DEF) are not synchronous anymore.

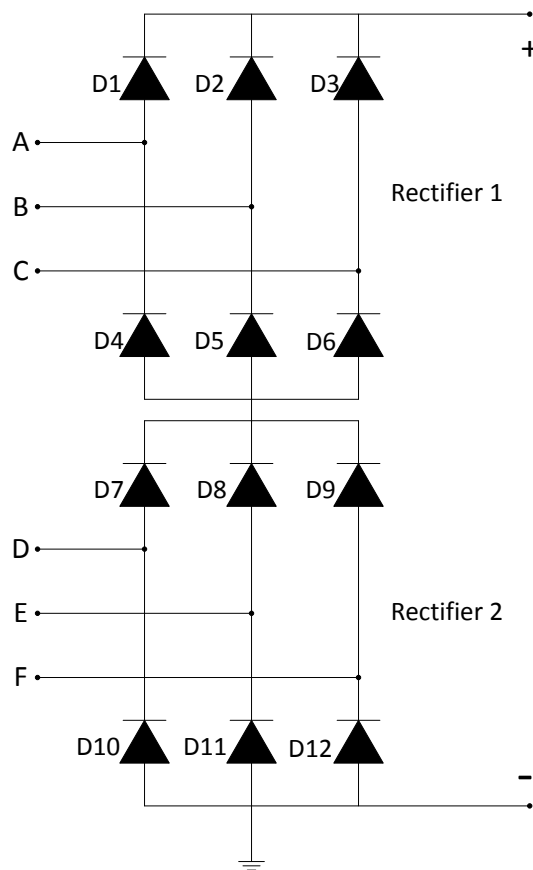


Figure 3.5: Series-connected 12-pulse bridge rectifier

By studying the two 6-pulse rectifiers individually, their voltages can be plotted as in Figure 3.6. Here, the AC-voltage of Rectifier 1 are the phase-A voltage, while the AC-voltage for Rectifier 2 corresponds to the phase-D voltage. Isolated, the two 6-pulse rectifiers generates a 6-pulse DC-voltage each. Equation 3.2 expressed the DC-voltage from $-\frac{\pi}{6} < \omega t < \frac{\pi}{6}$. We will now let this expression describe the DC-voltage of Rectifier 1 in Figure 3.5. The DC-voltage of Rectifier 2 can then be described as

$$v_{DC2} = \sqrt{2}V_{LL} \cdot \cos\left(\omega t - \frac{\pi}{6}\right) \quad \text{where} \quad 0 < \omega t < \frac{\pi}{3} \quad (3.6)$$

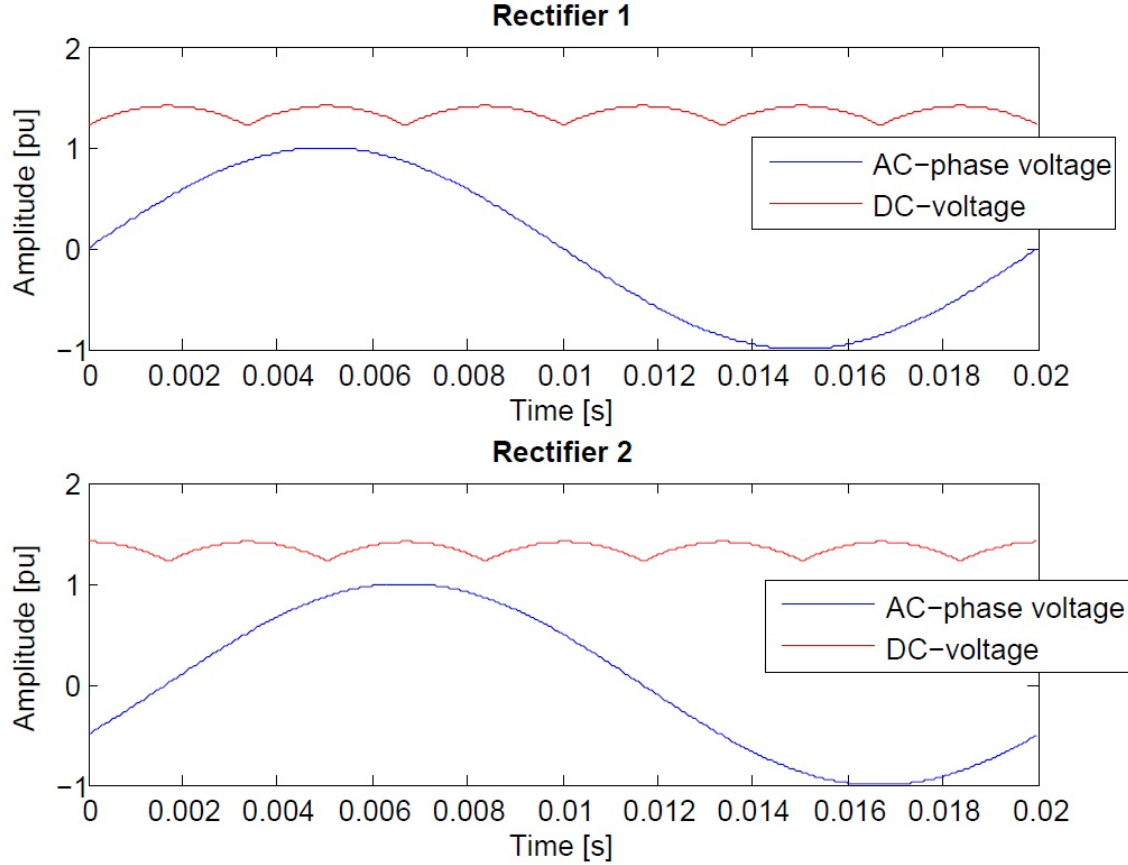


Figure 3.6: Input- and output voltage for Rectifier 1 and 2

Due to the 30 degree phase-shift between input phase-sets ABC and DEF, the 6-pulse DC-voltages generated by Rectifier 1 and 2 are also shifted by 30 electrical degrees. By adding the DC-voltages from Rectifier 1 and 2, we get the total output DC-voltage.

$$v_{DC} = v_{DC_1} + v_{DC_2} = \sqrt{2}V_{LL} \cdot \left[\cos(\omega t) + \cos\left(\omega t - \frac{\pi}{6}\right) \right], \quad 0 < \omega t < \frac{\pi}{6} \quad (3.7)$$

Figure 3.7 shows the DC-voltage of the complete series-connected 12-pulse rectifier for one period of line-frequency. In Figure 3.7, 1 pu is equal to the line-to-line input voltage, V_{LL} .

As we can see, the DC-voltage now consists of 12 pulses per period of line-frequency, hence the name *12-pulse rectifier*. The average DC-voltage of a series connected 12-pulse rectifier can further be calculated as

$$V_{dc} = \frac{1}{\pi/6} \int_0^{\pi/6} \sqrt{2}V_{LL} [\cos(\omega t) + \cos(\omega t - \frac{\pi}{6})] d\omega t = \frac{6}{\pi} \sqrt{2}V_{LL} \approx 2.70V_{LL} \quad (3.8)$$

which is equal to two times the DC-voltage of a 6-pulse rectifiers, as would be expected by two series connected 6-pulse rectifiers.

An advantage of using a 12-pulse rectifier compared to a 6-pulse rectifier, is lower harmonic current injection into the AC system. When the 5th harmonic currents from the

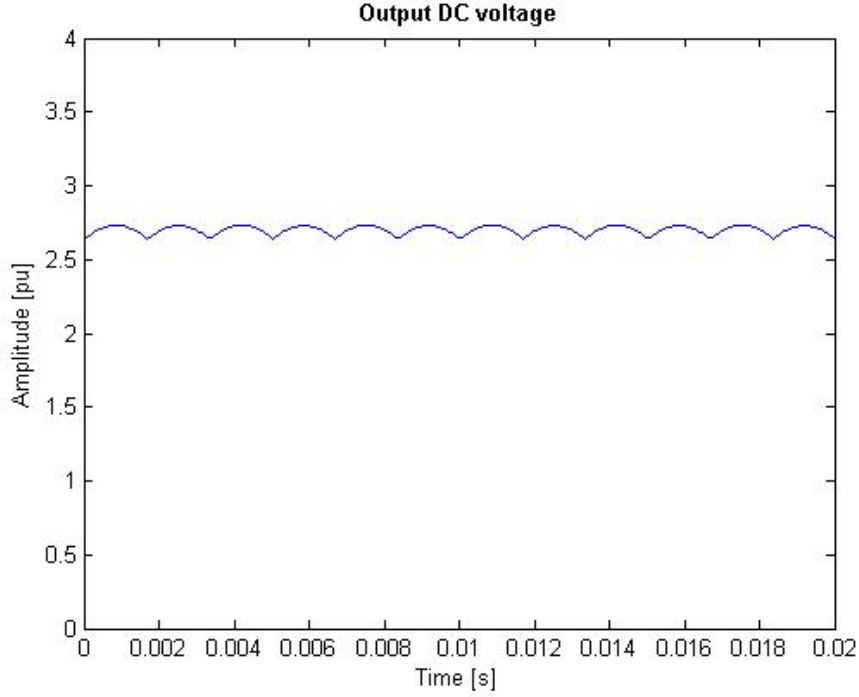


Figure 3.7: Output DC-voltage of an ideal 12-pulse rectifier

rectifiers (which are 30 degrees shifted to each other) are injected into one common phase at the primary winding of the three-winding transformer, they are set in anti-phase. This causes cancellation of the 5th harmonic current. The same applies to the 7th, 17th, 19th, 29th, 31th etc. harmonics. With the third harmonic and its multiples gone as well, we are left with a harmonic spectrum given by

$$h_{12p} = 12k \pm 1 \quad \text{where } k = 1, 2, 3... \quad (3.9)$$

with amplitudes given by Equation 3.4. The total 12-pulse spectrum is shown in Figure 3.8.

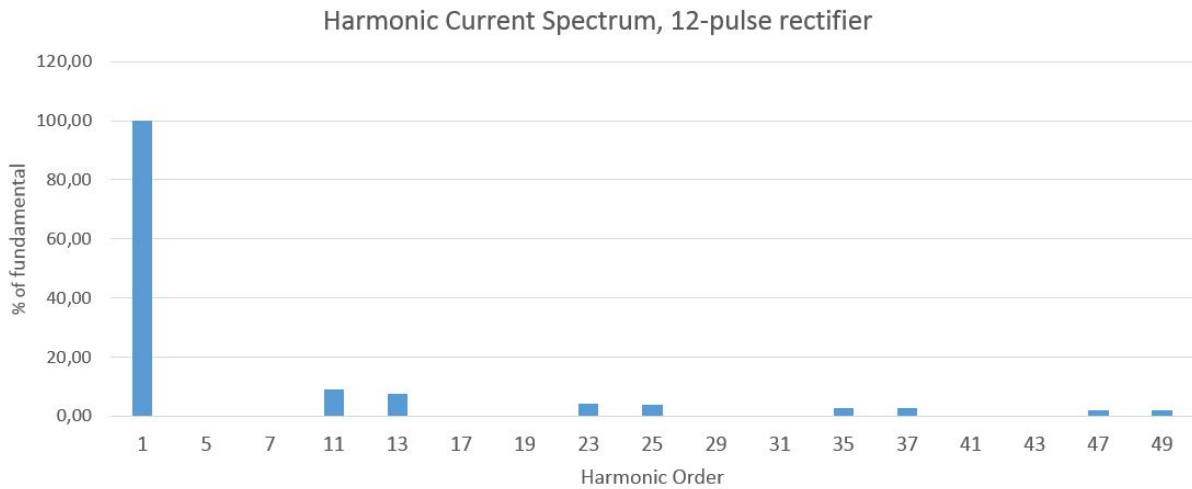


Figure 3.8: Harmonic current spectrum of a 12-pulse rectifier

In many cases, a 12-pulse rectifier may still cause too much harmonic current injection. By connecting two 12-pulse rectifiers together, a 24-pulse rectifier can be obtained. The two 12-pulse rectifiers must be shifted 15 electrical degrees with respect to each other. In other words, this means four 6-pulse rectifiers with electrical displacements of 0, 15, 30, and 45 electrical degrees. This gives a DC-voltage with 24 pulses for each period of line-frequency. This construction method further reduces the injected harmonic currents. Harmonic order 11, 13, 35, 37 etc. are injected into the primary winding of the transformer and set in anti-phase. Cancellation occurs, and the injected harmonic current spectrum will now be limited to

$$h_{24p} = 24k \pm 1 \quad \text{where } k = 1, 2, 3... \quad (3.10)$$

The amplitude of each harmonic is still given by Equation 3.4.

Likewise, both 18-pulse rectifiers (three 6-pulse rectifiers) and 36-pulse rectifiers (six 6-pulse or three 12-pulse rectifiers) can be made. However, an increase in pulses quickly increases both cost and complexity of the VSD system.

3.1.3 Static Var Compensator (SVC) Harmonics

In the electrical systems considered in this thesis, long subsea cables dominates the network construction. Such long cables may lead to large production of reactive power. To avoid large capacitive currents and boosted voltages, compensation measures needs to be taken. SVCs will be utilized for this purpose. A thyristor-controlled reactor (TCR) can regulate the amount of consumed reactive power by adjusting the firing-angle of the thyristors. Figure 3.9 shows a single-line model of the TCR.

Depending on the firing-angle of the thyristor, the current waveform is more or less distorted from its original sinusoidal form. Current harmonics are therefore generated. PowerFactory calculates the injected harmonic currents from the SVC according to the following equation [10]

$$i_{acb} = \frac{4}{\pi \cdot f_{fund}} \frac{\sin(\alpha') \cos(n\alpha') - n \cos(\alpha') \sin(n\alpha')}{n(n^2 - 1)} \quad (3.11)$$

where

$$\alpha' = \alpha - \frac{\pi}{2} \quad (3.12)$$

$$n = 2k + 1, \quad k = 1, 2, 3...$$

α is the firing-angle of the thyristors where 90° correspond to full conduction of the thyristor and 180° correspond to no conduction. The firing-angle is determined by the control setup of the SVC (discussed later).

The harmonic contribution of the SVC is far lower than the contribution of the rectifiers. However, they should be taken into account to maintain the accuracy of the network model.

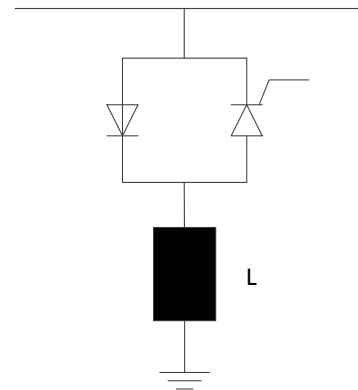


Figure 3.9: Model of a thyristor-controlled reactor (TCR)

3.2 Network Impedance and Resonance

The way harmonic currents behaves in a power system, heavily depends on the impedances of the system. At every busbar in a power system, an equivalent network impedance can be calculated (calculation method is discussed in Section 5.1.3). This represents the total impedance seen from the busbar. If a large harmonic current is fed into a busbar with a large network impedance, a large harmonic voltage will be generated. A solid understanding of the network impedances of the system is therefore crucial to understand the harmonic currents' behavior, and how they manifests themselves as harmonic voltages. Such an understanding is also vital to a harmonic mitigation process. We know that the reactances of an inductance and a capacitance can be expressed as

$$\begin{aligned} X_L &= \omega L \\ X_C &= \frac{-1}{\omega C} \end{aligned} \quad (3.13)$$

where $\omega = 2\pi \cdot f$ and f is the frequency. From Equation 3.13 we know that the magnitude of the reactances changes for different frequencies. The network impedance of a busbar therefore changes substantially as the applied frequency is changed. The 13th harmonic current experiences another network impedance at a given busbar, than the fundamental frequency current. At certain frequencies, resonance phenomena may occur. At these frequencies, the network impedance changes drastically within a short frequency range. This can have extreme impact on the harmonics' behavior. The next section will discuss the mechanisms behind series- and parallel resonance.

3.2.1 Series- and Parallel Resonance

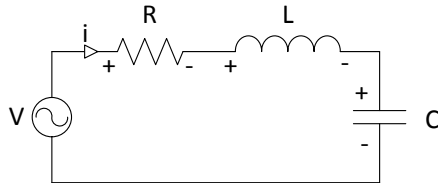


Figure 3.10: Series RLC circuit, [1]

Figure 3.10 shows a simple series RLC circuit. The circuit's inductance and capacitance can be represented in the frequency-domain as the reactances in Equation 3.13. The total reactance of the circuit can be expressed as

$$X_T = X_L + X_C \quad (3.14)$$

At a specific frequency, the circuit's total reactance X_T , goes to zero. This particular frequency is called the *resonance frequency*. Since the reactance now has decreased to zero, the circuit's total impedance has decreased dramatically (only consisting of the circuit's resistance). From Equation 3.13 and 3.14, the resonance frequency can be expressed as

$$f_{resonance} = \frac{1}{2\pi\sqrt{L \cdot C}} \quad [Hz] \quad (3.15)$$

This phenomenon is called *series resonance* and is characterized by a sudden drop in impedance magnitude. However, for the network type considered in this thesis, *parallel*

resonance usually poses more severe challenges than *series resonance* [1, 5].

Figure 3.11 shows a simple parallel RLC circuit. At the circuit's resonance frequency, the imaginary parts of the circuit's *admittances* goes to zero. The current $I_L - I_C$ goes to zero, causing the entire current to be fed through the resistance. The circuit's total impedance therefore increases dramatically, since the parallel connection in a sense vanishes. This phenomenon is called *parallel resonance*. The circuit's resonance frequency can be expressed by Equation 3.15.

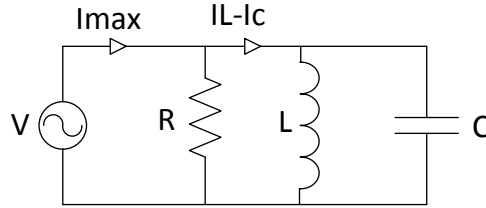


Figure 3.11: Parallel RLC circuit, [1]

3.2.2 Network Impedance Characteristics

As a tool to better understand the observed harmonics, equivalent network impedances will be calculated frequently throughout this thesis. By calculating a busbar's equivalent network impedance over a given frequency range, it is possible to generate a plot of the impedance. From now on, such plots will be referred to as a *network impedance characteristic*.

As mentioned, parallel resonances manifests themselves as a drastic increase in the circuit's impedance. Let us consider the parallel circuit in Figure 3.11. By inserting parameters $R = 1000\Omega$, $L = 4mH$ and $C = 2\mu F$, the network impedance characteristic may be calculated. Here, it is calculated as a parallel connection of the resistance R , the inductance L and the capacitance C . The resulting network impedance characteristic is shown in Figure 3.12.

With the parameters above, the circuit's resonance frequency may be calculated analytically by utilizing Equation 3.15. This results in a resonance frequency of $f_{resonance} = 1779.4 Hz$ which is confirmed by the clear parallel resonance top observed in Figure 3.12. As expected, the impedance magnitude of the parallel resonance is 1000Ω , since the impedance of the circuit now is only determined by its 1000Ω resistance.

An interesting aspect of the network impedance characteristic is how it acts if the circuit's electrical parameters changes. As will be clarified later, one of the most likely resonance problems in this thesis will be parallel resonance between cable capacitances and transformer inductances. What happens if the length of the cable is increased? What happens if the inductance of the transformer is reduced? To answer these questions we need to look at Equation 3.15. The total capacitance of a cable can be written as

$$C = C' \cdot l \quad [F] \quad (3.16)$$

where C' is the capacitance per kilometer and l is the cable's length in kilometers. A longer cable therefore results in a larger capacitance. By increasing the capacitance C

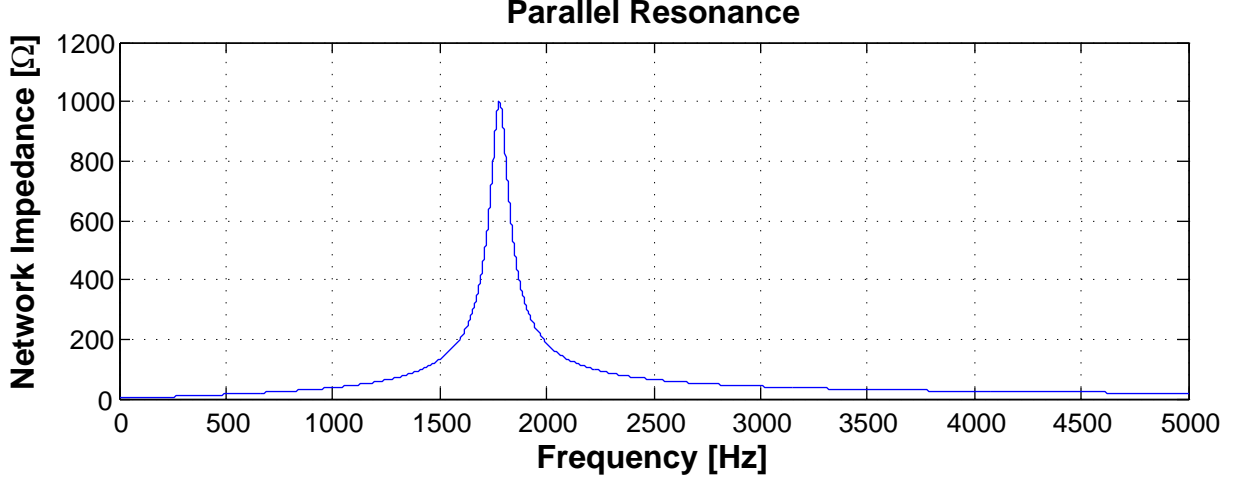


Figure 3.12: Network impedance characteristic of parallel RLC circuit in Figure 3.11

in Equation 3.15, the resonance frequency decreases. A parallel resonance (as shown in Figure 3.12) is therefore shifted towards lower frequencies. If the resonating inductance of a transformer is reduced, the inductance L in Equation 3.15 is reduced, causing increased resonance frequency.

In this way, the designer has the possibility to manipulate the network impedance characteristic and its resonance frequencies. By slightly adjusting the short-circuit impedance of a transformer, or the length or type of a cable, the harmonic content could be reduced substantially. However, due to other designing criterion, the designer might not have the possibility to change the parameter enough to avoid resonance problems.

3.3 Harmonic Current Amplification

If a resonating parallel RLC circuit carries a current with the same frequency (or nearly the same) as the resonance frequency, harmonic current amplification may occur. The 'tank' circuit (parallel-connection of a capacitance and an inductance) is excited, which causes the energy to oscillate from being stored in the capacitance (electric field) to being stored in the inductance (magnetic field). This phenomena can amplify the harmonic current several times. The increased harmonic current can further cause harmonic voltage problems when injected into a busbar. Below, the mechanisms causing such current amplification are explained in a relevant cable example.

The circuit in Figure 3.13 consist of an AC current source, a simplified cable and a network equivalent impedance. By adding the cable's resistance and inductance to $Z_{network}$, the circuit can be further simplified. The new impedance is called Z_{system} . The new circuit is shown in Figure 3.14, where $Z_C = -j\frac{1}{2\pi f \cdot C}$. Note that the current flowing out of *end 2* of the cable in Figure 3.13, is the same as I_S in Figure 3.14. With currents as defined by Figure 3.14, the current injected into the system Z_{system} , can be described as

$$I_s = \frac{Z_c}{Z_{system} + Z_c} \cdot I_h \quad (3.17)$$

Let us now assume that the cable's capacitance, represented by Z_c , resonates with the system Z_{system} , at a harmonic order h . This results in a parallel resonance circuit, as

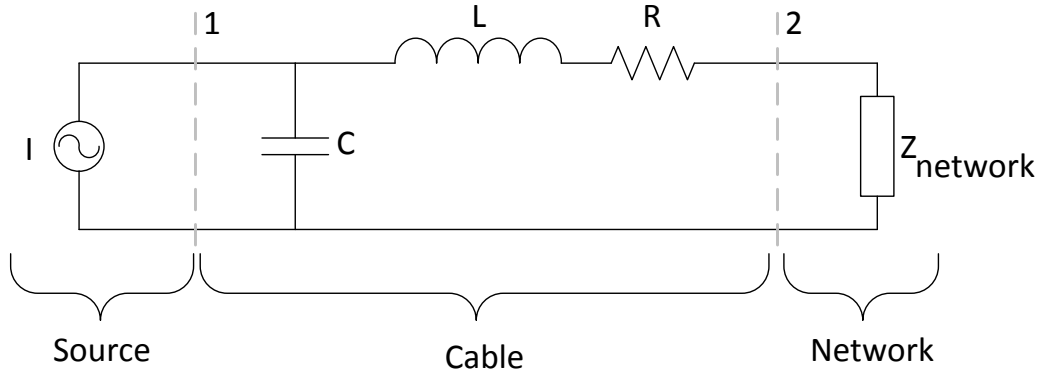


Figure 3.13: Simplified source-cable-network circuit

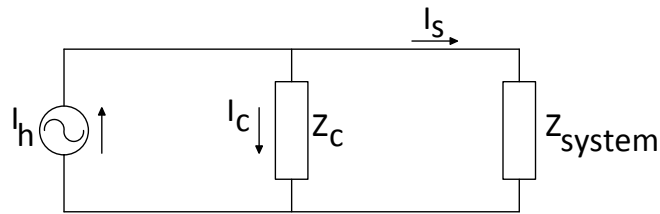


Figure 3.14: Simplified cable circuit with harmonic current amplification

described in Section 3.2.1. For harmonic order h we have

$$\text{Im}(Y_{system}) + \text{Im}(Y_c) = 0 \quad (3.18)$$

where $Y_{system} = 1/Z_{system}$ and $Y_c = 1/Z_c$. The current source on the left-hand side, now injects a harmonic current I_h , of harmonic order h , into the cable. Due to the parallel resonating circuit, the magnitude of the denominator in Equation 3.17 has decreased dramatically. Now, the numerator of Equation 3.17 might be several times larger than the denominator, leading to a current amplification through the cable. The magnitude of this amplification, depends on the cable- and system parameters, and how close the injected harmonic current's frequency is to the circuit's resonance frequency. An amplified harmonic current fed into a high impedance busbar may further cause harmonic voltages of very large magnitudes. It is therefore extremely important to keep such current amplification to an absolute minimum.

By inserting values for the parameters in Figure 3.13, the current amplification can be calculated. With $C' = 0.23 \mu F/km$, $L' = 0.38 mH/km$ and $R' = 0.119 \Omega/km$, the cable roughly corresponds to a $U_m = 36kV$, $185 mm^2$ subsea power cable (same type as the one utilized as step-out cable in the *Short Step-out*). Let us assume a cable length of $30 km$ and the inductance of $Z_{network}$ to be equal to $0.736 mH$. This gives a resonance frequency at the 11^{th} harmonic ($550 Hz$). The current amplification has been calculated for frequencies ranging from 1 to $2500 Hz$ for two different values of $Re(Z_{network})$. Figure 3.15 shows the plots.

With a $Re(Z_{network}) = 1\Omega$, the damping in the circuit is very low. At resonance, the imaginary part of the denominator of Equation 3.17 becomes zero, as discussed earlier. Due to the very low real part, the denominator's magnitude becomes very small, leading to an amplification of ~ 9 times, as the current flows through the cable. If the

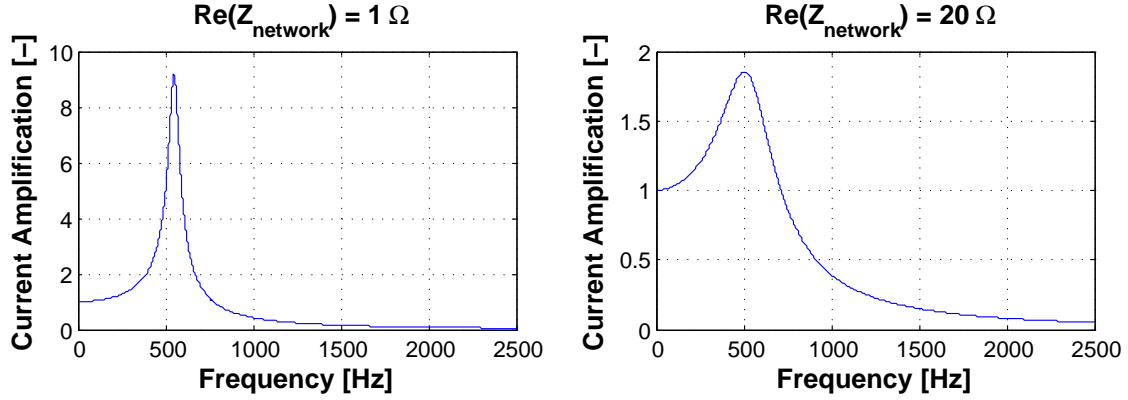


Figure 3.15: Possible current amplification in a 30 km long, $U_m = 36kV$, $185 mm^2$ subsea power cable

$Re(Z_{network})$ becomes even lower, the current amplification increases. If it is set to zero, the cable resistance offers the only damping in the circuit, causing an amplification of nearly 12 times the injected current. On the other hand, if the resistances are increased, the current amplification is decreased. With a $Re(Z_{network}) = 20\Omega$, the amplification is reduced to below two times the injected current.

The example above describes harmonic current amplification through a cable. However, a cable is not the only 'tank' circuit which can be excited and cause amplified harmonic currents. Looking back at Figure 3.14, let us now assume that the current I_h is a harmonic current injected into a busbar, by a cable. The end of *another* cable is connected to the same busbar. Its capacitance can be represented by the reactance Z_c , in Figure 3.14. Z_{system} could represent a transformer. Under certain conditions, the harmonic current injected into the busbar may therefore be further excited by other nearby cables or capacitive components. A harmonic current can first be amplified through a cable, before being further amplified as it is excited by another cable's capacitance. The second cable do not need to carry a fundamental load current. Such *double amplification* could clearly cause very large harmonic currents, which would lead to extreme harmonic voltages.

When conducting Harmonic Load Flow simulations in PowerFactory, it is possible to generate harmonic current spectra from both ends of a cable. Harmonic current amplification (or a *double amplification*) is therefore easily detectable. If current amplification is found, it also reveals which capacitance is resonating with the system. When the resonating capacitance is identified, harmonic mitigation becomes easier. Changing cable type (capacitance value) or cable length, could be enough to shift the resonance to another frequency and avoid current amplification, ending up with lower harmonic voltages.

3.4 Frequency Selective Circuits

Frequency selective circuits are used in a wide selection of electrical equipment. This includes electronics, communication equipment etc.. These circuits are selective in which frequencies are let through. Frequency selective circuits can be divided into three main categories; high-pass filter, band-pass filter and low-pass filter. Only the latter will be discussed here. A qualitative description of relevant low-pass filters will be given. How such filter-circuits can occur naturally in the power system will also be discussed.

3.4.1 RL Low-Pass Filter

Figure 3.16 shows a series RL low-pass filter circuit. The reactance of the inductor can be written as $Z_L = j\omega L$ where $\omega = 2\pi \cdot f$ and f is the applied frequency. It is clear that the reactance's magnitude increases with increasing frequency.

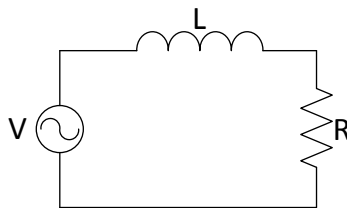


Figure 3.16: Series RL low-pass filter

As the applied frequency is low, a large part of the circuit's voltage is placed across the resistance R . However, as the frequency increases, an increasingly portion of the voltage drop is placed across the inductor, due to its increasing reactance. With a frequency $f = \infty$, the inductor's reactance becomes infinite, and the inductor acts as an open-circuit, therefore carrying the entire voltage drop.

The leakage inductance of a transformer can act as a low-pass filter in a power system. At high frequencies, a relatively large portion of the harmonic voltage is placed across the transformer, instead of spreading further throughout the system.

3.4.2 RC Low-Pass Filter

Figure 3.17 shows a series RC low-pass filter circuit. The capacitance's reactance can be written as $X_C = \frac{1}{\omega C}$ where $\omega = 2\pi \cdot f$ and f is the applied frequency. With increasing frequency, the magnitude of the capacitance's reactance decreases.

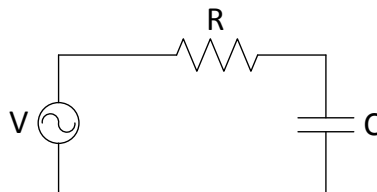


Figure 3.17: Series RC low-pass filter

When the applied frequency is low, only a small current is fed through the capacitance, due to its large reactance. Most of the voltage drop is therefore placed across the capacitance. But as the frequency increases, the magnitude of the reactance decreases, causing

a larger current to flow through the capacitance. If the frequency is infinite, the reactance of the capacitance is equal to zero, causing the capacitor to act as a short-circuit. The entire voltage is now placed across the resistance. This phenomenon was actually demonstrated in Figure 3.15; As the frequency approached 2500 Hz (harmonic order 50), nearly none of the injected current was visible at the other end, but was instead fed through the capacitance.

The capacitance of a long power cable may act as such a low-pass filter. The longer the cable, the larger the capacitance C , which further causes a lower shunt reactance.

3.4.3 LCL Low-Pass Filter

By combining the filtering abilities of both the RL- and the RC low-pass filters, a LCL low-pass filter can be obtained. Figure 3.18 shows such a filter. Harmonic voltages are effectively dampened across the inductances (large reactance magnitude at high frequencies) while harmonic currents are fed through the capacitance (low reactance magnitude at high frequencies).

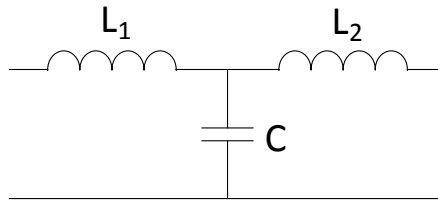


Figure 3.18: LCL low-pass filter

LCL filters can be intentionally constructed and tuned to filter a certain range of frequencies. By installing such filters between power electronics (as a VSD) and the utility, harmonics can be reduced considerably. However, the LCL filtering effect may also occur more or less naturally in a power system. A long subsea power cable, with one transformer in each end, could (very simplified) form a circuit as the one in Figure 3.18. This is the case for the *Long Step-out* where the step-out cable has a step-up transformer connected to one end, and a step-down transformer connected to the other end. As we will see later, this has a substantial damping effect on both current- and voltage harmonics.

3.5 Potential Problems Caused by Harmonics

From the above, it is clear that harmonic currents and voltages of some amplitude are most likely present in any electrical power system with frequency converters, rectifiers or other similar power electronics. Space-harmonics, caused by the non-sinusoidal winding distribution in electrical rotating machinery, the no-load current of a transformer, or any other non-linear component, may also cause increased harmonics in a power system. When discussing harmonics or harmonic content in a power system, it is usually referred to the steady-state conditions. Some upper harmonic limits are usually determined to assure correct operation and to avoid damage to the electrical components. Such standards are discussed in Section 3.7.

In the same manner as the fundamental current, harmonic currents cause ohmic losses in cables and conductors. Due to the skin-effect, experienced by the harmonic currents, the ohmic resistance becomes large for high-frequency harmonics. This causes excessive heating in the electrical components. For overhead lines, this is not a very serious problem, due to the self-repairing air insulation and effective cooling. However, the cooling of power cables are far less effective, and the harmonic current losses could lead to increased operational temperature. The excessive heating of XLPE (cross-linked polyethylene) power cables was studied by Patil and Gandhare [11]. As very large harmonic currents are fed through such cables, the power cable losses can increase by tens of percent, in turn causing the operational temperature to increase beyond the maximal operational temperature of the cable. The increased temperature causes a deterioration of the XLPE insulation. This may shorten the cable's lifetime to only a fraction of its originally expected lifetime.

The excessive heating described above, may not only occur in power cables, but also in transformers, motors, generators, capacitor banks etc. Increased iron or eddy current losses might also be a result of harmonics. It is clear that to high levels of harmonic current may become very expensive in the case of damaged or failed components.

Some electrical components might rely on accurate zero crossing of the voltage or current, to operate as intended. Other equipment might be very sensitive to the voltage- or current waveform. The waveform distortion caused by harmonics, could therefore lead to incorrect operation. Circuit breakers, fuses or relays might not be able to operate as desired under high-level harmonic conditions. Harmonics can result in failure, damage or tripping of such components, for no apparent reason.

Telecommunications, computers and similar components may be very sensitive to the voltage- or current waveform, along with electromagnetic interference. A utility with high harmonic content, might lead to damages, failures, interference or other unwanted effects on such equipment.

With the effects harmonics may have on a power system in mind, it is clear that the harmonics content should be minimized. The next section will discuss some relevant techniques which can lower the harmonics content.

3.6 Harmonic Mitigation

As mentioned in Section 2, placing the VSD topside is currently the most used approach. The harmonics in the cable system is then heavily dependent of the switching pattern of the VSD, and *not* the rectifier. The designer is then given the possibility to optimize the switching pattern to avoid harmonic resonance and to keep the harmonics at a minimum. This was done in the technology qualification testing for the Åsgard Subsea Gas Compression [8], and was also discussed by Råd [7]. Since the harmonics in the systems discussed in this thesis are determined by the rectifier, the possibility for this mitigation technique is lost. Further, this section will discuss some harmonic mitigation techniques relevant for the systems under consideration.

3.6.1 Rectifier Choice

As discussed in Section 3.1.1 and 3.1.2, the choice of rectifier type affects the harmonics present in the system, considerably. Going from a 12-pulse rectifier to a 24-pulse rectifier leads to less harmonic current injections. The electrical system will therefore not be as vulnerable for possible parallel resonances or current amplifications. In this thesis, 12-pulse rectifiers will be utilized. By studying the harmonics present in the systems, it can be further determined if 24-pulse rectifiers (or even higher pulse rectifiers) are required, or not.

3.6.2 Transformer Phase-Shift

By using the same principle as was done in the construction of 12- and 24-pulse rectifiers, harmonics can be limited by introducing phase-shifts in three-winding transformers. Harmonic currents from different network branches can be set in anti-phase which leads to damping (or ideally, total cancellation) of harmonics. If the subsea power system has a three-winding step-down transformer, the secondary and tertiary winding could be shifted 15 electrical degrees with respect to each other. If identical 12-pulse harmonic current spectra are fed into the secondary and tertiary winding, the phase-shift will result in cancellation of the 11th, 13th, 17th, 19th etc. harmonic currents, as in a 24-pulse rectifier. However, if this method is to function optimally, the harmonic spectra injected into the secondary and tertiary windings needs to be identical. To assure reduction of harmonics, there is need for two harmonic currents to be set in anti-phase. Otherwise, there is no reduction nor cancellation, at all. This method will be utilized on the three-winding step-down transformer in the *Long Step-out* topology.

3.6.3 Active- and Passive Harmonic Filtering

Both active- and passive harmonic filters are available on the market, with purpose to reduce the harmonic content in power systems. A passive filter can be designed as a low-pass filter (as discussed earlier) which can reduce high frequency components in the system. Another possibility is the use of specially tuned filters for specific harmonic frequencies. These filters consists of a series-connected inductance and a capacitance, shunt-connected to the line. Such a filter can act as a harmonic energy source. In this way, the filter can supply the loads with their demanded harmonic current, instead of being supplied by the utility (analogous to a capacitor bank supplying reactive power to

a highly inductive load). The harmonic content throughout the system is then reduced. Also, by inserting reactors in the system, harmonic content can be suppressed.

If the loads are highly dynamic in their operation, active filtering might be a good solution. With fast-switching semiconductors, the filter injects the same harmonic currents as are present in the system, but in anti-phase. In this way, the unwanted harmonics may be heavily reduced. This demands high switching frequencies by the filter, which in turn can cause problems with electromagnetic interference for sensitive equipment. Semiconductors can also be used in rectifiers to create a so-called *active front-end*. An active rectifier can reduce the harmonics injected into the system, utilizing an optimized switching scheme.

Installing either active- or passive filters, specifically made for harmonic mitigation, increases the complexity and cost of the power system. Such filter should therefore be the "last way out" when designing a subsea power system, with its extreme requirements to low maintenance and high reliability.

3.7 International Standards Concerning Harmonics

Two of the most applied international standards (or guidelines) concerning harmonic content in electrical power systems, are the IEC 61000-2-4 and the IEEE Std 519-2014. The IEEE standard has a strong focus on current harmonics, and also takes the short-circuit currents of the system into account, when determining the recommended upper harmonic limits. For the systems under consideration in this thesis, the IEEE 519-2014 would set the voltage THD limit to 5 % for busbars with voltages up to 69 kV, and 2.5 % for busbars with higher rated voltages [12].

The IEC standard on the other hand, has more of its focus placed on the voltage harmonics. The requirements presented by this standard depends on the sensitivity of the network under consideration (public network, industrial applications etc.). In Statoil's industrial power systems, the IEC 61000-2-4 Class 2 is used to define acceptable harmonic content, and will therefore be utilized in this thesis. The standard defines the total harmonic distortion (THD) as [2]

$$THD = \sqrt{\sum_{h=2}^{h=H} \left(\frac{Q_h}{Q_1}\right)^2} \quad (3.19)$$

where Q represents voltage or current, Q_1 is the RMS value of the fundamental frequency component, Q_h is the RMS value of the harmonic component of order h , and H is the maximal harmonic order considered in the standard ($H = 50$). The standard describes harmonic voltage limits at Points of Common Coupling (PCC). A PCC is defined by the IEC standard as; "*Point on a public power supply network, electrically nearest to a particular load, at which other loads are, or could be, connected*" [2]. The Class 2 part of the standard is applied to industrial and non-public power systems. The maximum voltage THD for Class 2 is by the standard set to 8 %. Table 3.1 presents the individual harmonic voltage limits at a PCC, proposed by the IEC standard. Figure 3.19 shows the resulting harmonic voltage spectrum (fundamental not included), based on Table 3.1. Note that these are individual limits. If a voltage contains the entire harmonic spectrum in Figure 3.19, the THD would become too high ($\sim 11.5\%$).

Odd harmonics non-multiples of three		Odd harmonics multiples of three		Even order harmonics	
Harmonic order h	Class 2 U_h [%]	Harmonic order h	Class 2 U_h [%]	Harmonic order h	Class 2 U_h [%]
5	6	3	5	2	2
7	5	9	1.5	4	1
11	3.5	15	0.4	6	0.5
13	3	21	0.3	8	0.5
17	2	$21 < h \leq 45$	0.2	10	0.5
$17 < h \leq 49$	x_1			$10 < h \leq 50$	x_2
$x_1 = 2.27 \cdot (17/h) - 0.27$					
$x_2 = 0.25 \cdot (10/h) + 0.25$					

Table 3.1: IEC 61000-2-4 Class 2 harmonic voltage limits, [2]

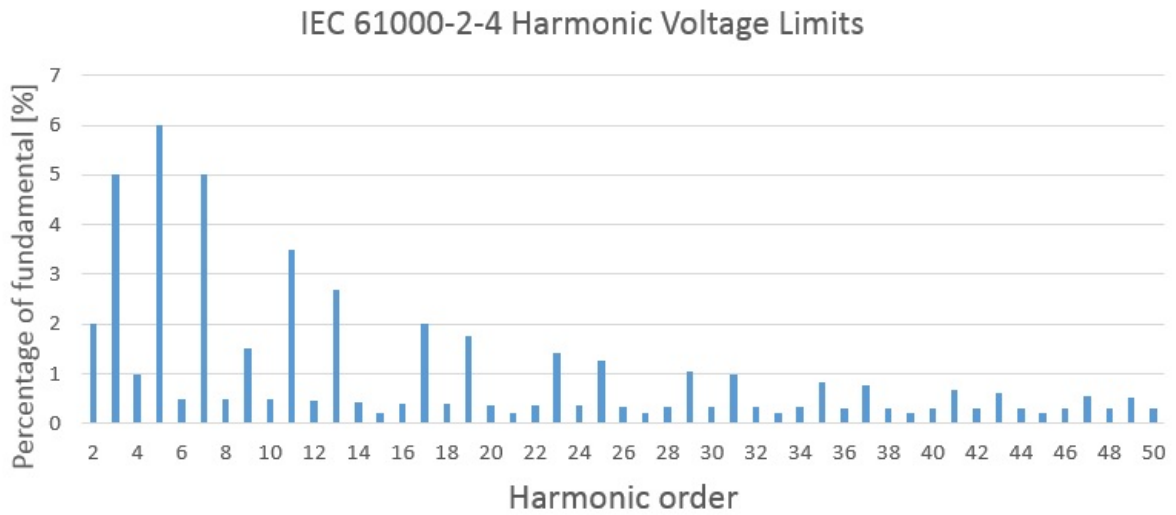


Figure 3.19: IEC 61000-2-4 Class 2 harmonic voltage spectrum

THD can also be used for current harmonics, however, whenever a THD value or level is referred to further in this thesis, it is *always* referred to a *voltage* THD. Table 3.1 and the maximum voltage THD of 8% will be used as a basis when assessing the results of this thesis. Due to the harmonic content in the calculations in this thesis, even- and multiples-of-three harmonics are not of interest.

4 Network Component Simplification and Modeling

This section will discuss the PowerFactory modeling of the various network components, simplifications made to the system, as well as the implementation of the *Long Step-out* and *Short Step-out* in PowerFactory, as a whole.

4.1 Transformer Modeling

The positive- and negative sequence transformer model in Figure 4.1, is used by PowerFactory as a basis for all calculations. The per-unit model of the transformer uses a complex winding ratio with magnitude 1:1. This enables the model to take the transformer's vector group into account. Further, the base values of the impedances are defined as follows, [13]

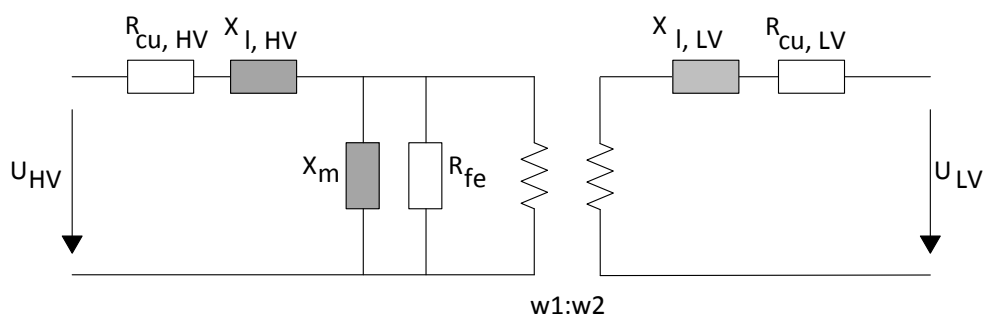


Figure 4.1: Positive- and negative sequence model of two-winding transformer, in Ohms

$$\begin{aligned} Z_{r,HV} &= \frac{U_{r,HV}^2}{S_r} \\ Z_{r,LV} &= \frac{U_{r,LV}^2}{S_r} \end{aligned} \quad (4.1)$$

and the short-circuit impedance as

$$z_{sc} = \frac{U_{sc}}{100} \quad (4.2)$$

where $U_{r,HV}$ and $U_{r,LV}$ are the rated voltages at HV- and LV-side, S_r is the rated apparent power and U_{sc} is the short-circuit voltage.

The topside step-up transformers in both *Long Step-out* and *Short Step-out* are equipped with tap-changers at their high-voltage side. In the PowerFactory model, an additional ideal transformer is then inserted on the HV-side of the original transformer model. The winding ratio of the additional transformer is determined by the tap-position. If tap-changing causes phase-shifts, a complex winding ratio is used. For even more accurate modeling, the parameters of the original transformer model can be set to be tap-dependent. This will not be done in this thesis. The control setup for the tap-changers are discussed in Section 4.7.1 and 4.8.1 for the *Long Step-out* and *Short Step-out*, respectively.

When modeling a three-winding transformer, the user can define where to place the tap-changing transformer, the magnetizing reactance and the iron loss resistance. Figure 4.2 shows the general model for three-winding transformers used by PowerFactory. In

the figure, the tap-changer is placed at the star-point, and all possible locations for magnetizing reactance and core-loss resistance, are shown (HV-side, MV-side, LV-side and star-point).

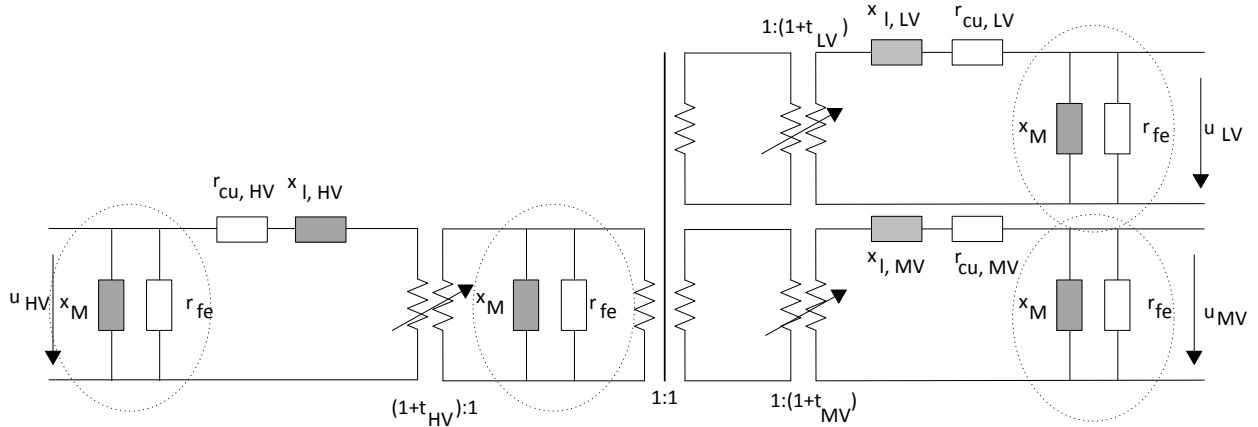


Figure 4.2: Positive- and negative sequence model of three-winding transformer, in per unit

To best be able to model high-frequency behavior of a transformer, frequency-dependence may be included for the transformer's internal parameters. However, this will not be done in the modeling in this thesis.

4.2 Cable Modeling

Accurate cable modeling is extremely important to assure correct and reliable results, when studying harmonic behavior in power systems. PowerFactory offers two main methods when modeling power lines or power cables; geometric and constructional input or electrical parameter input.

By the use of the cable's constructional data (conductor cross-sectional area, insulation thickness, sheaths, etc.), PowerFactory can calculate the electrical parameters itself based on both standard electromagnetism equations (Maxwell's equations) and more complex cable modeling methods to obtain frequency-dependent parameters. Likewise, the construction of an overhead line tower (distance between conductors, earth/grounding lines, etc.) can be used as input to model an overhead power line. However, when utilizing the constructional data given in the manufacturers' product brochures as input, this method have proven to be problematic. Unable to make the parameter calculations in PowerFactory converge, the constructional parameters cable model is not usable. Therefore, only the electrical parameters modeling will be utilized in this thesis.

When modeling the cables with electrical parameters as input, the numerical problems are avoided. Electrical sequence parameters per km are used as input. All parameters needed for the basic model, can normally be found in manufacturers' product brochures. However, by using the electrical parameter modeling, the parameters are not modeled to be frequency-dependent. Due to skin effect and proximity effect, the resistance of the cable's conductor changes for various frequencies. As the frequency increases, the current is forced to flow through the outer layers of the copper conductor, increasing the current density and rising the electrical resistance. Matrices describing the frequency-dependence of the cable parameters, can manually be included in the cable model. How the frequency-dependencies are calculated, is discussed in Section 4.2.2.

4.2.1 Distributed Parameters Model

When the length of a cable or line is of the same magnitude as the wavelength of the applied frequency, traditional circuit theory is no longer applicable. Instead of modeling the cables as π -equivalents, a distributed parameters model should be utilized. Such a model takes the distributed nature of the electrical parameters (resistance, capacitance, inductance, etc.) into account. Long cables dominate the cable systems under consideration in this thesis, and an accurate cable model is extremely important, both for low and high frequencies. A distributed parameters model of the cable is also important to assure correct network impedances in the system (discussed in Section 4.2.3). The general formulation of the distributed parameters model used in PowerFactory, is based on the circuit in Figure 4.3.

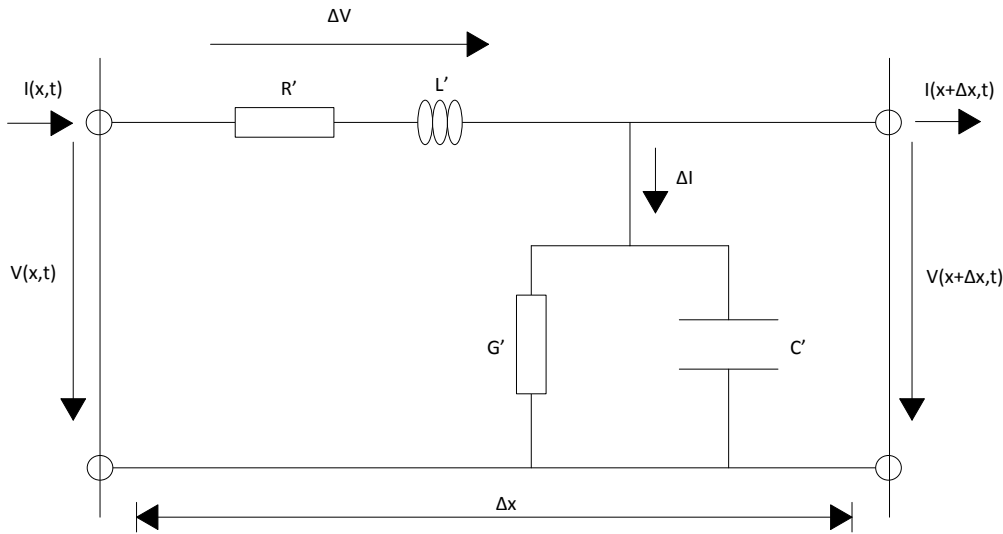


Figure 4.3: Distributed parameters model for cable modeling in PowerFactory

For each length Δx , the cable is described by its resistance R' , inductance L' , conductance G' and capacitance C' , per length unit Δx . By expressing the electrical parameters as impedance and admittance per length unit, we can express the rate of voltage- and current change, as follows [14]

$$\begin{aligned}\frac{\partial}{\partial x}V &= I(x) \cdot Z' \\ \frac{\partial}{\partial x}I &= V(x) \cdot Y'\end{aligned}\tag{4.3}$$

Taking the second derivative and rearranging gives

$$\begin{aligned}\frac{\partial^2}{\partial x^2}V &= Z' \cdot Y' \cdot V(x) \\ \frac{\partial^2}{\partial x^2}I &= Z' \cdot Y' \cdot I(x)\end{aligned}\tag{4.4}$$

which have the general solution

$$\begin{aligned}V(x) &= K_1 \cdot e^{\gamma x} + K_2 \cdot e^{-\gamma x} \\ Z_C \cdot I(x) &= -K_1 \cdot e^{\gamma x} + K_2 \cdot e^{-\gamma x}\end{aligned}\tag{4.5}$$

where

$$Z_C = \sqrt{\frac{Z'}{Y'}} \quad (4.6)$$

is the surge impedance of the cable, and

$$\gamma = \sqrt{Z' \cdot Y'} = \alpha + j\beta \quad (4.7)$$

is the propagation factor of the cable. The constants K_1 and K_2 can be determined from boundary conditions. The particular solution of Equation 4.5 further gives

$$\begin{bmatrix} V_r \\ I_r \end{bmatrix} = \begin{bmatrix} \cosh\gamma \cdot l & -Z_C \cdot \sinh\gamma \cdot l \\ \frac{1}{Z_C} \cdot \sinh\gamma \cdot l & -\cosh\gamma \cdot l \end{bmatrix} = \begin{bmatrix} A & B \\ C & D \end{bmatrix} \cdot \begin{bmatrix} V_s \\ I_s \end{bmatrix} \quad (4.8)$$

From the equations above, we can write the impedance and admittance of an exact long cable model circuit (Figure 4.4) as

$$\begin{aligned} Z &= Z_C \cdot \sinh\gamma \cdot l = Z' \cdot l \cdot \frac{\sinh\gamma \cdot l}{\gamma \cdot l} \\ Y &= \frac{\cosh\gamma \cdot l - 1}{Z_C \cdot \sinh\gamma \cdot l} = \frac{1}{2} \cdot Y' \cdot l \cdot \frac{\tanh(\frac{\gamma \cdot l}{2})}{\frac{\gamma \cdot l}{2}} \end{aligned} \quad (4.9)$$

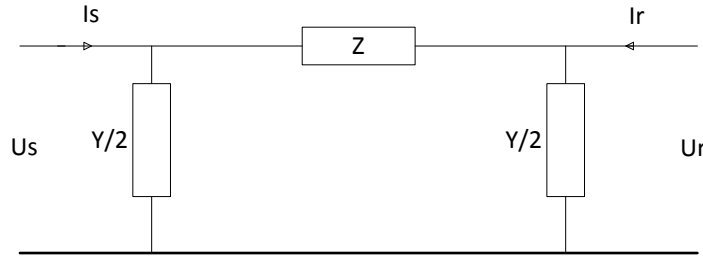


Figure 4.4: Equivalent circuit for long cable model with distributed parameters [1]

The distributed parameters model discussed above, is defined in the frequency-domain. It is therefore used by PowerFactory in all steady state calculations as load flow, harmonic load flow, frequency sweep, short-circuit as well as RMS-simulations (electromechanical). For EMT-simulations (electromagnetic transient) the model is converted from frequency-domain to time-domain by the use of Bergeron's method for solutions in time-domain [14].

4.2.2 Frequency-Dependent Resistances

To include frequency-dependence to the cable conductor resistances, a resistance characteristic for every utilized conductor cross-sectional area, has been calculated. By utilizing the method provided by the IEC 60287-1-1, frequency-dependent resistances have been calculated for frequencies ranging from 1 to 2500 Hz. The resistance characteristics can

further be included in their respective cable types, in the PowerFactory model. The method proposed by the IEC 60287-1-1 calculates the resistance as follows [15]; the AC resistance is calculated from

$$R = R' \cdot (1 + y_s + y_p) \quad (4.10)$$

where R is the AC resistance per length unit at maximum operational temperature. R' is the conductor's DC resistance per length unit at maximum operational temperature. y_s and y_p are the skin-effect factor and the proximity-effect factor, respectively, and are frequency-dependent. The DC resistance is calculated from

$$R' = R_0 \cdot [1 + \alpha_{20}(\theta - 20)] \quad (4.11)$$

where R_0 is the DC resistance at $20^\circ C$ per length unit, and is collected from IEC 60228 [16] as specified by the IEC 60287-1-1. α_{20} is the mass-temperature coefficient and is equal to $3.93 \cdot 10^{-3}$ for copper conductors. θ is the maximal operational temperature for the cable, and is set to $90^\circ C$ for the XLPE cables used in this thesis. The skin-effect factor is given by

$$\begin{aligned} y_s &= \frac{x_s^4}{192 + 0.8 \cdot x_s^4}, & 0 < x_s \leq 2.8 \\ y_s &= -0.136 - 0.0177 \cdot x_s + 0.0563 \cdot x_s^2, & 2.8 < x_s \leq 3.8 \\ y_s &= 0.354 \cdot x_s - 0.733, & x_s > 3.8 \end{aligned} \quad (4.12)$$

where

$$x_s^2 = \frac{8\pi f}{R'} \cdot 10^{-7} k_s \quad (4.13)$$

where f is the frequency, and k_s is equal to 1 for round, stranded conductors with extruded insulation (XLPE cables). The proximity-effect factor for three-core cables or three single-core cables (with round conductors) is given by

$$y_p = \frac{x_p^4}{192 + 0.8 \cdot x_p^4} \left(\frac{d_c}{s} \right)^2 \left[0.312 \cdot \left(\frac{d_c}{s} \right)^2 + \frac{1.18}{\frac{x_p^4}{192 + 0.8 \cdot x_p^4} + 0.27} \right] \quad (4.14)$$

where

$$x_p^2 = \frac{8\pi f}{R'} \cdot 10^{-7} k_p \quad (4.15)$$

d_c is the diameter of the conductor, and s is the distance between the conductors. k_p is equal to 1 for stranded conductors with extruded insulation. Based on the method described above, the frequency-dependent resistances are calculated for cables operating at their maximum operational temperature. However, an operating temperature of $90^\circ C$ is not realistic for a subsea power system. Due to the cooling effect of the ocean water, an operating temperature of $70^\circ C$ is assumed. To compensate for the lower temperature, a factor of 0.94 is multiplied to the resistances, for all frequencies [17]. The resulting frequency-dependent resistances are included in the cable models. Plots of the frequency-dependent resistances can be found in Appendix A.

To obtain an even more accurate cable model, the cable inductances should be modeled as frequency-dependent. Due to changes in the mutual coupling between the conductors for increasing frequency, the cable inductance normally decreases somewhat for higher frequencies. With Equation 3.15 in mind, we know that a lowered L causes increased resonance-frequency. Due to both the time constrain of this thesis, and the available data, frequency-dependent inductances are not included.

4.2.3 Cable Impedance

A cable model with only one π -equivalent would only include one resonance frequency, much alike the parallel resonance in the network impedance characteristic in Figure 3.12. Including an infinite number of π -equivalents is the same as modeling the cable with distributed parameters. Then, all resonance frequencies are included. Distributed parameters are therefore very important when high frequency phenomena are studied. By also including frequency-dependency as discussed in Section 4.2.2, the damping of the higher resonance frequencies are taken into account. Figure 4.5 shows the impedance, measured at one of the ends of an unloaded 100 km long $U_m = 123kV$, 240 mm^2 subsea power cable (same type as used as step-out cable in the *Long Step-out*). The red plot shows the impedance when utilizing a constant cable resistance, for an operational temperature of $70^\circ C$. The blue plot shows the impedance when frequency-dependent resistances are included.

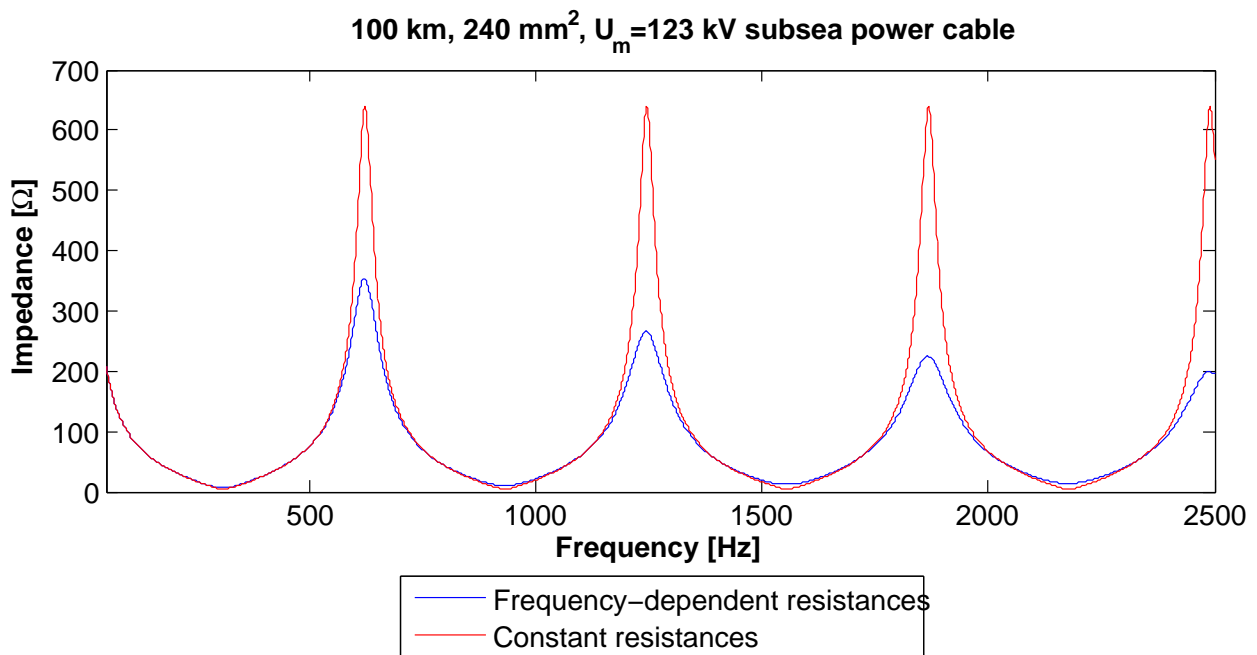


Figure 4.5: Impedance of cable section with a distributed parameters model

4.3 VSD Modeling

Section 3.1 discussed the mechanisms behind the harmonic current generation by rectifiers. An accurate model of the subsea VSDs are crucial to get a trustworthy system for harmonic studies. Since this thesis only focuses on the harmonic behavior at the supply-side of the VSD, some major simplifications may be done to the VSD modeling.

The main components of a VSD is its rectifier, a DC-link (with smoothing capacitor) and an inverter. Instead of modeling the entire VSD, only the rectifier and the DC-link will be modeled. The load (compressor or pump) will be modeled as a DC-load connected to the VSD's DC-link. modeling if the load is discussed in Section 4.4. There are several advantages to this approach. Modeling an inverter can be very complex. A complete control- and drive circuit system has to be modeled to assure correct semiconductor switching operation. Increasing a network model's complexity also increases the number of possible sources of error. As discussed in Section 3.1, only the harmonics caused by the rectifier has relevance to the analysis' in this thesis. Despite the simplifications described above, this VSD modeling should be fairly accurate.

4.3.1 Rectifier Model

The built-in 6-pulse bridge module in PowerFactory can be modeled either as a three-phase diode rectifier or a three-phase line-commutated rectifier/inverter (thyristor-controlled). Based on the background study conducted in the specialization project [1], only the diode rectifier will be used, and thus discussed here.

In steady-state calculations, PowerFactory uses a fundamental frequency model heavily based on Equation 3.3 and 4.16, where the latter describe the DC-side's active power flow [18].

$$P_d = U_d \cdot I_d \quad (4.16)$$

The equations used in these calculations, are the same for both the diode rectifier and the thyristor rectifier (fire angle set to zero for the diode rectifier), and are based on modeling the rectifier as a load where the active and reactive power are constant. To include the DC-voltage drop caused by commutation, a voltage ΔU_d is subtracted from the DC-voltage, where

$$\Delta U_d = -\frac{3}{\pi} X_{cr} \cdot I_d \quad (4.17)$$

where X_{cr} is the commutation reactance. This results in a DC-voltage of

$$U_{dc} = 1.35 \cdot V_{LL} - \Delta U_d \quad (4.18)$$

Ohmic losses are included in the same manner.

In harmonic studies, the rectifier is always modeled as a current source load. The fundamental AC current is determined by the power drawn by the load connected to the rectifier's DC-bus, from on a preceding load flow calculation. When modeled as an *ideal rectifier*, the injected harmonic current spectrum is defined according to the theoretical current spectrum of a 6-pulse rectifier, as described in Section 3.1.1. The DC-current is therefore constant.

The VSDs modeled in the *Long Step-out* and *Short Step-out*, will all be modeled as 12-pulse bridge rectifiers. This will be realized by series-connecting two 6-pulse rectifiers, as shown in Figure 3.5. A three-winding transformer model, with a 30 electrical degree

phase-shift between its secondary (wye-connected) and tertiary (delta-connected) winding, will be used to supply the rectifiers.

Two different 6-pulse bridge rectifier models are available in PowerFactory. The first one have the negative DC-terminal automatically grounded while both DC terminals are accessible for the other. Otherwise, the models are identical. By combining these rectifier models, a 12-pulse rectifier is created. Figure 4.6 shows the final PowerFactory implementation which corresponds to Figure 3.5.

Figure 4.7 shows the results of an EMT-simulation test of the VSD model in Figure 4.6. The lower plot shows the voltage at one of the phases, at the supply-side (HV-side) of the transformer, while the upper shows the voltage at the DC-bus. No filtering (smoothing capacitor) is utilized at the DC-bus in the EMT-simulation test. This, to emphasize the twelve pulses. Here, the 12-pulses at the DC-bus are clearly visible. The harmonics caused by the rectifier are also visible at the AC-voltage.

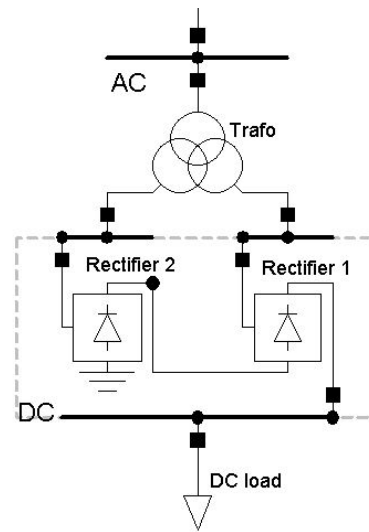


Figure 4.6: Single-line representation of a 12-pulse rectifier implemented in PowerFactory

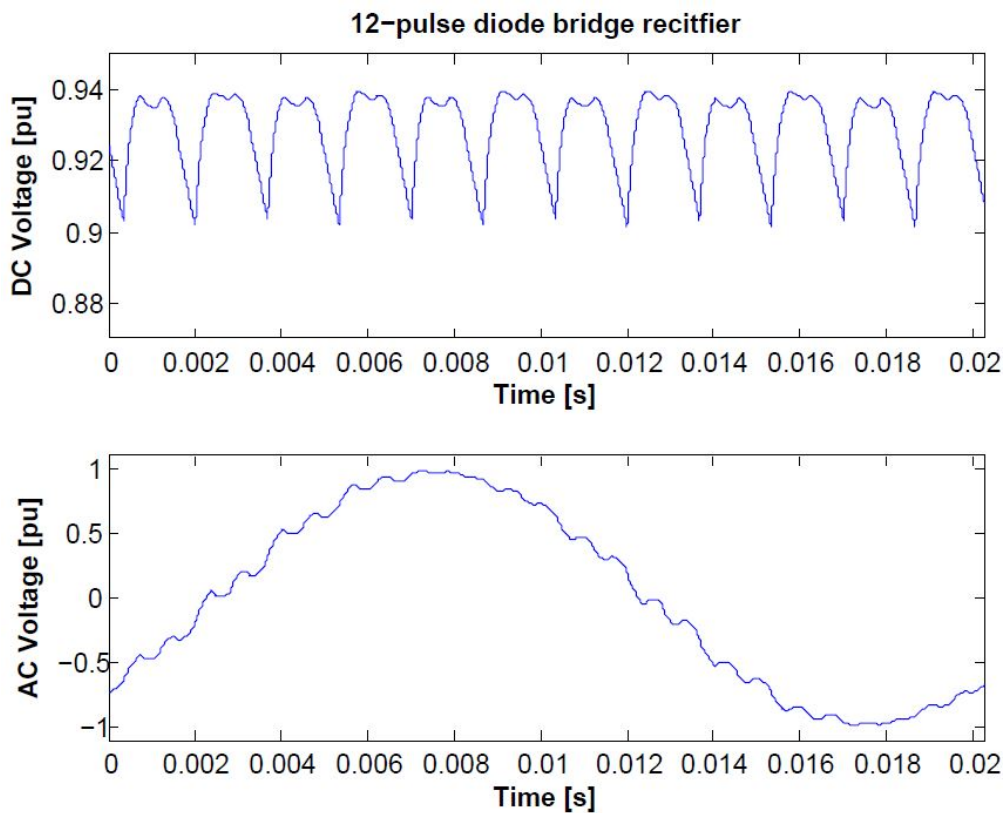


Figure 4.7: DC- and AC voltages of PowerFactory 12-pulse rectifier model

For certain scenarios, it is interesting to get an indication on the system performance if 24-pulse rectifiers were utilized, instead of 12-pulse rectifiers. The implementation of the 12-pulse rectifier, as shown in Figure 4.6, offers flexibility to decide the injected harmonic current spectrum. As described above, each 6-pulse rectifier injects a 6-pulse current spectrum. By changing this to a 12-pulse spectrum, and reducing the phase-shift between the secondary and tertiary windings of the VSD transformer from 30 to 15 degrees, a theoretical 24-pulse current spectrum (with constant DC current) is injected into the cable system.

However, in reality, a 24-pulse rectifier is *not* constructed in this way, but normally by utilizing a 5-winding transformer where phase-displaced 6-pulse rectifiers are connected to four of these windings. Modeling the 24-pulse rectifier as described above, therefore assumes that the network impedance *do not change* when shifting from a 12-pulse to a 24-pulse rectifier. This is an unsafe and uncertain assumption, and the 24-pulse model will therefore *only* be used as a rough indication on how the system may perform, when utilizing 24-pulse rectifiers. In the same manner, the rectifiers can be modified to inject 36-pulse current spectra. This involves the same assumptions and uncertainty as the 24-pulse modification, and will *only* be used in special cases to get a rough indication of the system's performance.

4.4 Load Modeling

As mentioned in the previous section, the PWM-inverter, electrical motor and its mechanical load, are simplified to be represented by a DC-load connected to the VSD's DC-bus. The load will be modeled as a current source load. Alternatively, the load could be modeled as an impedance, but the current source is closer to the electrical motor load's true behavior.

The DC load model is always single-phase and is shown in Figure 4.8. In steady-state simulations, the load is characterized by its active power flow, P. Due to the modeling of the rectifier described above, the only objective of the DC-load is to determine the fundamental current, which in turn determines the amplitudes of the harmonic currents injected by the rectifier.

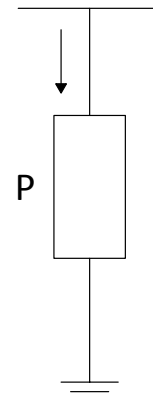


Figure 4.8: Single-phase DC current source load model

4.5 Topside Grid Modeling

To represent the topside power plant, a built-in grid element is used. The grid element is modeled as a voltage source with an internal impedance. In load flow analysis, the grid element is set to be a SL Bus (slack bus). Using this setting, the element controls the voltage, angle and frequency of the busbar it is connected to.

Figure 4.9 shows the positive-sequence model of the grid element used in harmonic calculations. The impedance is defined as

$$Z1 = R1 + jX1 \quad (4.19)$$

where $R1$ and $X1$ are calculated from the short-circuit properties of the grid module. Many of the topside loads and components would be electrical motors and transformers. Due to their inductive nature, the R/X ratio is set to 0.1. The maximum short-circuit power is set to 570 MVA for the grid module, which corresponds to a short-circuit current of ~ 30 kA for the 11 kV system.

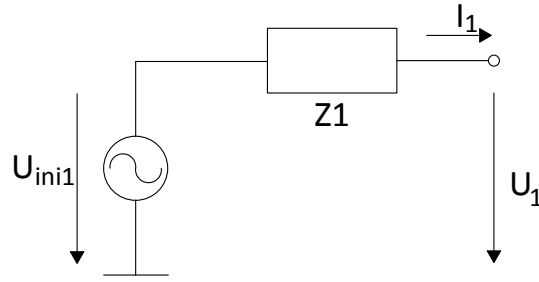


Figure 4.9: Positive-sequence model of grid element

For harmonic and frequency sweep calculations, harmonic voltages and frequency dependencies can be added to the model. Since this thesis' focus is the phenomena in the subsea cable system, no harmonics will be added to the grid element. All harmonics visible at topside will therefore be a result of the subsea harmonic injection, and harmonics caused by the Static Var Compensator.

4.6 Static Var Compensator Modeling

To keep topside voltages and currents under control, reactive power compensation is required. This is mainly due to the reactive power produced by the long step-out cable. The compensation is done by the use of a SVC. This is a system consisting of a combination of a shunt capacitor bank and a shunt reactor. The shunt reactor is thyristor-controlled, and the capacitors can be both permanently/ mechanically connected, or thyristor-controlled. Only the TCR will be utilized here.

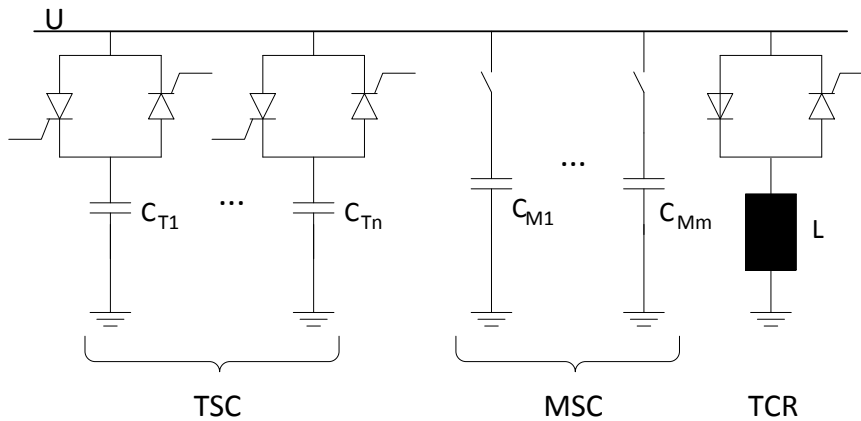


Figure 4.10: General model of Static Var Compensator (SVC) system

The topside SVCs implemented in the network topology models will be balanced and operated at reactive power control. The details concerning the control of the SVCs are discussed in Section 4.7.2 and 4.8.2 for the *Long Step-out* and *Short Step-out*, respectively. The need for reactive compensation is due to an *excess* of reactive power. The harmonic content generated by the SVCs is mainly caused by the TCR, and was discussed in Section 3.1.3.

4.7 Long Step-out Implementation in PowerFactory

Based on Section 2.1 and the simplifications and modeling discussed above, the *Long Step-out* has been implemented in DIgSILENT PowerFactory. Figure 4.11 shows the construction, voltage levels and naming of the most important electrical components.

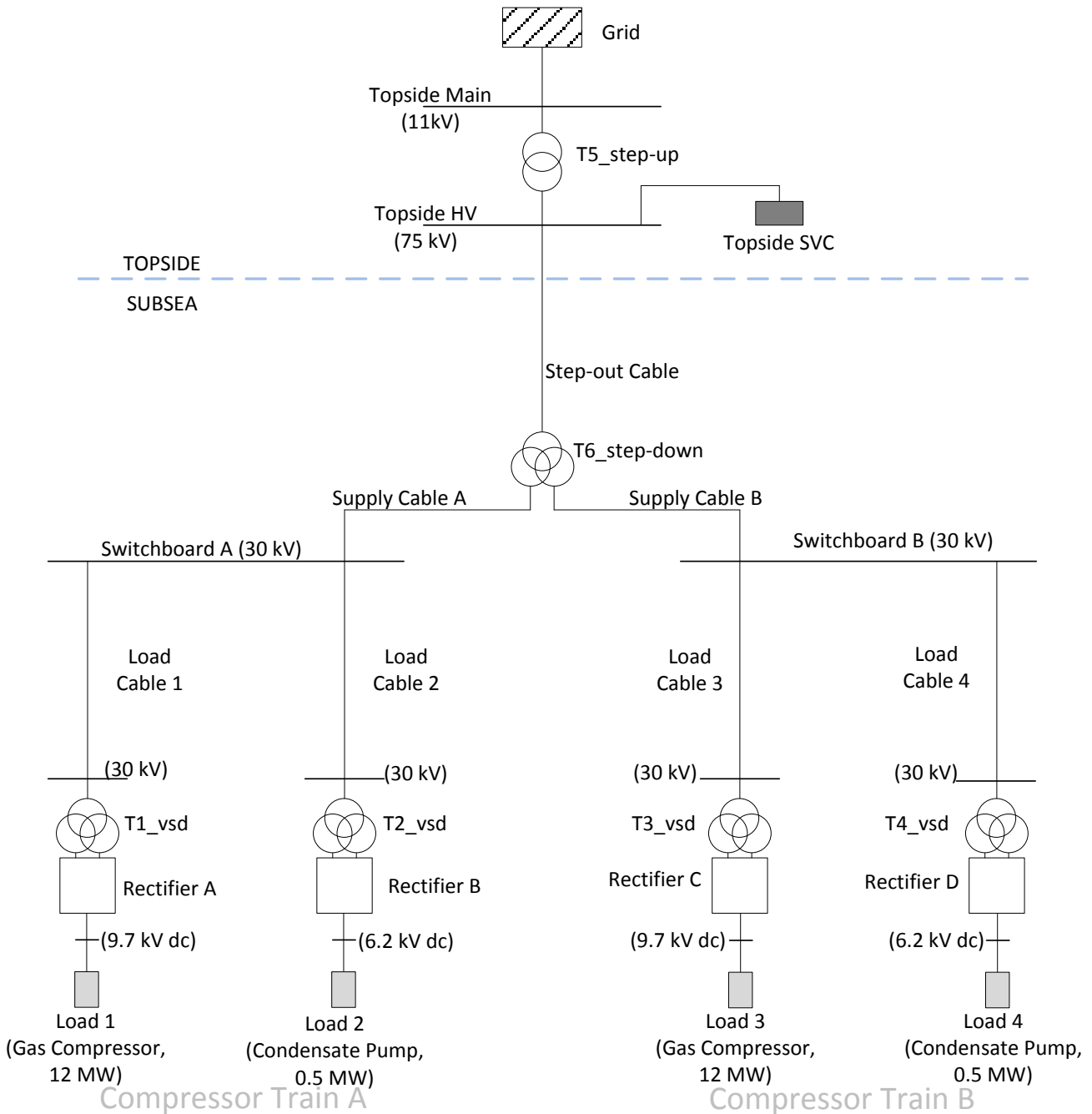


Figure 4.11: PowerFactory implementation and naming of the *Long Step-out*

A 64/110 (123) kV cable has been chosen as step-out cable in this topology. An operational voltage of 75 kV is selected. This applies to all variants simulated. However,

this is a simplification. For a real power system, the cable type and operational voltage would be optimized for every variant. With a large voltage rating, the insulations thickness increases, which in turn increases the distance between the conductor and the screen. This results in lower cable capacitance and less reactive power production. Due to technological limitations, cables and components with $U_m = 36kV$ have been used in the subsea distribution system. In cooperation with Statoil ASA, realistic cable length intervals have been defined for all cable sections. Table 4.1 shows these lengths, which are used as outer limits and basis for all further simulations and calculations. Appendix B presents the network components' electrical parameters and ratings. The rectifiers *Rectifier A* through *D* are implemented as shown in Figure 4.6.

Cable	Length interval [km]
Step-out Cable	50 - 200
Supply Cable A	0.02 - 0.7
Supply Cable B	0.02 - 5.0
Load Cable 1 & 2	0.02 - 0.7
Load Cable 3 & 4	0.02 - 0.7
Load cables supplying the same compressor train always have equal length	

Table 4.1: Long Step-out cable lengths

4.7.1 Voltage Control (Topside Transformer Tap-Changer)

The topside step-up transformer, *T5_step-up*, has a $\pm 10 \cdot 1\%$ tap-changer on its high-voltage side. To keep the subsea voltages as close to rated values as possible, the tap-changer's reference busbar is set to be *Switchboard A* (the subsea switchgear in *Compressor Train A*). This configuration allows the voltage at *Topside HV* to fluctuate somewhat, compared to its rated voltage. The tap-changer can then increase the voltage on *Topside HV* to compensate for the voltage drop across the *Step-out Cable*, and keep the subsea voltages at desired levels.

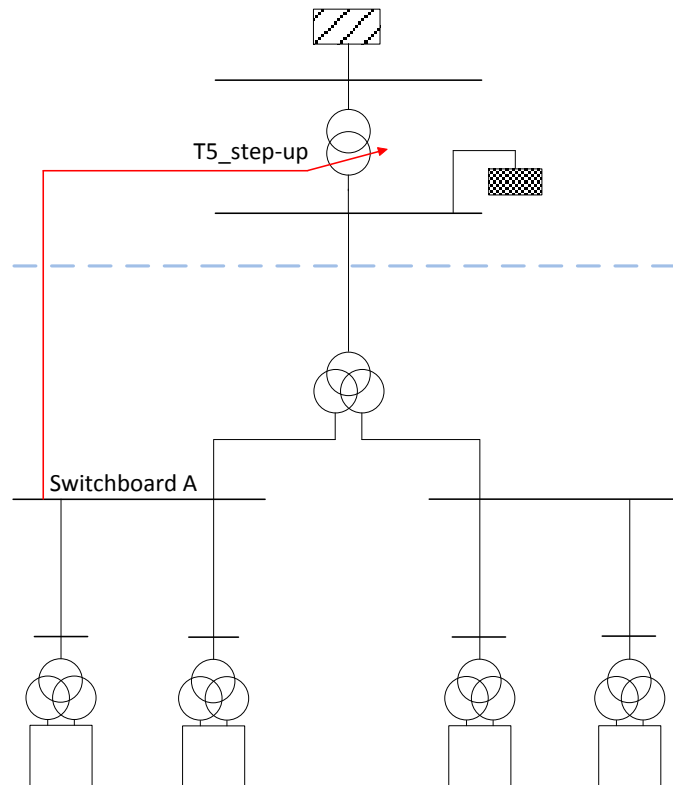


Figure 4.12: Schematic representation of tap-changer control system

4.7.2 Reactive Power Control (Topside SVC)

In a realistic system, the reactive power compensation system would most likely consist of passive reactors covering the reactive power base load, and an active system (normally a static synchronous compensator) to cover the dynamic behavior. This has been simplified to one larger SVC in the *Long Step-out*. A SVC element can be set to control the voltage, reactive power, or the power factor. With the tap-changer control method described, a voltage control setup at the *Topside HV* busbar becomes difficult. Since the voltage is allowed to fluctuate, the SVC will counteract the transformer tap-changing, which in turn can cause overloading of the *T5_step-up* transformer. Instead, the SVC is set to control the reactive power flow injected into the *Topside Main* busbar from the subsea system. If the reactive power flow from *Topside HV* into *Topside Main* exceeds 5 MVAR, the SVC starts consuming reactive power. The very low reactive current flowing through transformer *T5_step-up*, keeps the transformer loading low.

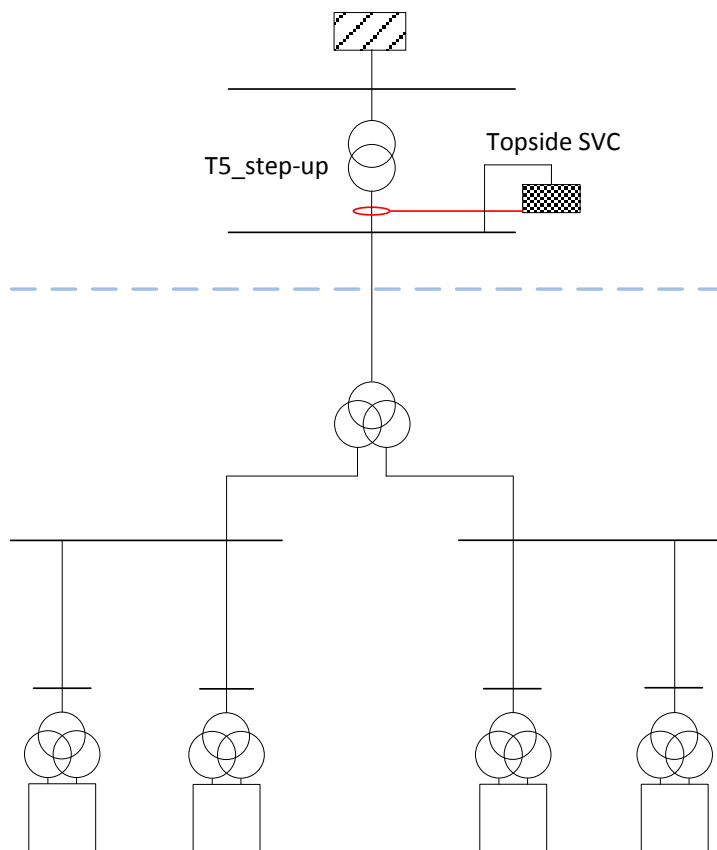


Figure 4.13: Schematic representation of reactive power control system

4.8 Short Step-out Implementation in PowerFactory

Based on Section 2.2 and the component modeling and simplifications discussed previously, the *Short Step-out* has been implemented in DIgSILENT PowerFactory. Figure 4.14 shows the construction, voltage levels and naming of the most important components. With no subsea step-down transformer, all electrical equipment from the *Topside HV* switchboard and downwards, have rating $U_m = 36kV$ and are operated at 30 kV. The rectifiers *Rectifier A* through *D* are implemented as shown in Figure 4.6.

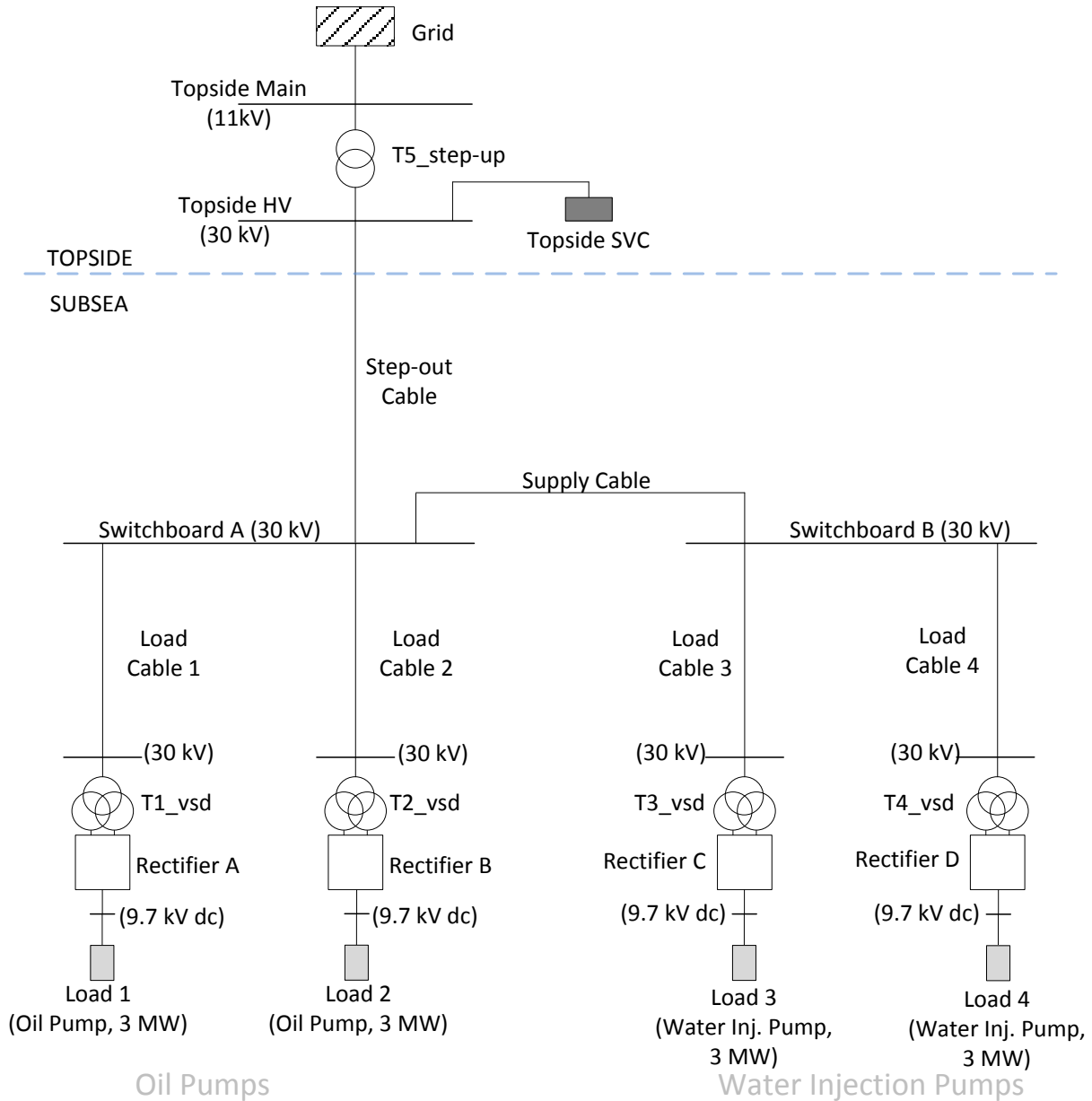


Figure 4.14: PowerFactory implementation and naming of the *Short Step-out*

Table 4.2 describes the relevant cable lengths of the *Short Step-out*. Here, all cable

length can vary independently of each other. Appendix B presents the network component’s electrical parameters.

Cable	Length interval [km]
Step-out Cable	1.0 - 60
Supply Cable	4.0 - 6.0
Load Cable 1	0.02 - 5.0
Load Cable 2	0.02 - 5.0
Load Cable 3	0.02 - 5.0
Load Cable 4	0.02 - 5.0

Table 4.2: *Short Step-out* cable lengths

4.8.1 Voltage Control (Topside Transformer Tap-Changer)

To control the voltage at the subsea switchboards, the *T5_step-up* transformer is equipped with a $\pm 10 \cdot 1\%$ tap-changer at its high-voltage side. Its reference busbar is set to be *Switchboard A*, allowing the voltage at *Topside HV* to fluctuate in the same manner as for the *Long Step-out*.

4.8.2 Reactive Power Control (Topside SVC)

As for the *Long Step-out*, the *Topside SVC* controls the reactive power flow from *Topside HV* into *Topside Main*. Here, the SVC will begin consuming reactive power when the reactive power flow exceeds 1.5 MVar.

4.9 System Design Criteria

All cables in the topologies are dimensioned to have a maximum loading of 90% in load flow calculations. This criteria needs to be fulfilled for all cable lengths simulated (see Table 4.1 and 4.2). In addition, the voltage drop across a cable must be kept below 15%. The latter criteria is most relevant for the step-out cable, due to its long length and high power rating. In addition, a small conductor cross-sectional area is desirable. This, due to both electrical properties and cost. Electrical parameters for all cables are collected from data sheets of relevant manufacturers.

Transformer parameters are based on typical values for traditional topside transformers. To determine an appropriate value for short-circuit impedance, the recognized minimum values of short-circuit impedance in IEC 60076-5 are used [19].

It shall be noted that the components are not dimensioned as thorough as it would be in the designing phase of a real system. Short-circuit properties, no-load conditions (Ferranti-rise effects and possible ferro-resonance) etc. would then have had to be taken into account, when designing the system. A step-out cable of 200 km clearly pushes the limits of what is possible with AC technology. As stated by Song-Manguelle et al. [20], there is an upper length limit for subsea AC power cables. By lowering the voltage and using reactive compensation, the maximum length can be stretched somewhat. For even longer distances, either a low-frequency AC- or a DC - system should be considered. This further rises challenged with switchgear (DC) and larger transformer sizes (low-frequency AC), but this is beyond the scope of this thesis.

5 Simulation Software, Strategy and Methodology

This section will discuss the method and tools utilized when conducting the simulations done in this thesis. In addition, the overall strategy of the simulation process, is discussed.

5.1 Simulation Software - DIgSILENT PowerFactory 15.1

As for the specialization project, fall 2014, the simulation software DIgSILENT PowerFactory 15.1 will be utilized. Several tool packages are available in the software, ranging from traditional load flow and EMT calculations, to technical-economical optimization and reliability tools. The electrical systems are constructed in a single-line diagram interface, where all components and parameters can be accessed and specified. Further, result variables can be defined and extracted. The DIgSILENT Programming Language (DPL) allows the user to create unique tools, using coded scripts, made for a specific simulation setup. Optimization analysis or series simulations may then be executed in an orderly and systematic way. The DIgSILENT Programming Language is further discussed in Section 5.1.4.

Even though they are few, there are some disadvantages with the use of DIgSILENT PowerFactory. Due to its complexity, the user must be quite experienced to get the benefit of the software's true potential. Since PowerFactory offers a variety of tool packages, a very large number of parameters can be included in the models. The user therefore has to know what parameters are important for his specific simulation setup. In addition to its complexity, PowerFactory is not an open-source software. The specific calculation methods utilized by PowerFactory, might not always be clear. In some cases, this could lead to more difficult troubleshooting and identification of possible sources of error.

On the other hand, PowerFactory conducts its calculations very fast, even for large and complex power systems. Along with user definable simulation options, such as step sizes and estimation limits, the simulation tools are relatively user-friendly.

As mentioned earlier, MATLAB will be used when post-processing the results from the PowerFactory calculations. MATLAB offers more flexibility in the post-processing, in addition to more visual flexibility when plotting the results. In the next sections, the PowerFactory tools utilized in this thesis are briefly presented.

5.1.1 Load Flow

The PowerFactory Load Flow calculation tool will in this thesis mainly be utilized in the designing process of the electrical systems. This, to prevent overloading of cables and transformers, and to assure acceptable busbar voltages. PowerFactory utilizes traditional load flow calculation methods where the nodes are defined as PV nodes, PQ nodes, Slack nodes or Device nodes (special node such as SVCs or converters). For the AC Load Flow calculations, the Newton-Raphson method is used to solve the non-linear equations. The user is given the choice between two formulations; current equations or power equations. Only the power equation formulation will be utilized here. The calculation tool has an outer loop control to take transformer tapping and SVC control correctly into account. The loop control checks if the voltages are within the desired limits. If not, the tap-changers are adjusted (if possible) and the load flow calculation is repeated.

5.1.2 Harmonic Load Flow

To calculate harmonic voltages and currents, the Harmonic Load Flow tool is utilized. The user has in advance defined the system's harmonic sources. PowerFactory identifies all harmonic orders present in the system, based on these sources. Load flow calculations are then conducted on each of the harmonic orders. A new system impedance matrix is calculated for each harmonic order (due to the change in network impedance, discussed earlier).

As a result of such calculations, harmonic current- and voltage spectra can be generated. In addition, the total harmonic distortion (THD) of currents or voltages may be calculated. Combined, these results gives the user a good overview of the harmonic conditions in the system.

5.1.3 Frequency Sweep

During Load Flow or Harmonic Load Flow calculations, PowerFactory calculates the system's impedances only for the relevant frequencies. To get a deeper understanding of the network impedances of the system, the Frequency Sweep tool is utilized. The user defines upper and lower frequency limits, in addition to an incremental step size. Automatic step-size adaption is also possible. The system's impedance matrix is then calculated for every frequency in this range. When the system's impedance matrix is calculated, current sources are set to zero Ampere (open-circuited), and voltage sources are set to zero Volt (short-circuited) [21, 22]. The calculations are therefore conducted on a "dead" power system.

As a result of a Frequency Sweep, the network impedance characteristic (as discussed in Section 3.2.2) can be plotted for any busbar in the system. Potential series- and parallel resonances are therefore easily detectable. Throughout this thesis, the Harmonic Load Flow tool will be utilized in combination with the Frequency Sweep tool, to investigate the harmonic condition.

5.1.4 DIgSILENT Programming Language (DPL)

DIgSILENT Programming Language (DPL) is an internal programming language for the DIgSILENT PowerFactory software. The syntax is similar to that of MATLAB or C, and gives the user the possibility to create his own, specially tailored, simulation tools. Almost all parameters and variables can be accessed, changed or extracted using DPL. In this thesis, DPL will be used to construct a series scan simulation setup, for the harmonic and resonance analysis, which can scan through several network variations, and collect specific results for each variation. How the DPL scripts are constructed, are discussed in Section 5.2.3.

5.2 Simulation Strategy

In the simulations to be done, a large number of network topology variations will be simulated, where the topology's cable lengths are slightly changed for each variant. This applies to both the *Long Step-out* and the *Short Step-out*. An orderly and systematic simulation method is therefore very important. By utilizing the DIgSILENT Programming Language (DPL), simulation scripts have been developed for both topologies. The script allows the user to define minimum and maximum length limits, in addition to an incremental step-size, for all cables in the system. A small incremental step-size increases the resolution, and therefore also the accuracy. However, the required computational power, and the total simulation duration, also increases. A trade-off between simulation resolution and simulation duration must therefore be determined, as often is the case for computer simulation tools. For each variant of the system, a Load Flow and a Harmonic Load Flow calculation are conducted. Key results are collected and stored in a result matrix, along with the lengths of each cable. This makes the identification of problematic variants for further analysis easy. Such a series simulation, where all cable lengths are varied, will from this point on be referred to as a *Series Scan*. Section 5.2.3 presents a simplified pseudo-code of the DPL scripts. The complete scripts can be found in Appendix D.

Initially, complete Series Scan simulations will be conducted on both the *Long Step-out* and the *Short Step-out*, to get an overview of the harmonic content in the systems. The simulation resolution, limits and incremental step sized are described in Section 5.2.1 and 5.2.2 for the *Long Step-out* and *Short Step-out*, respectively. Further, the topologies will be investigated in more detail to understand the reason behind potential problems, found during the Series Scan simulations.

Further, two specific variants of each topology will be investigated in detail. First, a worst-case variant will be identified and analyzed to illustrate the problematic potential of harmonic disturbance in a subsea power system. The second case will consider a variant with lower THD levels, and measures to lower the THD levels further, will be discussed.

Harmonics in an electrical power system may lead to several unwanted effects. Distorted voltage and current waveforms, incorrect operation of electrical equipment and excessive heating can be some results of excessive amounts of harmonics. This thesis will only consider distortion of the voltage waveform. The total harmonic distortion (THD) of the busbars' voltages will be used as an indication of the systems harmonic performance. The next two sections will discuss the settings used in the Series Scan simulations of the *Long Step-out* and the *Short Step-out*.

5.2.1 *Long Step-out* Series Scan Settings

The cables' length limits in Table 4.1 are used as the outer limits. Table 5.1 displays the cable length used in the initial Series Scan of the *Long Step-out*. All possible combinations of these lengths will be simulated, resulting in a total of 16 807 variations. Estimated simulation duration is 43 minutes.

***Long Step-out* cable lengths [km], initial Series Scan**

Step-out Cable	Supply Cable A	Supply Cable B	Load Cable 1&2*	Load Cable 3&4*
50	0.020	0.02	0.020	0.020
75	0.133	0.85	0.133	0.133
10	0.246	1.68	0.246	0.246
125	0.359	2.51	0.359	0.359
150	0.472	3.34	0.472	0.472
175	0.585	4.17	0.585	0.585
200	0.698	5.00	0.698	0.698

*Gas compressor and condensate pump belonging to the same compressor train have equal load cable lengths.

Total number of simulations: 16 807

Estimated simulation duration: 43 min

Table 5.1: Cable length variations for *Long Step-out*, initial Series Scan

5.2.2 *Short Step-out* Series Scan Settings

Table 4.2 defines the outer cable length limits of the *Short Step-out*. Table 5.2 shows the cable lengths used in the initial Series Scan of the *Short Step-out*, resulting in a total of 19 440 variations, and an estimated simulation duration of 50 minutes.

***Short Step-out* cable lengths [km], Initial Simulation**

Step-out Cable	Supply Cable	Load Cable 1	Load Cable 2	Load Cable 3	Load Cable 4
1.0	4.0	0.020	0.02	0.02	0.02
15.5	5.0	1.015	1.015	1.015	1.015
30.0	6.0	2.010	2.010	2.010	2.010
44.5		3.005	3.005	3.005	3.005
59.0		4.000	4.000	4.000	4.000
		4.995	4.995	4.995	4.995

Total number of simulations: 19 440

Estimated simulation duration: 50 min

Table 5.2: Cable length variations for *Short Step-out*, initial Series Scan

5.2.3 PowerFactory DPL Script (Pseudo-Code)

The scripts used for both the *Long Step-out* and the *Short Step-out* have the same basic construction, according to the pseudo-code presented below. As an example, only three cables are changing lengths in the pseudo-code.

```
Variable initialization
Identifying and assigning all objects (electrical components) needed
Initializing result matrix

while(length of Cable 1 <= Max length Cable 1) {
  while(length of Cable 2 <= Max length Cable 2) {
    while(length of Cable 3 <= Max length Cable 3) {

      Executing Load Flow Simulation
      Executing Harmonic Load Flow Simulation
      Writing results to result matrix

      Increase length of Cable 3
    }
    Increase length of Cable 2
  }
  Increase length of Cable 1
}
```

The full version of the DPL scripts used for Series Scan simulations, can be found in Appendix D.

6 Long Step-out Harmonics and Resonance Analysis

This section will present the results and findings of the harmonic analysis of the *Long Step-out* topology. The system's harmonic behavior will be studied to find possible tendencies, trends, patterns or relations among the observed harmonic and resonance phenomena. With a solid understanding of the harmonic behavior, potential harmonic mitigation becomes easier. Section 6.3 analyzes a worst-case variant of the *Long Step-out*, with respect to the busbars' THD levels. Section 6.4 investigates a variant of the *Long Step-out* with lower THD level, and discusses harmonic measures that could be applied to further lower the THD.

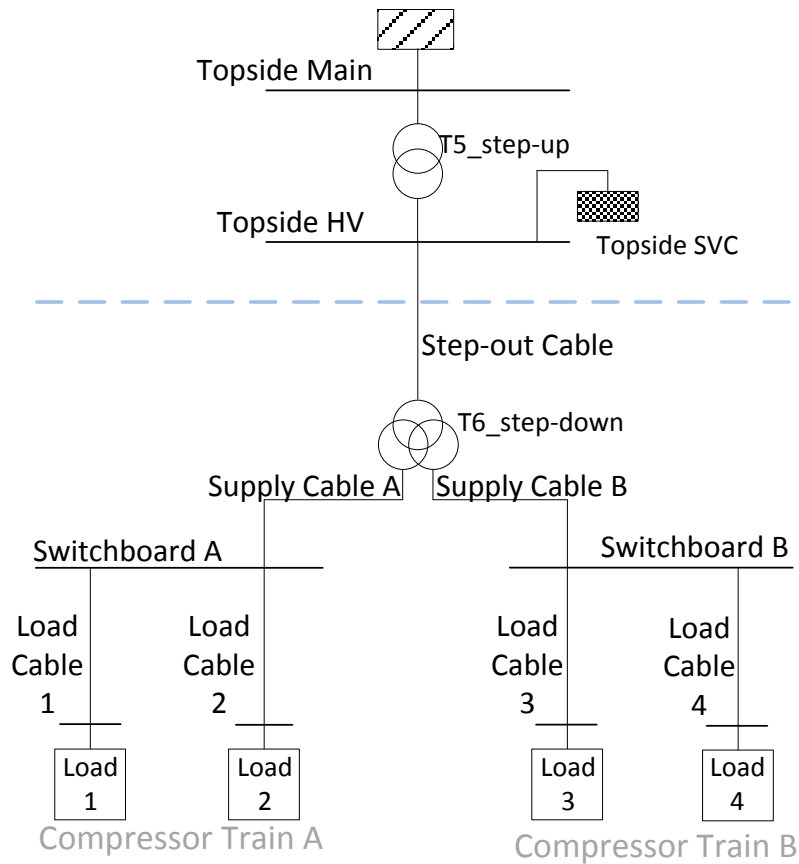


Figure 6.1: Main busbars and cables of *Long Step-out*

Figure 6.1 shows a sketch of the *Long Step-out*, with naming and location of the most important electrical components. These components will be referred to frequently in the following text. Whenever a *Long Step-out* electrical component (cable, transformer, busbar etc.) is referred to in the text, it will be written in *italic*. In the following text *Topside Main* and *Topside HV* will in some cases be referred to as the *topside busbars*. Likewise, *Switchboard A* and *Switchboard B* will in some cases be referred to as the *subsea busbars*. Due to the construction of the *Long Step-out* (described in Section 2.1) the length of *Load Cable 1* and *Load Cable 2* will *always* be the equal, when discussing the *Long Step-out* (likewise for *Load Cable 3* and *Load Cable 4*). In many cases, the load

cables in the *Long Step-out* will therefore be written as *Load Cable 1&2* and *Load Cable 3&4*. Table 6.1 is the same as Table 4.1, and defines the allowable length ranges of the various cables in the *Long Step-out*.

Cable	Length interval [km]
Step-out Cable	50 - 200
Supply Cable A	0.02 - 0.7
Supply Cable B	0.02 - 5.0
Load Cable 1&2	0.02 - 0.7
Load Cable 3&4	0.02 - 0.7

Load cables supplying the same compressor train always have equal length

Table 6.1: *Long Step-out* cable lengths

Figure 6.2 shows plots of the initial short-circuit currents at *Switchboard A* and *Switchboard B*, normalized to the busbars' respective load current, as the *Step-out Cable* length increases. All remaining cables are kept constant at their longest length, according to Table 6.1. As expected, the short-circuit current declines as the length of *Step-out Cable* increased. The load currents at *Switchboard A* and *Switchboard B* are identical and equal to 275 A. The short-circuit current is slightly lower for *Switchboard B* due to the longer *Supply Cable B* (5 km).

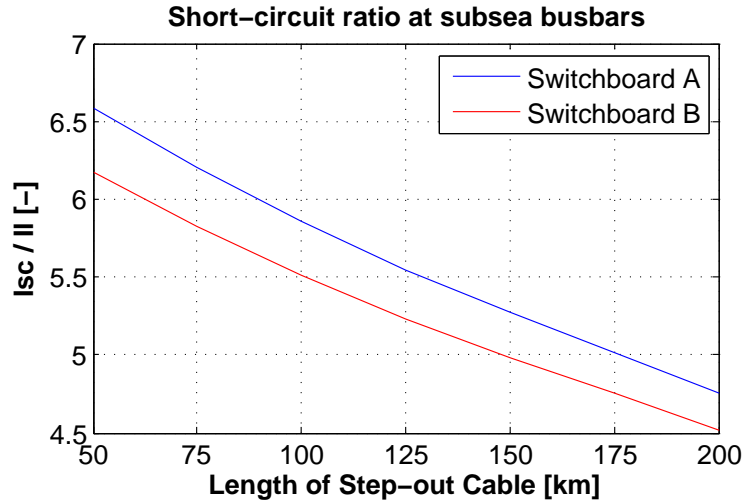


Figure 6.2: Short-circuit current ratio at subsea busbars

6.1 Long Step-out Series Scan

Series Scan simulations have been conducted on the *Long Step-out* with cable length limits and incremental step sizes as defined by Table 5.1. As can be seen from the pseudo-code (Section 5.2.3) of the script, the cable lengths are increased in a specific order. In the following results, the order of varying cable length are changed to best present the results in a way that reveals possible patterns or the significance of the various cables.

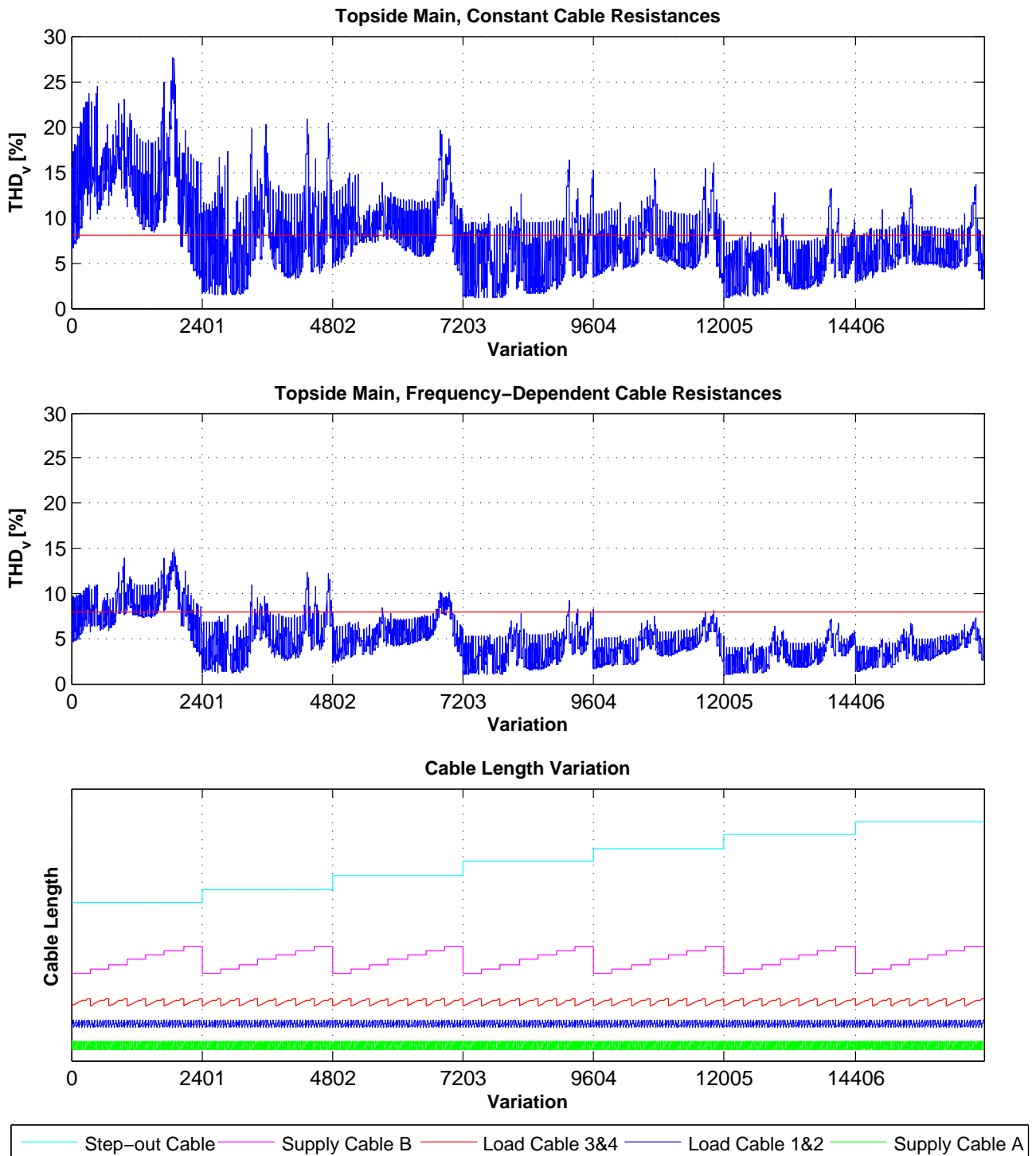


Figure 6.3: Long Step-out Series Scan; Topside Main THD levels

Figure 6.3 shows the THD levels at *Topside Main*, calculated from a Series Scan simulation. The horizontal red lines represents the IEC 61000-2-4 Class 2 THD limit of 8 %. The upper plot shows the results of a network model using constant cable resistances. The middle plot shows the results of a network model using frequency-dependent cable resistances (discussed in Section 4.2.2). The cable variation order used, is presented in the lower plot. Figure 6.3 illustrates the importance of an accurate and complete simulation model. Constant parameters would be a conservative assumption, however, the results becomes too deviant to draw trustworthy conclusions. For this reason, only frequency-dependent cable resistances will be used in all network models analyzed further in this thesis.

From the THD plot (*with* frequency-dependent resistances) in Figure 6.3, some possible patterns emerges through the variation range. A short length of *Step-out Cable* should be avoided to keep the *Topside Main* THD levels at a minimum. With length of 50 km (variation 0 through 2 401), the danger of exceeding the 8 % limit is substantial. For *Step-out Cable* lengths of 125 km and up (from variation 7 203 and up) the THD at *Topside Main* rarely tips above the limit. A long *Step-out Cable* reduced the THD levels but also reduces the influence of the other cables. In addition to a long *Step-out Cable*, the length of *Supply Cable B* should preferable be kept short to maintain the lowest possible THD levels. However, when investigating the results of Figure 6.3, the simulation resolution has to be kept in mind. Some of the cables are increased rather much in length for each step. Possible resonances can quickly be lost, due to the rough resolution.

Figure 6.4 shows the THD levels at *Topside HV* and *Switchboard B*, along with the cable length variation order (same as in Figure 6.3). The THD pattern of *Topside HV* behaves quite similar to that of *Topside Main*; longer *Step-out Cable* leads to lower THD, and the length of *Supply Cable B* should be kept short. A 50 km *Step-out Cable* should definitely be avoided. The THD levels are higher at *Topside HV* than at *Topside Main* for all variations. This is caused by the filtering effect of the topside transformer, as discussed in Section 3.4.

When moving down to *Switchboard B*, the THD pattern changes. Relatively small changes are made to the THD plot as the length of *Step-out Cable* increases. The length of *Supply Cable B* on the other hand, seems to have the most influence on *Switchboard B*'s THD level. Clearly, the length of *Supply Cable B* should be kept as short as possible to minimize the harmonic content. In addition, two length ranges of the *Supply Cable B* sticks out as hazardous, with respect to harmonics. Cable lengths of 0.85-2.5 km and > 4 km should be avoided. This pattern can also be seen in the THD plot of *Topside HV*. In addition, the THD level never tips below the 8% limit, implying that harmonic reduction measures are required to assure acceptable THD levels (according to the IEC standard). In fact, the minimum calculated *Switchboard B* THD in the Series Scan, is 17.1 %. This is suspiciously high to be the lowest THD level for the entire variation range.

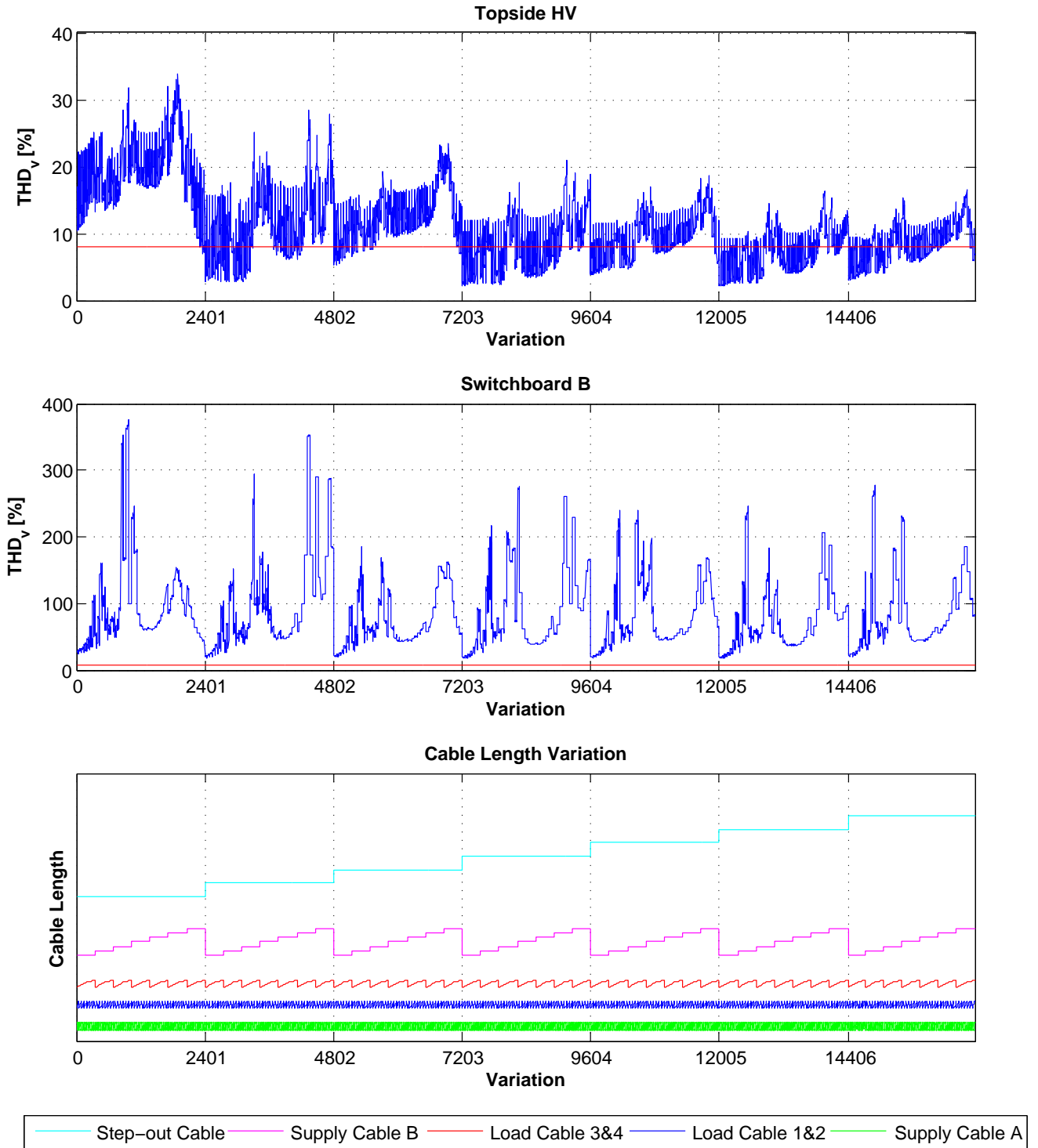


Figure 6.4: Long Step-out Series Scan; Topside HV and Switchboard B THD levels

To best present the THD plots at *Switchboard A*, the order of changing cable lengths must be changed. Figure 6.5 presents the THD levels, IEC limit and the corresponding order of changing cable length. For *Switchboard A*, the lengths of *Load Cable 1&2* should be kept as short as possible. In combination with a short *Supply Cable A*, this gives the lowest THD levels. However, if the lengths of *Load Cable 1&2* are long, a short *Supply Cable A* might not be the best anymore. The length of *Step-out Cable* should be kept long, as also was the case for the other busbars. As for *Switchboard B*, the THD at *Switchboard A* never tips below the 8% limit. The minimum THD is 17.24%. Also this, suspiciously high.

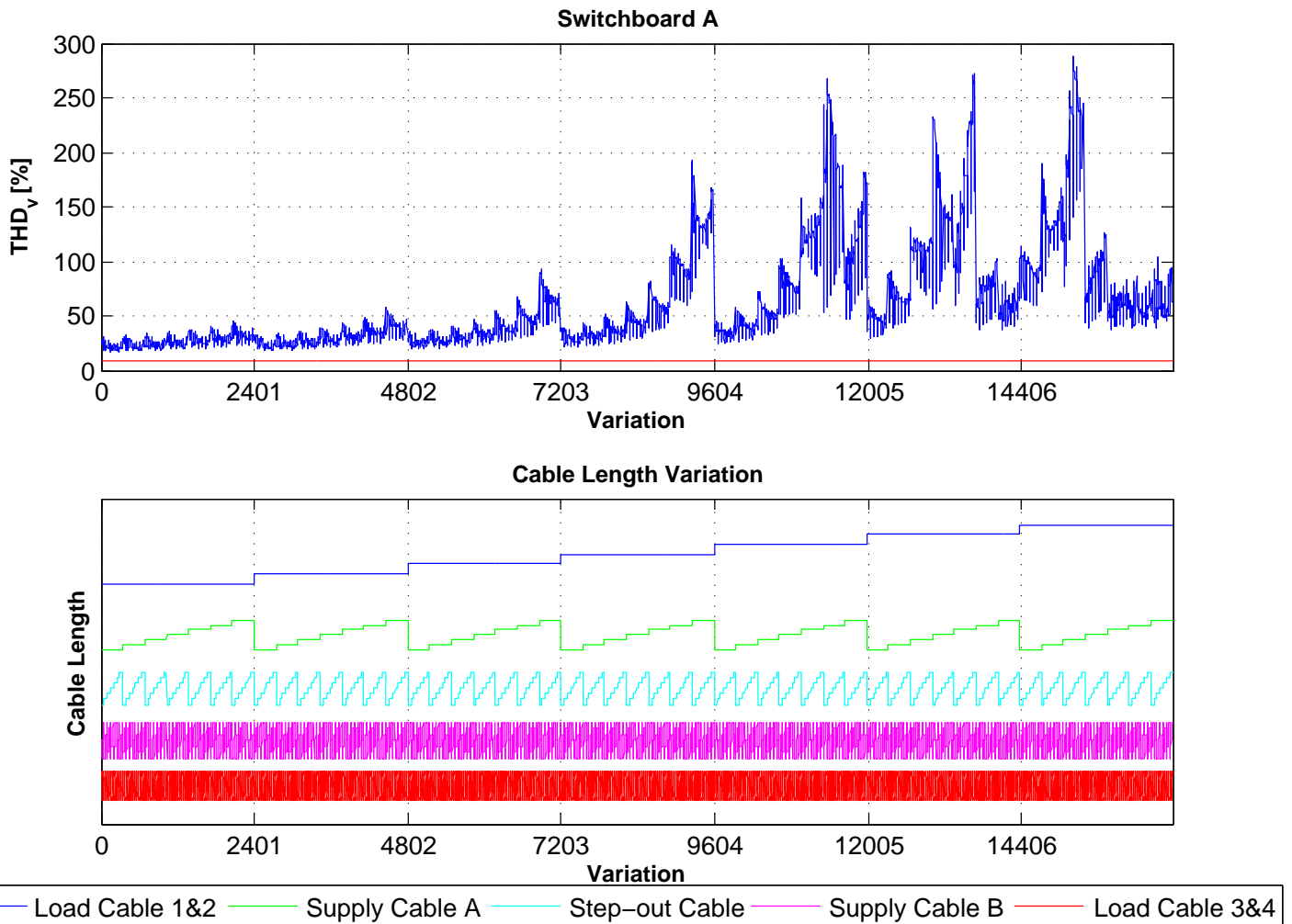


Figure 6.5: Long Step-out Series Scan; *Switchboard A* THD levels

The plots in Figure 6.3, 6.4 and 6.5 also gives information of the importance of each cable on the busbars' THD levels. For the THD plot of *Switchboard B* in Figure 6.4, this was particularly evident. If *Load Cable 1&2* and *Supply Cable A* had any significant influence on the *Switchboard B*'s THD level, "high-frequency noise" should be visible in the THD plot. However, this is not the case. The rather clean THD plot implies that *Load Cable 1&2* and *Supply Cable A* have very limited influence on the busbar's THD level, especially for long lengths of *Supply Cable B*. Likewise, the length of *Supply Cable B* and *Load Cable 3&4* have relatively low influence on the THD levels at *Switchboard A*.

The main reason for difference in the cables' harmonic influence on the busbars' THD levels, lies in the subsea *T6_step-down* transformer. To increase the decoupling between *Compressor Train A* and *Compressor Train B*, the three-winding transformer is designed to have a high short-circuit impedance between its secondary and tertiary winding (20 %). This protects each of the compressor trains against voltage drops or faults located at the other train. From Figure 6.4 we can see that the lengths of *Load Cable 1&2* and *Supply Cable A* affects the topside busbars' THD levels more, than the THD level at *Switchboard B*. Its important to be aware that this decoupling affects how harmonics spread throughout the electrical system.

6.2 Long Step-out Harmonic and Resonance Behavior

This section will investigate the harmonic behavior found in the previous section, in more detail. Figure 6.6 shows contour plots of the THD levels at *Topside Main* and *Switchboard A*, as the lengths of *Step-out Cable* and *Supply Cable A* are varied. All remaining cables are kept constant at their minimum length, according to Table 6.1.

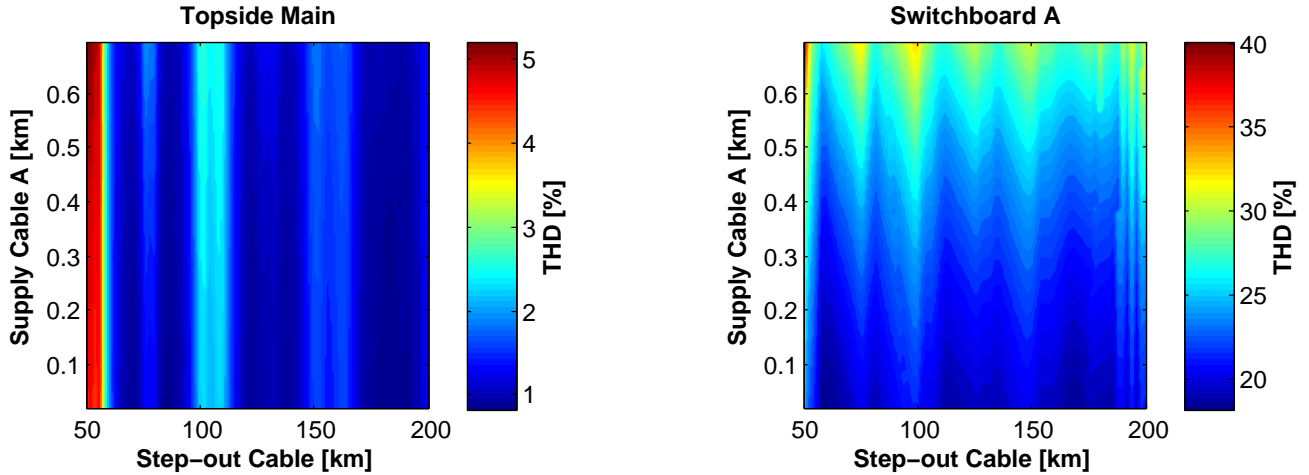


Figure 6.6: Long Step-out contour plots of *Topside Main* and *Switchboard A* THD levels

The THD contour plot of *Topside Main* in Figure 6.6 is dominated by vertical lines in the color scaling. This suggests that the length of *Step-out Cable* is far more important in determining the *Topside Main* THD level, than the length of *Supply Cable A* (which also was found in the previous section). Regardless of the lengths of *Step-out Cable* and *Supply Cable A*, the *Topside Main* THD is always below the 8% IEC limit, implying that as long as the lengths of *Load Cable 1&2*, *Load Cable 3&4* and *Supply Cable B* are kept short, the *Topside Main* THD will stay below the IEC limit.

At *Switchboard A*, the situation is somewhat different. Even though there are vertical lines of higher and lower THD levels, it seems like the length of *Supply Cable A* is the most influential on the busbar's THD level. The length of *Supply Cable A* should be kept as short as possible to obtain the lowest possible *Switchboard A* THD levels.

It shall be noted that the length range of the *Step-out Cable* is very large, compared to the length range of *Supply Cable A*, in these plots. In a system designing process, the designer might have the possibility to vary cable lengths within some hundred meters, to avoid resonance problems. The entire cable length ranges of Figure 6.6 are therefore not a completely realistic options for a specific system.

Figure 6.7 shows the THD levels the *Switchboard A* and *Switchboard B* as the lengths of *Step-out Cable* and *Supply Cable B* are varied. All other cables are kept constant at their minimum length. With respect to voltage levels, cable types and load configuration, *Compressor Train A* and *Compressor Train B* are identical. The only difference is the fact that *Supply Cable B* may have a length of up to 5 km, while *Supply Cable A* can only reach a length of 0.7 km. For this reason, the THD plots of *Switchboard A* in Figure 6.7 are identical to those in Figure 6.6, for *Supply Cable B* lengths up to 0.7 km.

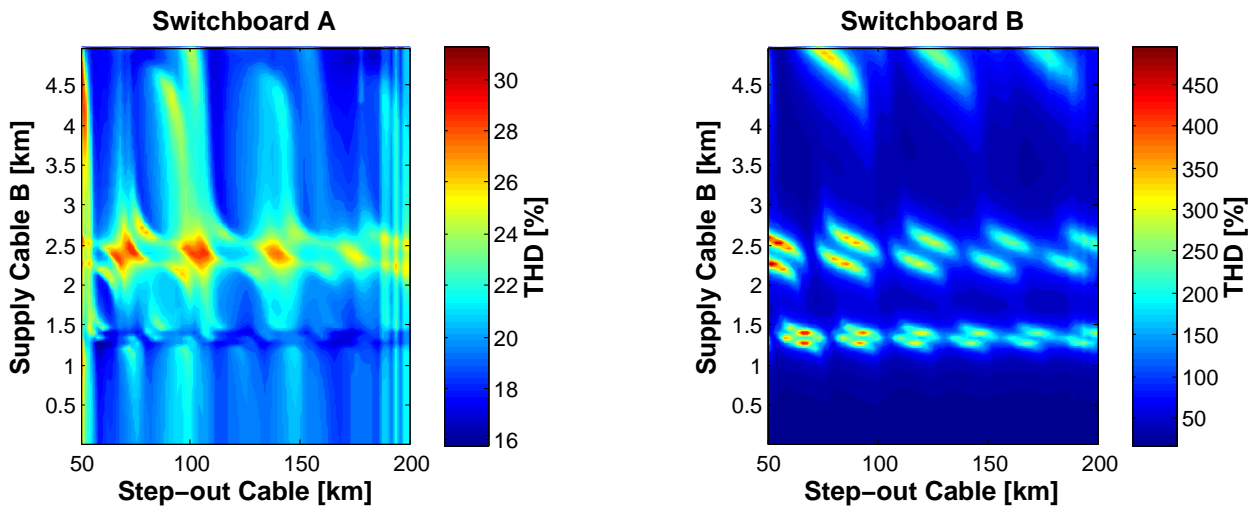


Figure 6.7: Long Step-out contour plots of *Switchboard A*, *Switchboard B* and *Topside Main* THD levels

For increasing lengths of *Supply Cable B*, its influence on the system's THD levels also increases. Especially in the THD plot of *Switchboard B*, three lengths of *Supply Cable B* are particularly hazardous; ~ 1.4 km, ~ 2.5 km and > 4.4 km. To understand what causes these increased THD levels, we must investigate the development of *Switchboard B*'s network impedance characteristic, as the length of *Supply Cable B* increases.

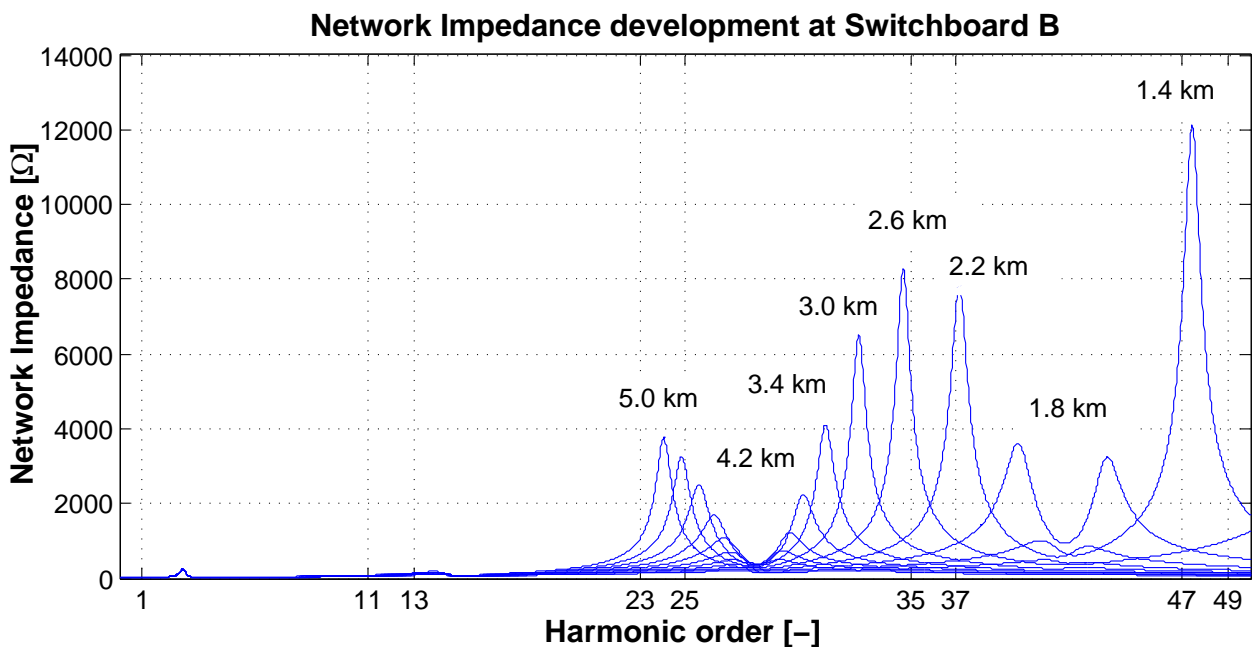


Figure 6.8: Development of *Switchboard B* network impedance characteristic

Figure 6.8 displays several plots of the network impedance characteristic at *Switchboard B* for different lengths of *Supply Cable B*. The lengths of *Supply Cable B* are shown above

the parallel resonance tops present for the respective lengths. The *Step-out Cable* is kept constant at 90 km, while all other cables are kept at their minimum lengths. In other words, Figure 6.8 shows the same topology variations as the plots in Figure 6.7 for a *Step-out Cable* length of 90 km.

With a *Supply Cable B* length of ~ 1.2 km, a large parallel resonance top is located close to harmonic order 49. The parallel resonance top is caused by a resonance between the capacitances of cables *Load Cable 3&4* and *Supply Cable B*, and the inductance of the *T6-step-down* transformer. Further, this causes amplification of the 49th harmonic current (as described in Section 3.3), which in turn causes a high 49th harmonic voltage, and high THD levels. As the length of *Supply Cable B* increases to ~ 1.4 km, the resonance top is shifted down to harmonic order 47. Now, the 47th harmonic current is amplified in *Load Cable 3&4* and *Supply Cable B*, causing increased THD levels. This explains the high THD levels for *Supply Cable B* lengths of 1.2 - 1.4 km in Figure 6.7.

As the length of *Supply Cable B* further increases, the parallel resonance top is shifted towards lower frequencies. With the harmonic current spectrum of a 12-pulse rectifier in mind (Figure 3.8), we know there is no current harmonics present for harmonic orders between 47 and 37. The THD levels therefore temporarily decreases. But as the length of *Supply Cable B* approaches 2.2 km, the parallel resonance top (the resonance frequency) is close to the 37th harmonic. Current amplification of the 37th harmonic occur, leading to increased THD levels. Further length increase of *Supply Cable B* shifts the resonance top down to harmonic order 35, once more causing current amplification and increased THD levels. This explains the high harmonic content when the length of *Supply Cable B* is between 2.2 - 2.7 km. Likewise, the high THD levels as *Supply Cable B* has a length above 4.5 km can be explained by the resonance top's location at harmonic order 25 and 23.

Although the THD plot of *Switchboard A* in Figure 6.7 has some of the same characteristics as the THD plot of *Switchboard B*, a low-level THD field at *Switchboard A* sticks out for a *Supply Cable B* length of ~ 1.4 km. Due to massive current amplification of the 47th and 49th harmonic in *Load Cable 3&4* and *Supply Cable B*, large harmonic currents at these frequencies are injected into the *T6-step-down* transformer. Due to the high frequency of the 47th and 49th harmonics (2350 and 2450 Hz) the inductances' reactances are of very large magnitudes. Most of the harmonic currents are fed into the *Step-out Cable*, but a relatively large part is also injected into *Supply Cable A*. This current injection *into* the *Compressor Train A* branch, suppresses all possible current amplifications of the 47th and 49th harmonic currents in *Load Cable 1&2* and *Supply Cable A*, which in turn lowers the THD levels.

Especially in the THD plots of *Topside Main* in Figure 6.6 and of *Switchboard A* in Figure 6.7, vertical lines in the color scaling are visible at certain lengths of the *Step-out Cable*. Lengths of ~ 55 km, 100 km, 110 km, 150 km and ~ 162 km, results in increased THD levels, regardless of the lengths of both *Supply Cable A* and *Supply Cable B*. These lines are caused by resonance between the *Step-out Cable* and the *T5-step-up* transformer. However, the increase in *Topside Main* THD caused by these resonances, are not of critical magnitudes compared to the resonances occurring in *Load Cable 1&2*, *Load Cable 3&4*, *Supply Cable A* and *Supply Cable B*.

Figure 6.9 shows the THD levels at *Switchboard A* and *Switchboard B* as the lengths of *Supply Cable A* and *Load Cable 1&2* are varied. The lengths of all other cables are kept constant to their respective maximum lengths, according to Table 6.1. When noticing the difference in the color scaling of the two plots, it is clear that the lengths of *Supply Cable A* and *Load Cable 1&2* have nearly no influence on the *Switchboard B* THD level. With a short-circuit impedance of 20% between the secondary and tertiary winding of the *T6_step-down* transformer, *Switchboard A* and *Switchboard B* are highly decoupled. Thus, the resonance and current amplification occurring at *Switchboard A* do not influence the conditions at *Switchboard B*, significantly.

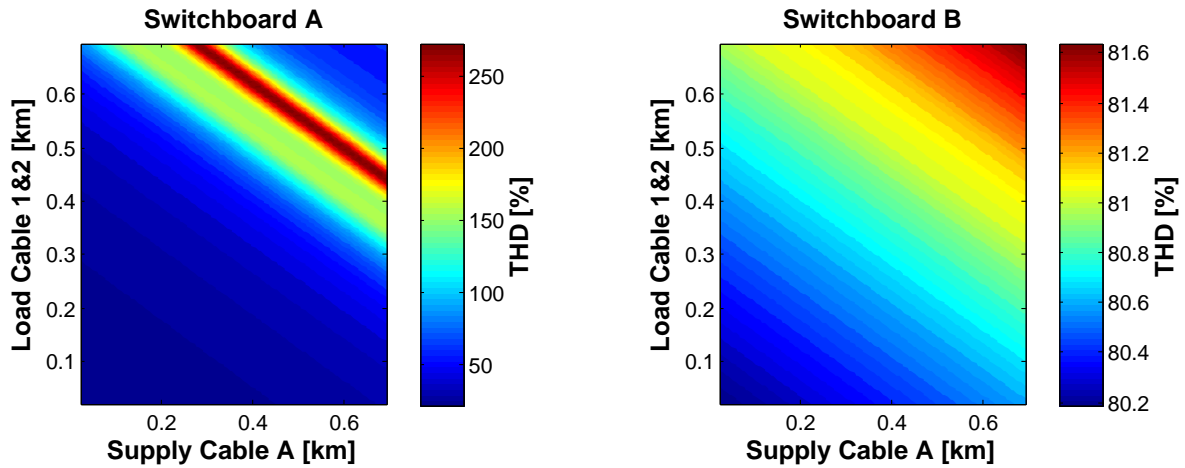


Figure 6.9: Long Step-out contour plots of *Switchboard A* and *Switchboard B* THD levels

It is clear that the lengths of *Supply Cable A* and *Load Cable 1&2* have extreme influence on the THD level at *Switchboard A*. Due to a parallel resonance close to harmonic order 47, powerful current amplification occurs in *Load Cable 1*. In addition, some current amplification occurs in *Load Cable 2*. However, for some specific length combinations of *Load Cable 1&2* and *Supply Cable A* (the more or less diagonal red high-level THD line in the THD plot of *Switchboard A*), the harmonic current injected by *Load Cable 1* is further excited by the capacitance of *Load Cable 2*. In Section 3.3, this was referred to as *double amplification*. The magnitude of the 47th harmonic current becomes extremely large, causing extreme THD levels at *Switchboard A*.

From the very large THD levels at *Switchboard A* in Figure 6.9, one could believe that the topside busbars' THD levels would be large as well. However, due to the effective damping of higher frequencies by the natural LCL low-pass filter (discussed in Section 3.4), the *Topside Main* THD levels remain below the 8% IEC limit. It is therefore clear that the THD levels observed at topside, are *not* representative for the subsea THD levels.

6.3 Case Study 1: *Long Step-out* Worst-Case THD Scenario

This section will analyze a worst-case variant of the *Long Step-out*, when it comes to THD levels. The case study is analyzed to illustrate the influence and severity harmonic disturbance may have on a power system. By utilizing the same DPL script as was used in Section 6.1, but with narrower cable length ranges, a worst-case topology variant has been identified. Table 6.2 presents the cable lengths defining the network topology variant. Only 12-pulse rectifiers, with their corresponding harmonic current injection, are used. This variant causes a *Topside Main* THD level of 14.9 %.

Cable	Length [km]
Step-out Cable	50
Supply Cable A	0.16
Supply Cable B	4.4
Load Cable 1&2	0.7
Load Cable 3&4	0.18

Load cables supplying the same compressor train always have equal length

Table 6.2: Cable lengths for Case Study 1

Figure 6.11 and 6.12 shows the harmonic current spectra in both ends of *Load Cable 1* and *Load Cable 2*, respectively. The blue spectra represent the current in the load-end of the cables, while the red spectra represents the currents injected into *Switchboard A*. The blue spectra are therefore identical to the 12-pulse harmonic current spectrum discussed in Section 3.1.2 (Figure 3.8). An explanatory partial sketch of the *Long Step-out* is presented in Figure 6.10. In addition to the current spectra, the network impedance characteristics, as seen from *Switchboard A*, are presented in both figures.

The network impedance characteristic of *Switchboard A* has a parallel resonance at harmonic order 47, caused by resonance between the capacitance of *Load Cable 1&2* and the short-circuit impedance of the *T6_step-down* transformer.

Load Cable 1 (supplying a gas compressor load) carries a fundamental frequency current of 259.09 A, while *Load Cable 2* (supplying a condensate pump load) carries a 10.79 A fundamental frequency current. From Figure 6.11 and 6.12 it may look like the amplification of the 47th harmonic current is extremely large in *Load Cable 2*, relative to the

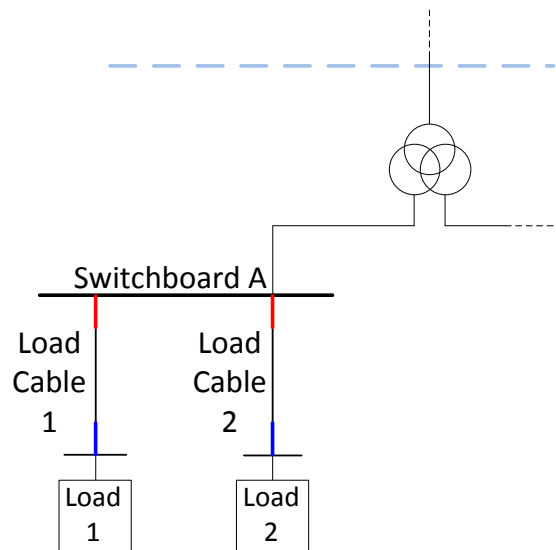


Figure 6.10: Explanatory sketch for Figure 6.11 and 6.12

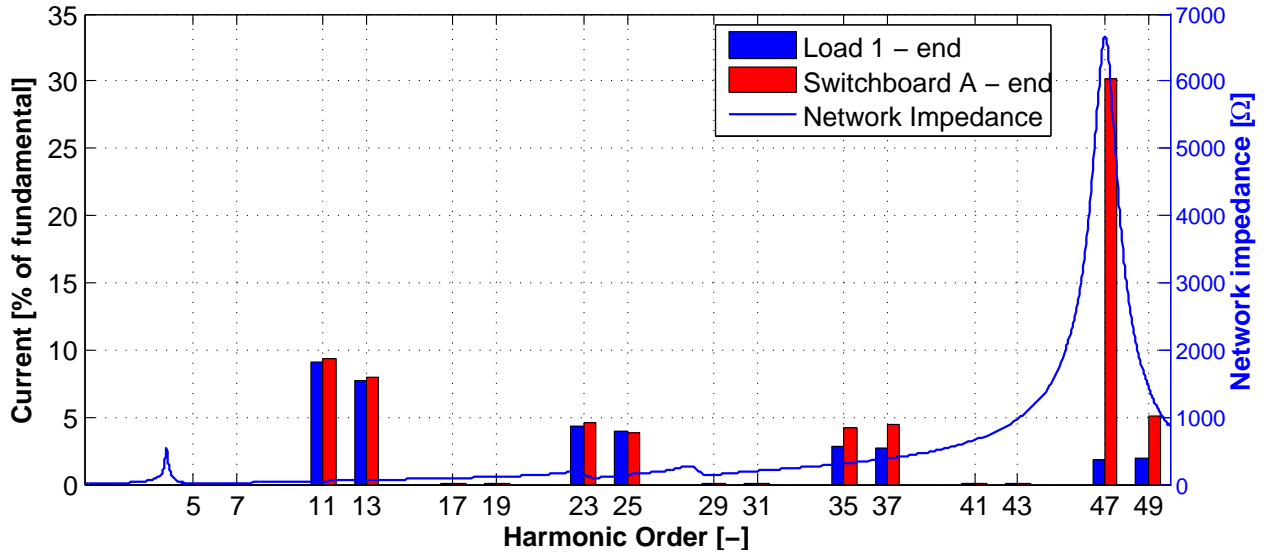


Figure 6.11: Case Study 1: Harmonic currents in *Load Cable 1* with network impedance characteristic seen from *Switchboard A*

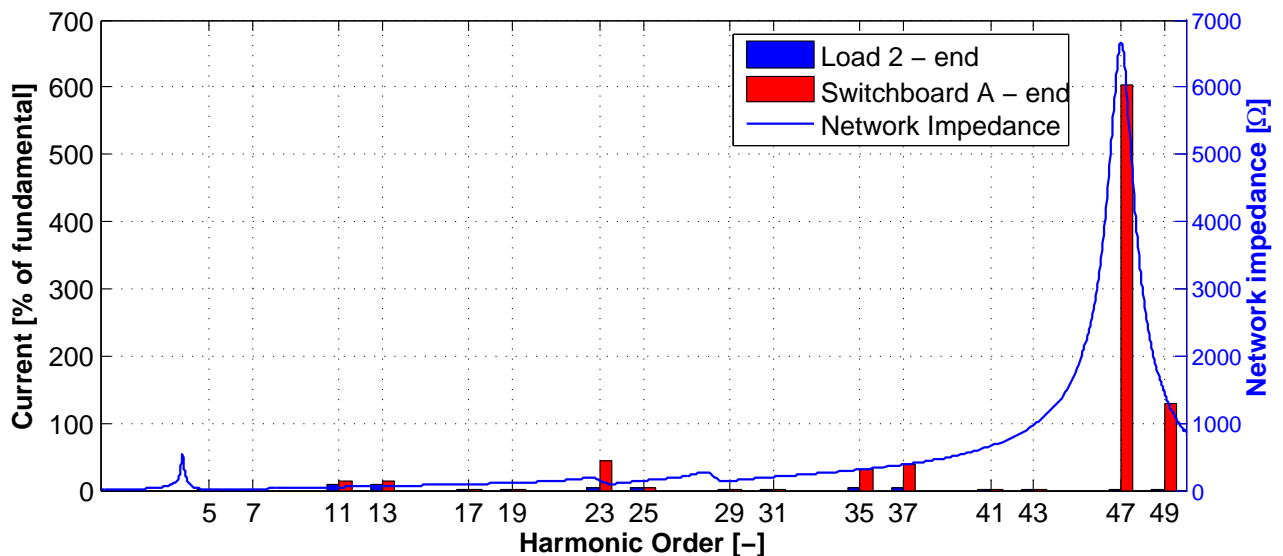


Figure 6.12: Case Study 1: Harmonic currents in *Load Cable 2* with network impedance characteristic seen from *Switchboard A*

injected current. However, the large current in the *Switchboard A* - end of *Load Cable 2* is not *only* caused by amplification of the injected current. As described previously, *double amplification* may occur at certain length combinations of *Load cable 1&2* and *Supply Cable A*. The 47th harmonic current is first amplified several times through *Load Cable 1*. As the current is injected into *Switchboard A*, it is further excited by the capacitance of *Load Cable 2*. The *double amplification* of the harmonic currents leads to extremely large harmonic voltages at *Switchboard A*. Figure 6.13 shows the harmonic voltage spectrum, the individual IEC limits and the network impedance characteristic of *Switchboard A*. The resulting THD at *Switchboard A* is 221.6 %.

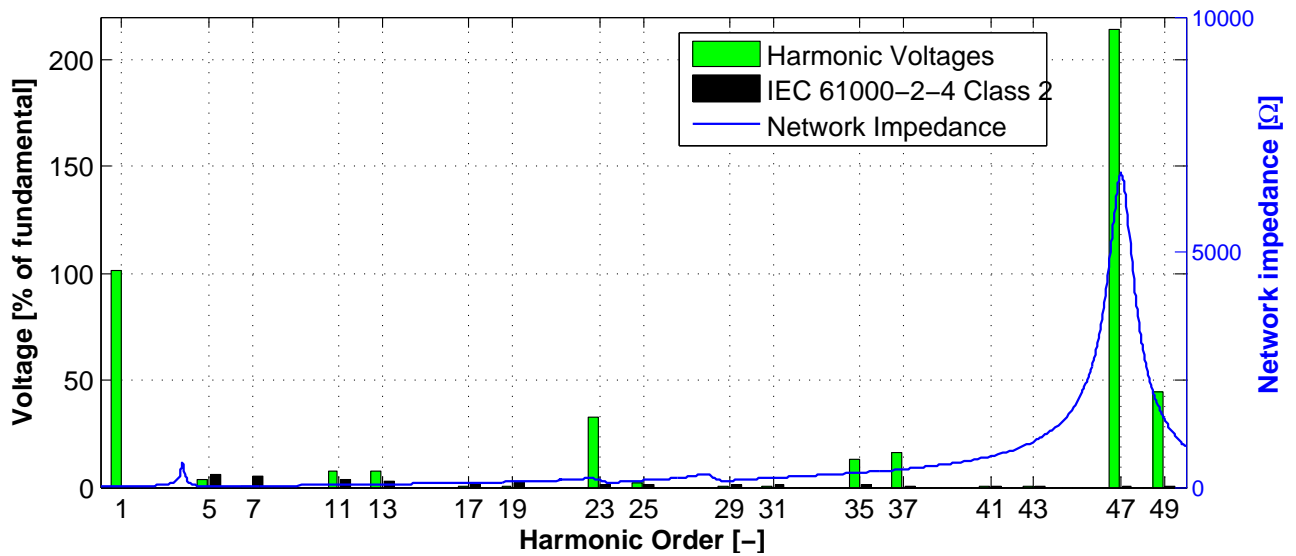


Figure 6.13: Case Study 1: Harmonic voltage spectrum and network impedance characteristic seen from *Switchboard A*

The harmonic currents from *Load Cable 1&2* are further injected into *Supply Cable A*. Also here, a slight amplification of the 47th harmonic current occurs, before it is injected into the windings of the *T6_step-down* transformer.

Due to parallel resonance, mainly between *Supply Cable B* and *T6_step-down* transformer, especially the 23rd harmonic current is amplified through *Supply Cable B*. The harmonic current spectra of *Supply Cable B* can be found in Figure C.2 in Appendix C.1.1.

Thus, large 47th (and some 49th) harmonic currents are injected into *T6_step-down* by *Supply Cable A*, while 23rd (and some 25th) harmonic currents are injected by *Supply Cable B*. In Section 3.6.2 the effect of phase-shifting the secondary and tertiary windings of a transformer, was discussed. However, the 15° phase-shift in *T6_step-down* transformer do not contribute to any cancellation of the 23rd, 25th, 47th or 49th harmonic currents, which can therefore flow relatively undisturbed through the transformer.

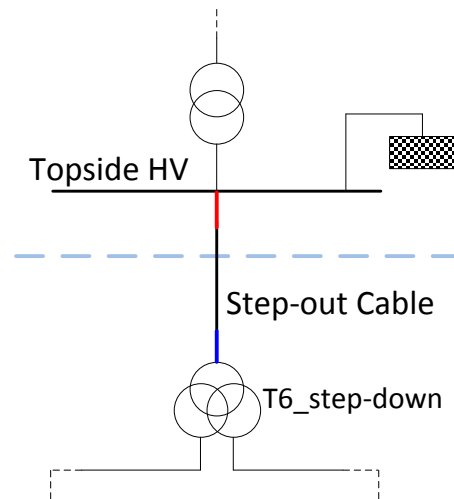


Figure 6.14: Explanatory sketch for Figure 6.15

Figure 6.15 presents the harmonic current spectra in both ends of the *Step-out Cable*, in addition to the network impedance characteristic seen from the *Topside Main* busbar. An explanatory partial sketch of the *Long Step-out* is presented in Figure 6.14. As ex-

pected, the current spectrum in the *T6_step-down* - end of the cable is dominated by the 23rd and 47th harmonic currents. Due to unequal current injections from *Supply Cable A* and *Supply Cable B*, 11th, 13th, 35th and 37th harmonic currents are still present in the *Step-out Cable*, despite the phase-shifting effect of the *T6_step-down* transformer.

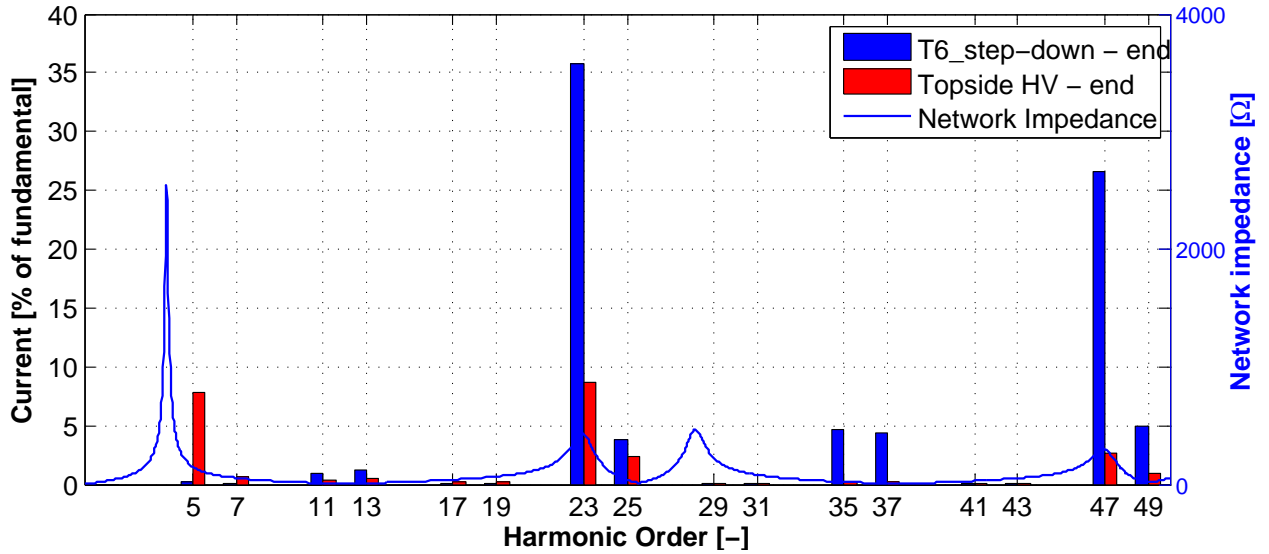


Figure 6.15: Case Study 1: Harmonic currents in *Step-out Cable* with network impedance characteristic seen from *Topside HV*

As the currents flow through the *Step-out Cable*, they are heavily dampened. Due to the filtering effect discussed in Section 3.4, most of the high frequency currents are fed through the capacitance of the cable. Figure 6.16 presents the harmonic voltage spectrum and network impedance characteristic at *Topside Main*, along with the individual IEC 61000-2-4 Class 2 harmonic voltage limits. Compared to the voltage spectrum at *Switchboard A* (Figure 6.13), it is clear that the natural LCL-filter has an incredible damping effect on the voltage harmonics. The 23rd, 25th, 47th and 49th harmonic voltages are still the problem which implies that substituting the 12-pulse rectifiers with 24-pulse rectifiers would not be sufficient to assure acceptable THD levels (as 24-pulse rectifiers would only cancel the 11th, 13th, 35th and 37th harmonics). With a *Topside Main* THD level of 14.9%, other measures (such as 36-pulse rectifiers) should be considered.

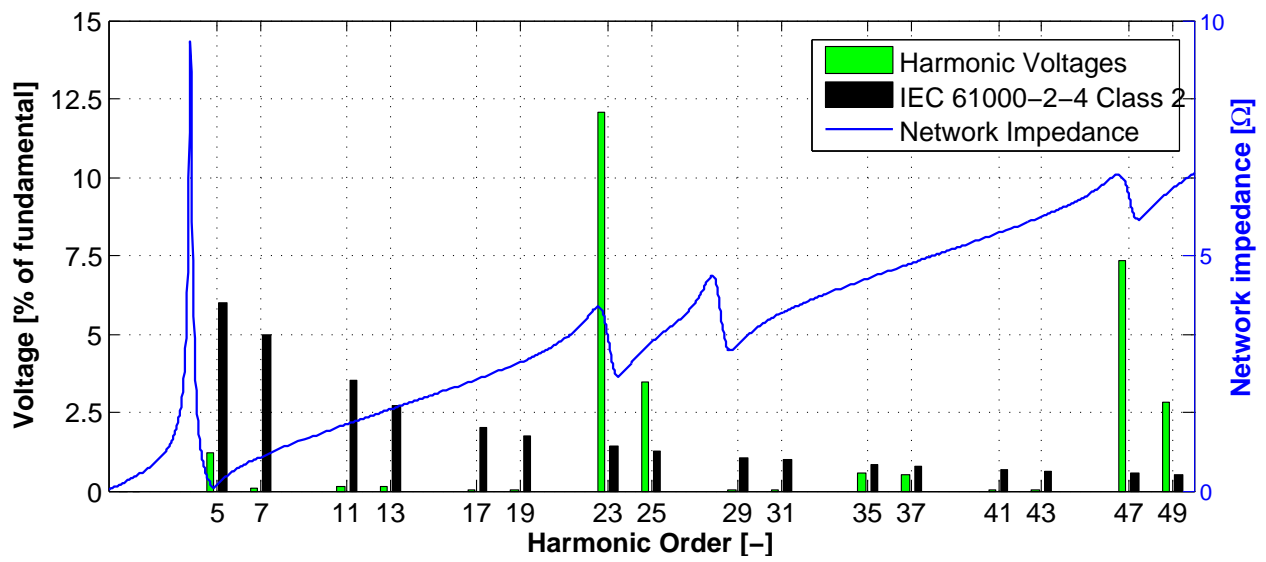


Figure 6.16: Case Study 1: Harmonic voltage spectrum and network impedance characteristic seen from *Topside Main*

6.4 Case Study 2: *Long Step-out* Lower THD Scenario

From Study Case 1, we know that the harmonic content in the *Long Step-out* may become extremely large under certain circumstances. This section will analyze a variant of the *Long Step-out* with considerably lower levels of harmonics. In addition, possible means (if necessary) to assure acceptable THD levels in the system, will be discussed. Table 6.3 defines the cable lengths of the *Long Step-out* Case Study 2 variant. Since *Supply Cable A* and *Supply Cable B*, and *Load Cable 1&2* and *Load Cable 3&4* have equal lengths in this variant, the branches supplying *Compressor Train A* and *Compressor Train B* are identical. With the findings of Section 6.1 (Series Scan) in mind, a long *Step-out Cable*

Cable	Length [km]
Step-out Cable	175
Supply Cable A	0.06
Supply Cable B	0.06
Load Cable 1&2	0.04
Load Cable 3&4	0.04

Load cables supplying the same compressor train always have equal length

Table 6.3: Cable lengths for Case Study 2

and the remaining cables kept short, should result in relatively low THD levels. Figure 6.17 shows the harmonic voltage spectrum and network impedance at *Switchboard A*. In addition, the individual harmonic limits of the IEC 61000-2-4 Class 2 are indicated as a black spectrum. With a resulting THD of 20.0 % at *Switchboard A*, this is clearly one of

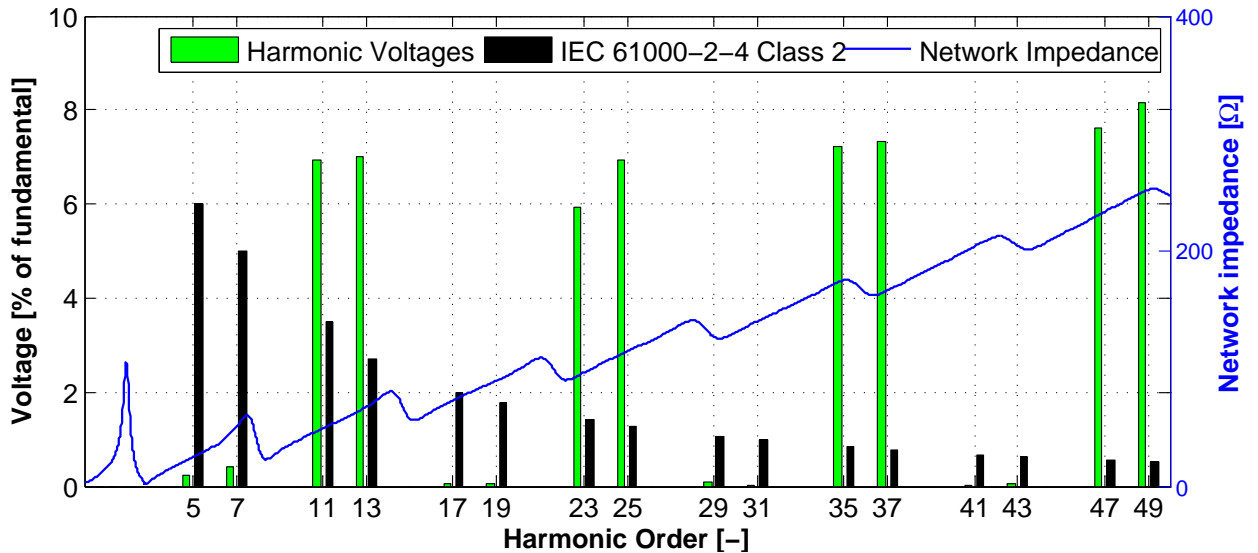


Figure 6.17: Case Study 2: Harmonic voltages and network impedance characteristic seen from *Switchboard A*

the variants with the lowest harmonic content, keeping Figure 6.5 in mind. The 11th, 13th, 23rd, 25th, 35th, 37th, 47th and 49th voltage harmonics are all above the limits specified

by the IEC standard, although no current amplification occurs in the surrounding cables. The voltage harmonics at harmonic order 5, 7, 17, 19 etc. are caused by the *Topside SVC*.

Since the lengths of *Supply Cable A* and *Load Cable 1&2* are very short (60 meters and 40 meters, respectively), their capacitances are relatively small which results in very high resonance frequencies. A possible parallel resonance is therefore located outside the harmonic order range, considered in this thesis. But even though the harmonic currents are not amplified, the THD level at *Switchboard A* (and *Switchboard B*) are way to high when using 12-pulse rectifiers.

No harmonic current amplification occur through *Supply Cable A* nor *Supply Cable B*. Figure 6.19 shows the harmonic current spectra of both ends of the *Step-out Cable*. Figure 6.18 offers an explanatory sketch. Since the systems supplying *Compressor Train A* and *Compressor Train B* are identical, the harmonic current spectra injected into the secondary and tertiary windings of *T6_step-down* transformer, are also identical. The 15° phase-shift between the secondary and tertiary windings, therefore cancel the 11th, 13th, 35th and 37th harmonic currents, completely. Only the 23rd, 25th, 47th and 49th harmonic currents are injected into the *Step-out Cable*. The fundamental current in the *T6_step-down* - end of the *Step-out Cable* has an amplitude of 213.45 A. Due to massive reactive power production

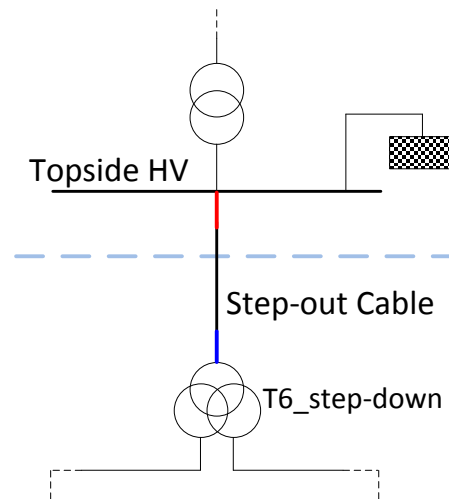


Figure 6.18: Explanatory sketch for Figure 6.19

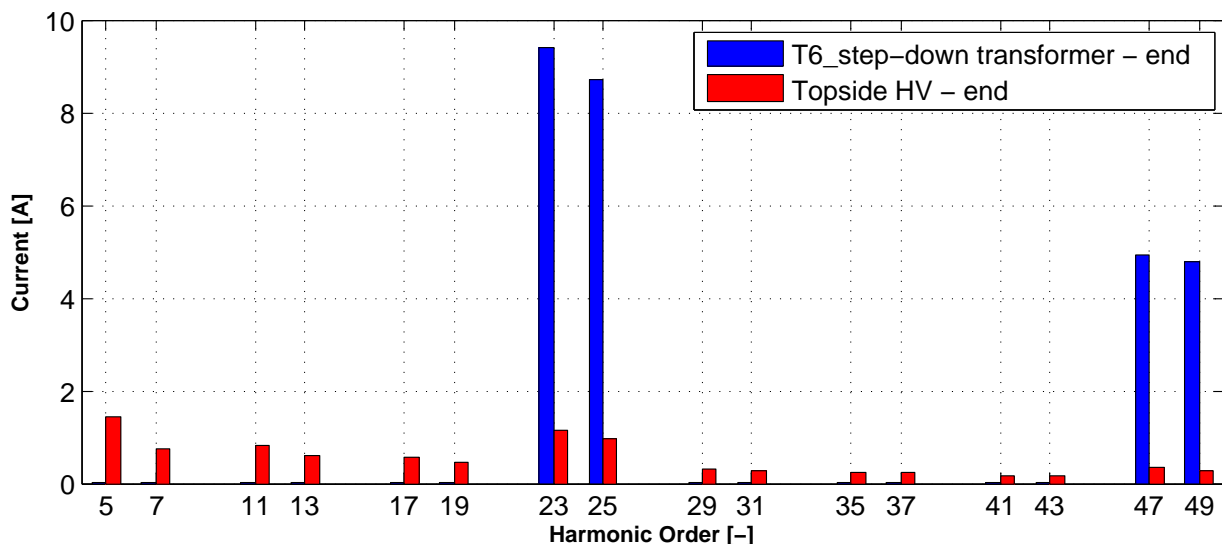


Figure 6.19: Case Study 2: Harmonic currents in *Step-out Cable*

in the very long *Step-out Cable* (175 km), the amplitude of the fundamental current in the

Topside HV - end of the *Step-out Cable*, is quite much larger than in the *T6_step-down* - end (396.98 A). For this reason, the spectra in Figure 6.19 are presented in Ampere instead of percentage of the fundamental. Throughout the cable, the 23rd, 25th, 47th and 49th harmonic currents are dampened to far lower levels. The currents of harmonic orders 5, 7, 11, 13, 17, 19, 29 etc. are mainly caused by the thyristor switching of the *Topside SVC*.

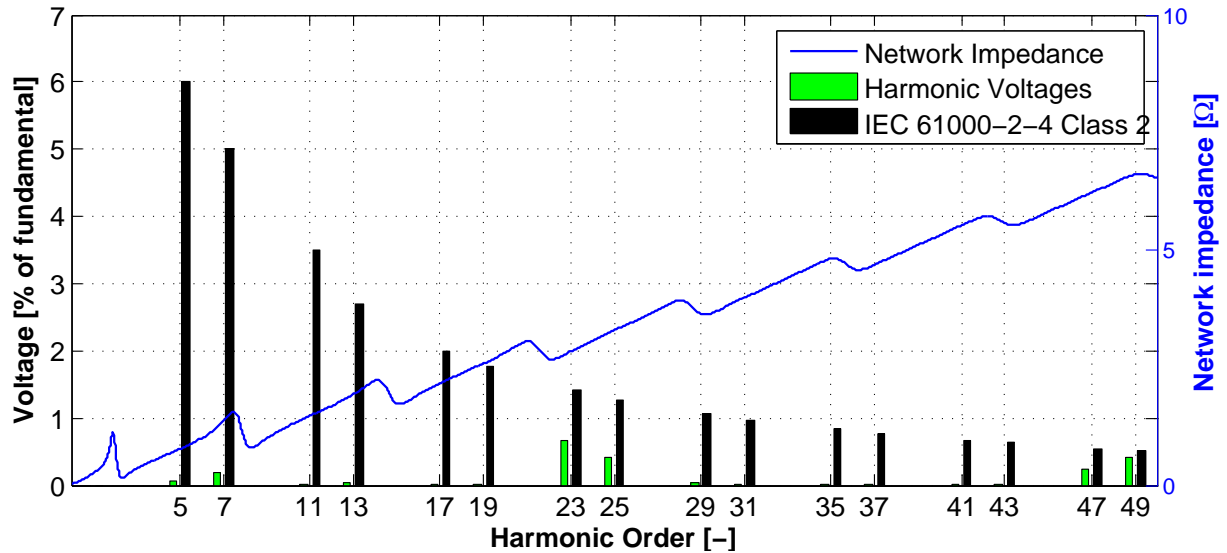


Figure 6.20: Case Study 2: Harmonic voltages and network impedance characteristic seen from *Topside Main*

Figure 6.20 presents the harmonic voltage spectrum and network impedance characteristic at *Topside Main*, along with the individual IEC limits. All harmonic voltages are below the limits proposed by the IEC 61000-2-4 Class 2. The resulting THD is 0.9%. The natural low-pass filters assures very low topside harmonic voltages, however, the THD levels at the subsea busbars are still above what is acceptable, even though no harmonic resonance nor current amplification occurs.

By modifying all the rectifiers to inject 24-pulse harmonic current spectra, as discussed in Section 4.3.1, new harmonic calculations have been conducted. The THD levels at *Switchboard A* and *Switchboard B* are now reduced to 14.2 % which still is above the 8 % IEC limit. Due to the phase-shift between the secondary and tertiary winding of *T6_step-down* transformer, the topside THD levels are not changed. By changing the injected harmonic current spectra corresponding to a 36-pulse rectifier, reduces the THD levels further. The THD levels at *Switchboard A* and *Switchboard B* are now 10.2 %.

No substantial harmonic resonance nor harmonic current amplification occurred in the topology variant studied in this section. Still, the 12-pulse harmonic current injections alone were enough to generate too high THD levels at the subsea busbars. Case Study 2 has emphasized that the harmonic content in the subsea distribution system (LV-side of the *T6_step-down* transformer) *must* be analyzed when investigating the harmonic behavior of such a system.

6.5 General Observations for the *Long Step-out*

From the analysis and case studies above, some general observations can be made regarding the harmonic behavior in the *Long Step-out*. The individual cables in the topology clearly have unequal influence on the THD levels at the separate busbars. Each cable has most influence on the most close-by busbar's THD level. Due to the evident decoupling of the system, caused by the high-impedance *T6_step-down* transformer, the harmonic behavior is rather complex. The longer the cables are, the larger their impedance becomes and their influence on the network impedance characteristic increases. Potential parallel resonances therefore becomes increasingly "rigid" in the network impedance characteristic.

As was shown in Case Study 1, one of the largest challenges with the *Long Step-out* topology is "local" resonance and harmonic current amplification between the load- or the supply cables, and the subsea *T6_step-down* transformer. Due to the decoupling of the transformer, extreme current amplification (and also *double amplification* of certain current injections) may occur in these cables, further causing very large harmonic voltages.

Generally, a long *Step-out Cable* with the remaining cables kept as short as possible results in the lowest THD levels, as was found in Section 6.1. It is also clear that the LCL-filtering effect in the system can easily mask problematic harmonic conditions at the subsea busbars, when observed from topside. Potential resonances caused by the *Step-out Cable* itself, is not nearly as problematic as the "local" resonances occurring in the load- and supply cables.

In a harmonic mitigation process of such a power system, it is interesting to know the effects of the individual harmonics. Series Scan simulations, similar to those conducted in Section 6.1, have therefore been conducted, only with a modification of the injected harmonic current spectra. Figure 6.21 and 6.22 shows the THD levels of the system busbars with the corresponding cable variation order. Here, the injected harmonic current spectra have been changed to consist of the 11th and 13th, *only* (in addition to the fundamental). This scenario is not realistic, but is only simulated to clarify the 11th and 13th harmonics' isolated impact on the system.

The 11th and 13th harmonic currents alone, are not problematic with respect to the topside burbars' THD levels. The THD at *Topside Main* is kept below 2 %, while the THD at *Topside HV* is always kept below 4 %. At the subsea busbars, on the other hand, the 11th and 13th harmonics causes problems. Regardless of the variation, the THD levels are above the IEC limit. To get a system with subsea THD levels within the IEC requirements, the 11th and 13th harmonics *have* to be reduced, which could be done by utilizing 24-pulse rectifiers.

Likewise, simulations with harmonic current injections limited to harmonic order 23 and 25, 35 and 37, 47 and 49 have been conducted. The THD plots of these simulations can be found in Appendix C.1.2. These simulations shows that harmonic orders 23, 25, 35, 37, 47 and 49 are far more problematic than the 11th and 13th harmonics. 24-pulse rectifiers alone will therefore not be enough to reduce the harmonic content at the subsea busbars to an acceptable level, as also was the result of Case Study 2.

These simulations emphasize the fact that harmonic mitigation may be very complex. Only an increase in the pulse number of the rectifiers might not solve a harmonic content problem. The network impedance characteristic should always be investigated in detail to be able to choose the best suitable mitigation technique.

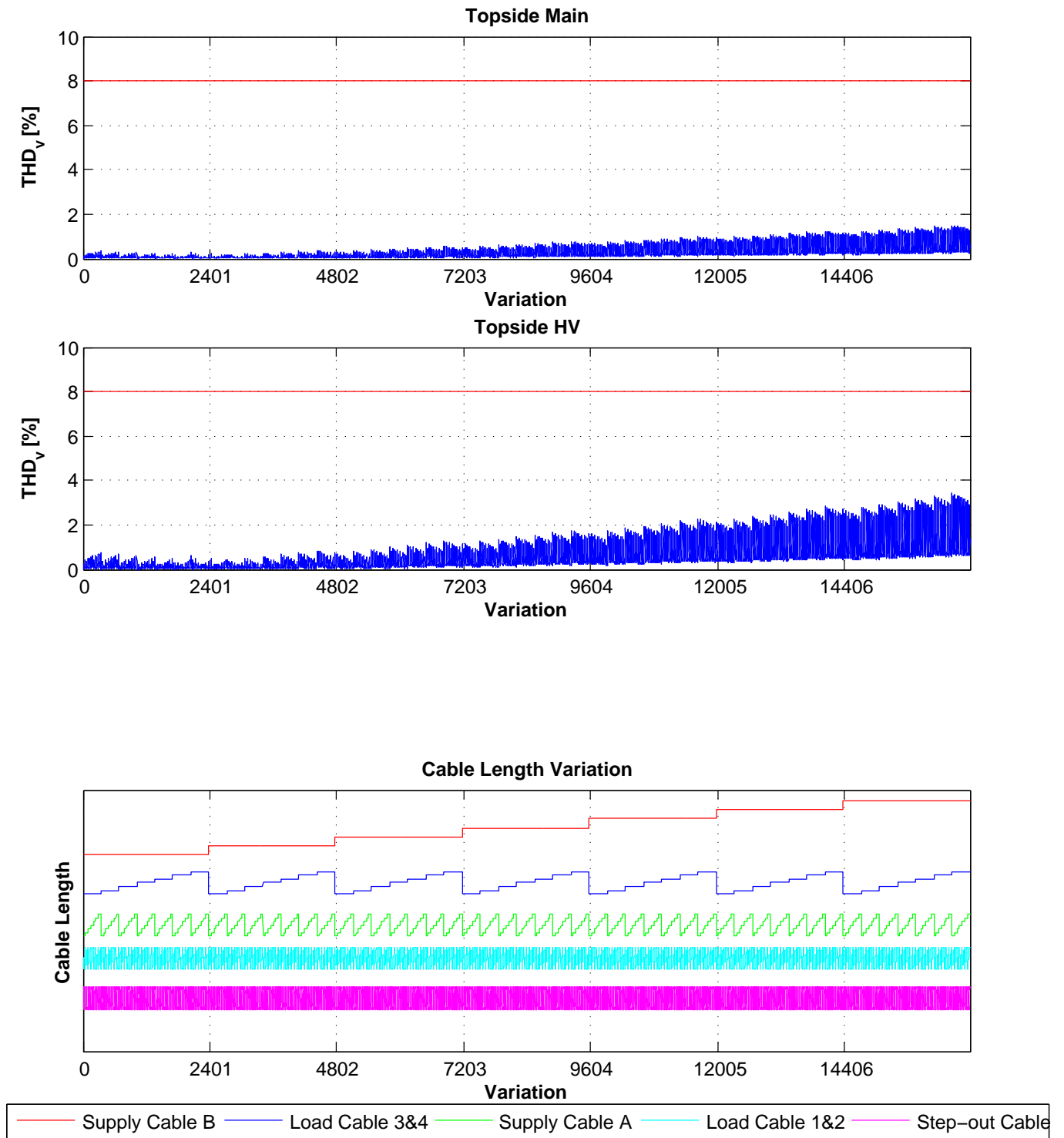


Figure 6.21: Topside busbars' THD levels with injected 11th and 13th harmonic currents, only

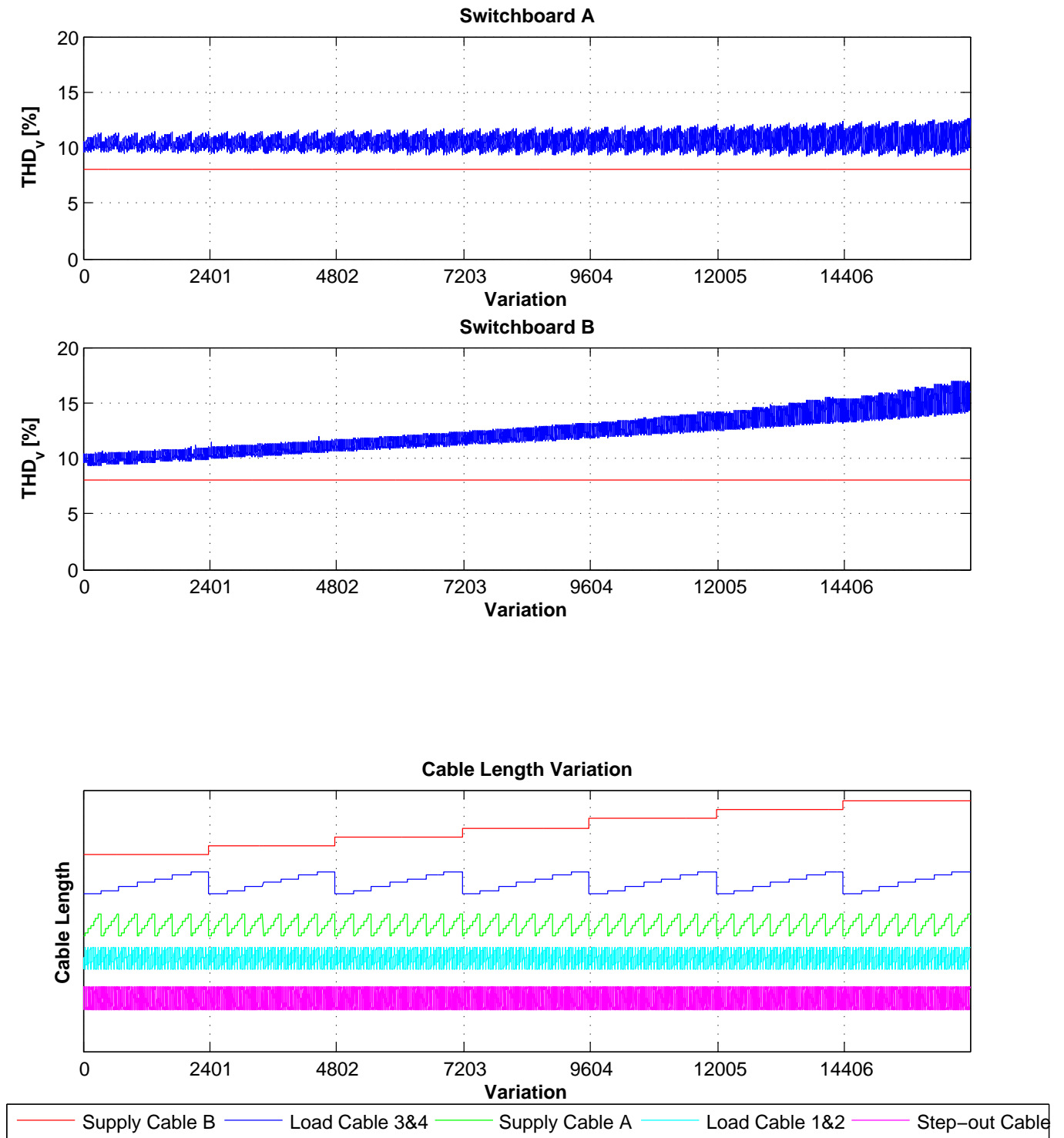


Figure 6.22: Subsea busbars' THD levels with injected 11th and 13th harmonic currents, only

7 *Short Step-out* Harmonics and Resonance Analysis

This section presents the results and findings of the harmonic analysis of the *Short Step-out* topology. As for the *Long Step-out*, the *Short Step-out* will be analyzed to reveal possible trends, patterns and relations. First, Series Scan simulations of the *Short Step-out* will be studied. Further, Section 7.2 will investigate the harmonic behavior in more detail. Case Study 3 (Section 7.3) discusses a worst-case variant of the *Short Step-out*, when it comes to THD levels. Case Study 4 (Section 7.4) discusses a variant with relatively low THD levels. Here, possible means (if necessary) to assure acceptable THD levels for the variant, will be discussed. Figure 7.1 shows a sketch of the *Short Step-out* topology

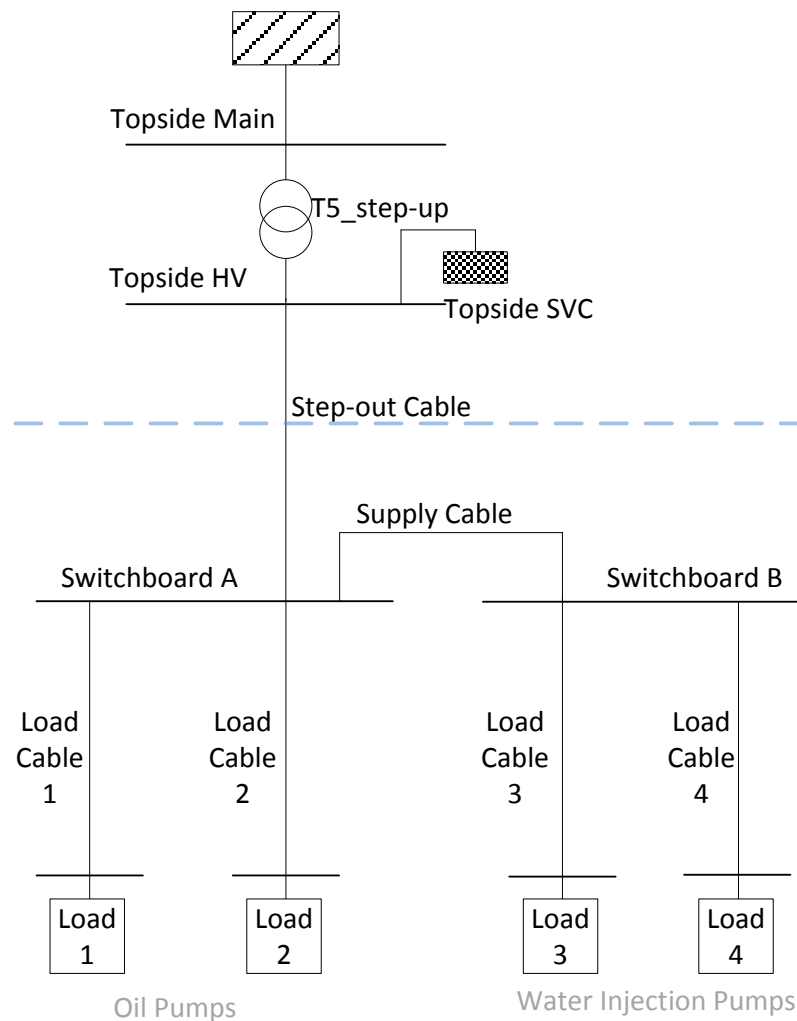


Figure 7.1: Main busbars and cables of the *Short Step-out*

with the naming and location of the system's most important electrical components. The different cables and busbars will be referred to repeatedly in the following text. All *Short Step-out* components will be written in *italic*, as it was done for the *Long Step-out*. Note that the four subsea loads of the *Short Step-out* are independent of each other. *Load*

Cable 1 through *Load Cable 4* can therefore have unequal lengths. Table 4.2 is rendered in Table 7.1, and defines the allowable cable lengths of the *Short Step-out* topology.

Cable	Length interval [km]
Step-out Cable	1.0 - 60
Supply Cable	4.0 - 6.0
Load Cable 1	0.02 - 5.0
Load Cable 2	0.02 - 5.0
Load Cable 3	0.02 - 5.0
Load Cable 4	0.02 - 5.0

Table 7.1: *Short Step-out* cable lengths

Figure 7.2 shows plots of the initial short-circuit currents at *Switchboard A* and *Switchboard B*, normalized to the busbars' respective load current, as the length of *Step-out Cable* increases. All remaining cables are kept constant at their longest length according to Table 7.1. As expected, the short-circuit current declines as the length of *Step-out Cable* increased. The load currents at *Switchboard A* and *Switchboard B* are identical, and equal to 135 A. The short-circuit current is slightly lower for *Switchboard B* due to the 5 km long *Supply Cable*.

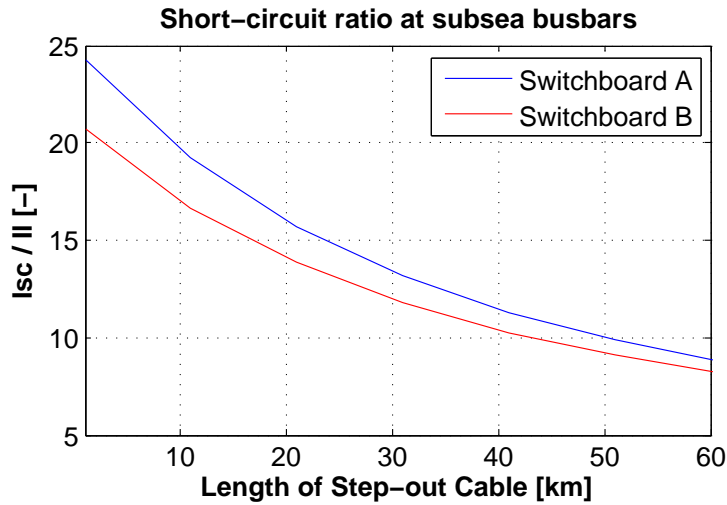


Figure 7.2: Short-circuit current ratio at subsea busbars

7.1 *Short Step-out Series Scan*

A Series Scan simulation with varying cable lengths according to Table 5.2, has been conducted on the *Short Step-out*. Figure 7.3 and 7.4 presents plots of the THD levels at the topside (*Topside Main* and *Topside HV*) and subsea (*Switchboard A* and *Switchboard B*) busbars. All calculations are done with frequency-dependent cable resistances. The order of varying cable length have been arranged to best present the results.

Compared to the *Long Step-out* results, the THD plots of the various busbars are much more alike for the *Short Step-out*. Qualitatively, the THD plots are nearly equal at all busbars. The similarity of the THD plots are caused by the absence of a subsea step-down transformer. As described earlier, the *T6_step-down* transformer in the *Long Step-out* has a filtering effect on the harmonics, but also a decoupling effect of the subsea power system. With a shorter *Step-out Cable* and lower load current, no step-down transformer is needed in the *Short Step-out*. The subsea busbars are therefore strongly connected to each other, as well as to the topside system. Without the filtering effect of a subsea step-down transformer (large series impedance), the harmonics are easily transmitted throughout the entire system.

Due to the strongly coupled system, the network impedance characteristics of the busbars are nearly equal, especially for *Switchboard A*, *Switchboard B* and *Topside HV*. The topside *T5_step-up* transformer offers some damping and decoupling between the two topside busbars. For the *Long Step-out* it became clear that most of the harmonic problems were caused by resonance between the subsea supply- or load cables, and the subsea step-down transformer. The absence of a subsea step-down transformer removes these problems and challenges from the *Short Step-out* topology.

From Figure 7.3 and 7.4, it is clear that the *Step-out Cable* is the most influential, when it comes to the busbars' THD levels. Variation 0 through 3 888 have a *Step-out Cable* length of 1 km which should definitely be avoided. Further, the harmonic problems seems to decline as the length of *Step-out Cable* increases. Also, the influence of the remaining cables seems to decrease substantially. Keeping the strong coupling in mind, this makes sense. As the length of *Step-out Cable* increases, its impedance becomes increasingly dominant in determining the network impedance characteristic at the system's busbars. When the *Step-out Cable* approaches its longest length, the remaining cables' impedances are not large enough to substantially affect the network impedance, and thereby affect the harmonic behavior. Their series-impedances are too small and their shunt-admittances are too large.

Two lengths of the *Step-out Cable* seems to assure particularly low THD levels; 30 km (variation 7 776 through 11 664) and 59 km (variation 15 552 through 19 440). Section 7.2 will now investigate the causes behind the high and low THD levels, found in Figure 7.3 and 7.4.

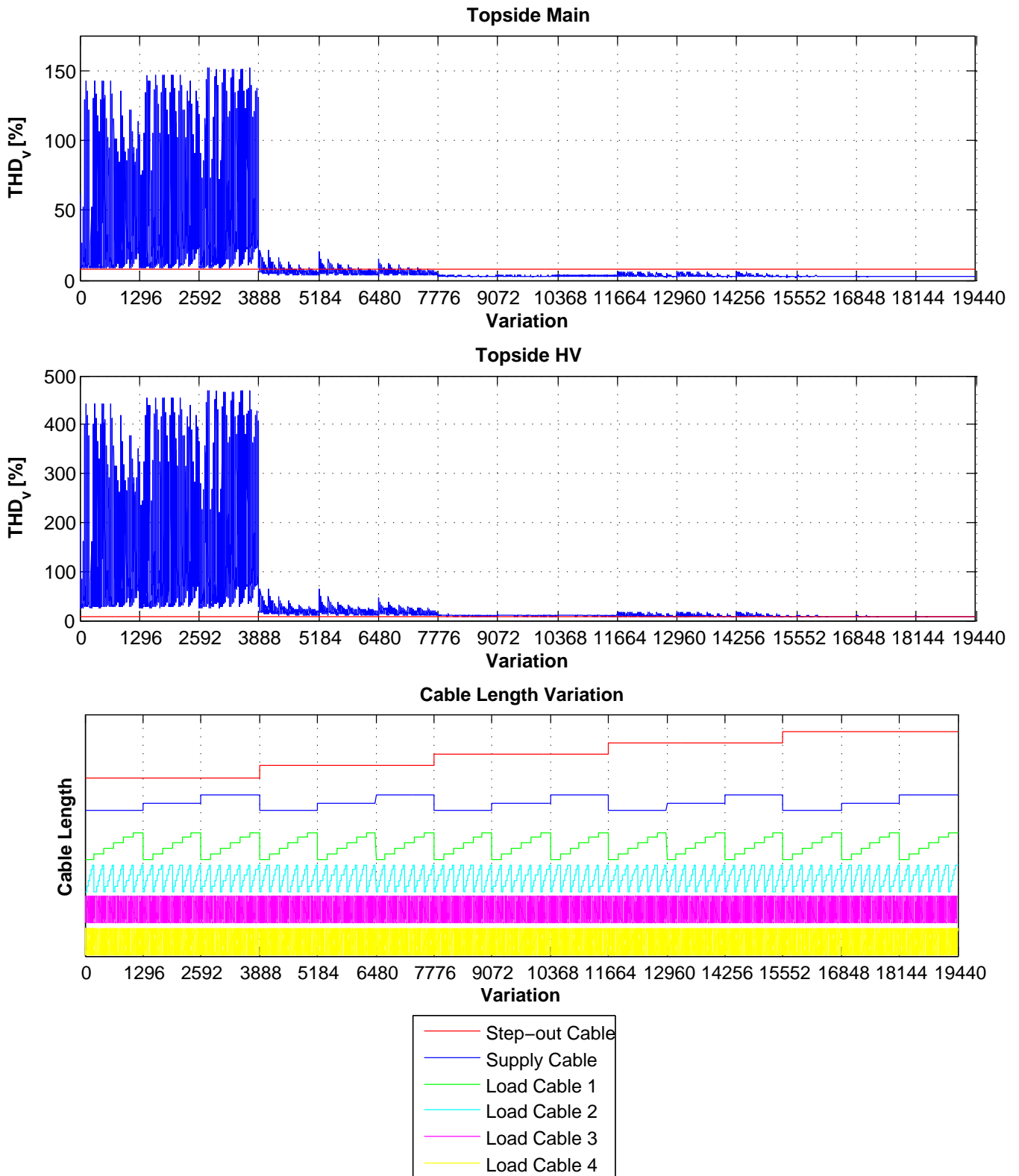


Figure 7.3: Short Step-out Series Scan; Topside Main and Topside HV THD levels

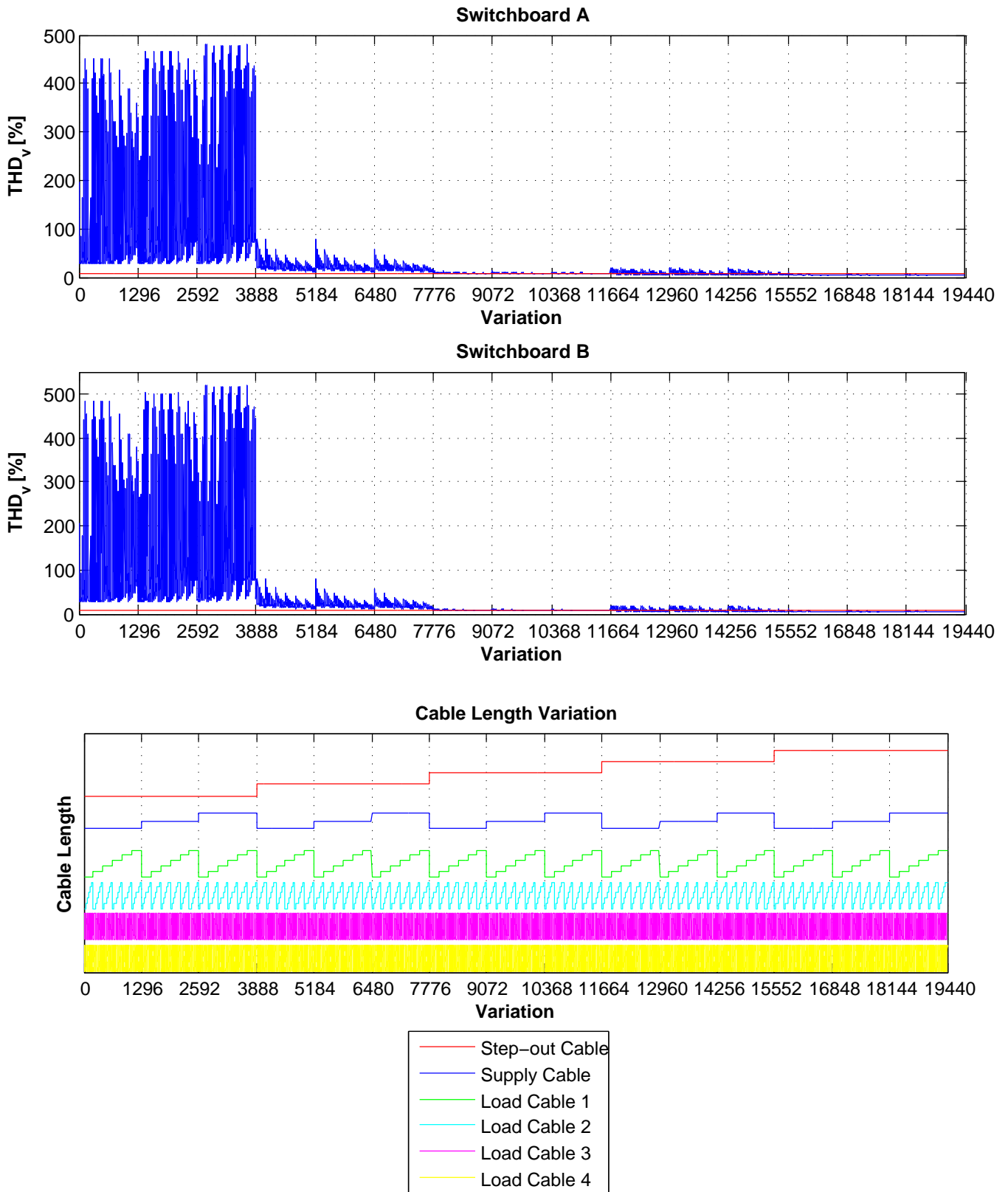


Figure 7.4: Short Step-out Series Scan; Switchboard A and Switchboard B THD levels

7.2 Short Step-out Harmonic and Resonance Behavior

To understand the influence the *Step-out Cable* has on the system's THD levels, let us consider Figure 7.5. Here, only the length of the *Step-out Cable* is varied. All other cable lengths are kept constant at their minimum length, according to Table 7.1. The blue plot represents the THD level at *Topside Main*, while the red represents the IEC 61000-2-4 Class 2 THD limit of 8 %. For lengths of up to 20 km, the THD level lies above

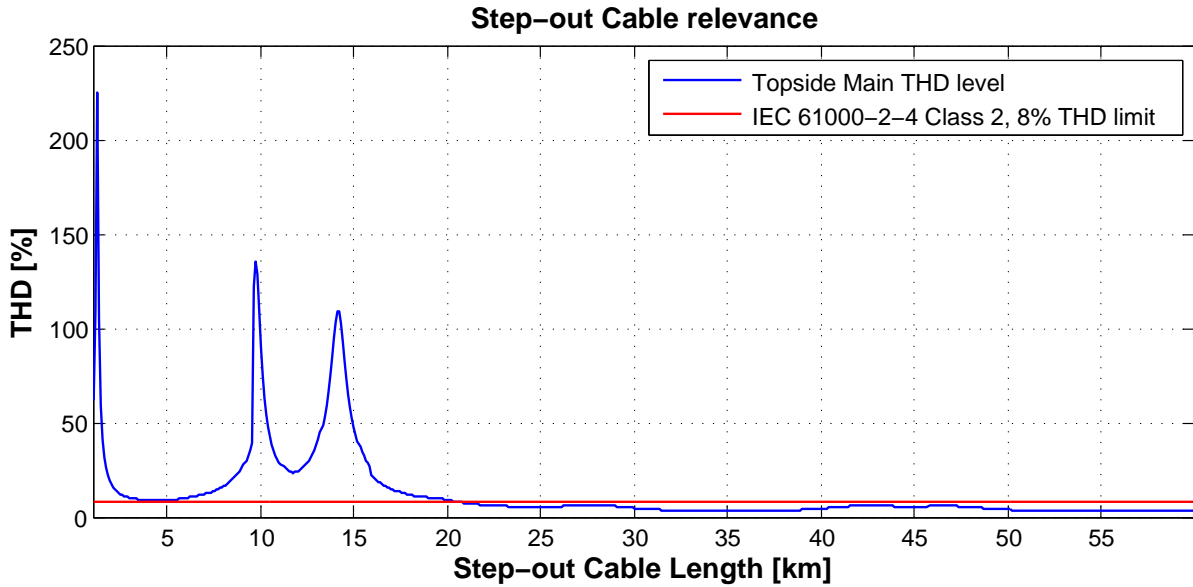


Figure 7.5: THD at *Topside Main* with varying *Step-out Cable* length

the IEC limit and especially three THD tops sticks out. To understand what happens in the system at these critical lengths, we need to investigate the network impedance characteristic of *Topside Main*. Figure 7.6 shows the network impedance characteristics at *Topside Main* with *Step-out Cable* lengths of 1 km and 60 km. The parallel resonance tops have been named as shown in the figure. As the length of *Step-out Cable* is increased, the cable's total capacitance increases and its resonance frequency decreases. Resonance Top 1 is shifted from harmonic order 23 to harmonic order ~ 5 , as the length of *Step-out Cable* is increased from 1 to 60 km. The key to understand the THD plot of Figure 7.5, is to understand the development of the network impedance as the *Step-out Cable* length increases. Figure 7.7 shows the development of the parallel resonance tops of the network impedance characteristic at *Topside Main*, as the length of the *Step-out Cable* increases. The development of both amplitude and resonance frequency are plotted.

Let us start with a *Step-out Cable* length of 1 km. All other cables are kept constant at their minimum allowable length. As we can see from both the upper plot of Figure 7.6 and from Figure 7.7, there is now only one resonance top present in the network impedance characteristic. Its amplitude is approximately 150Ω and it is located around the 23rd harmonic. This parallel resonance top is from now on referred to as Top 1. The resonance top is caused by the capacitance of *Supply Cable* resonating with the inductance of the *T5_step-up* transformer.

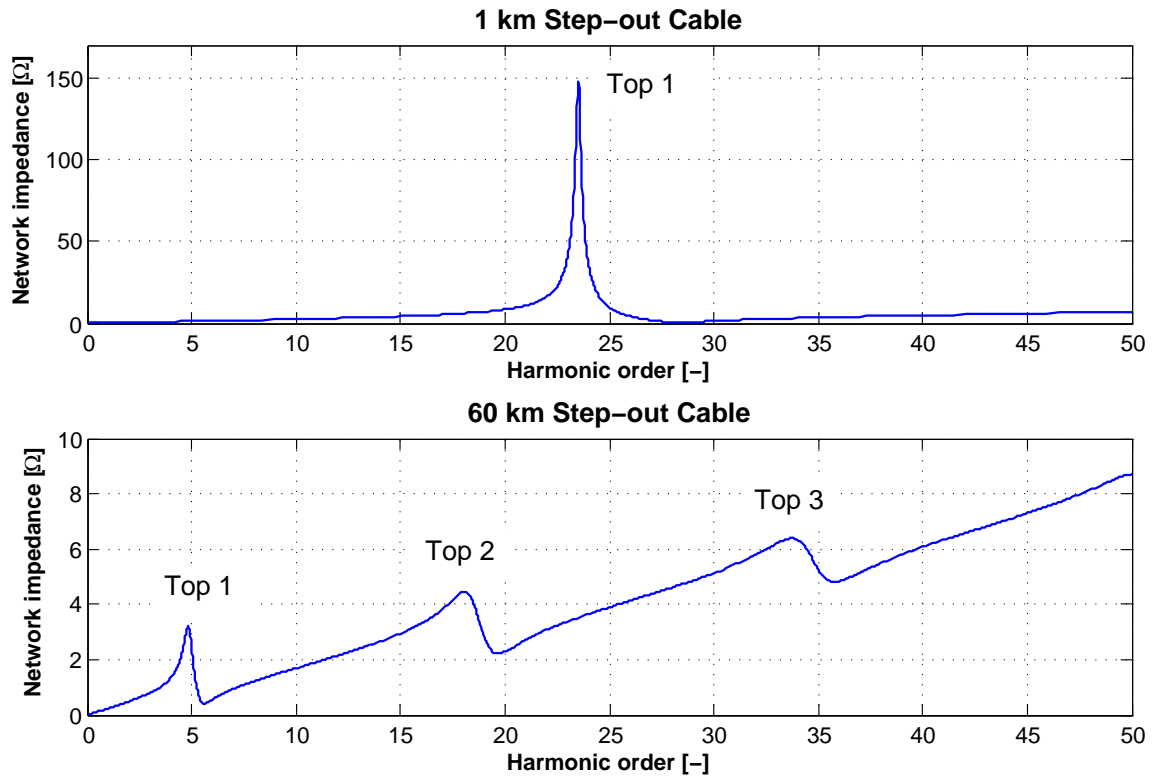


Figure 7.6: Network impedance characteristics at *Topside Main* with a *Step-out Cable* length of 1 km and 60 km

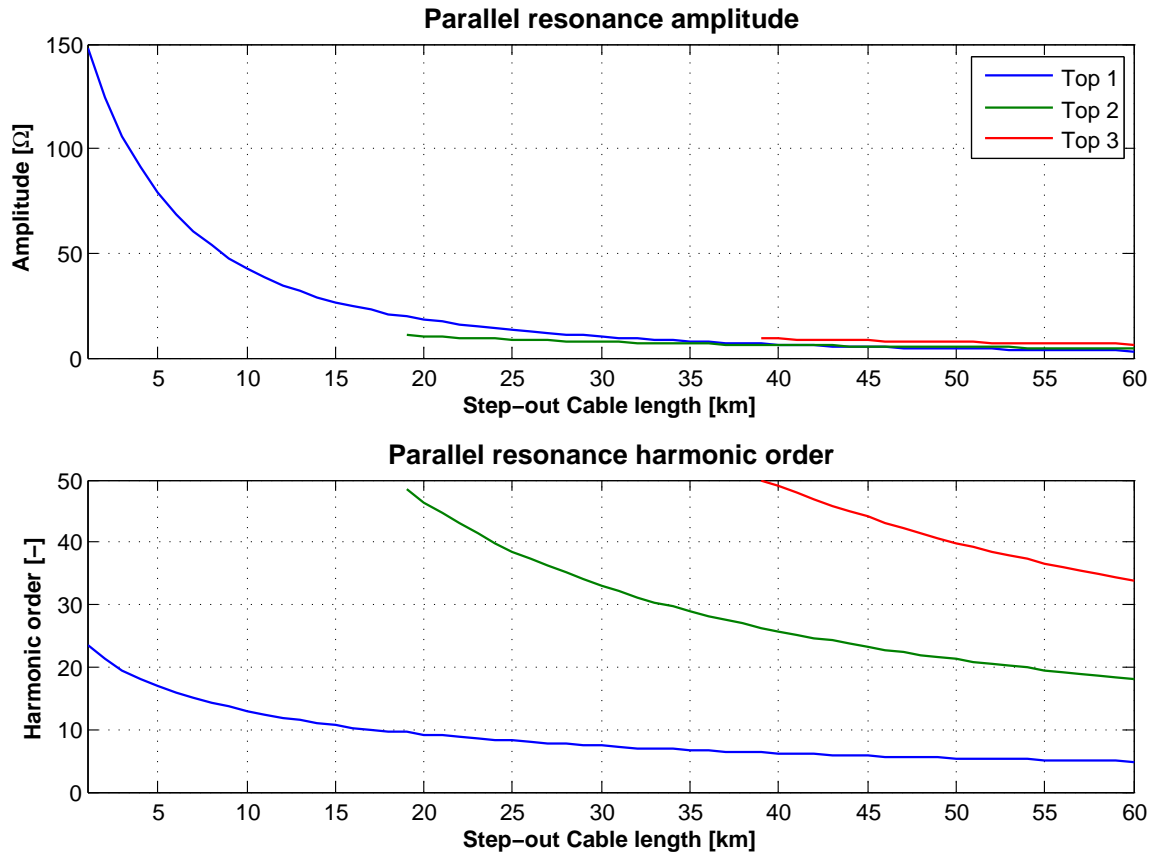


Figure 7.7: Development of harmonic order and amplitude of parallel resonances in the network impedance characteristic of *Topside Main*

Since a 23rd harmonic current is present in the system, a massive current amplification

occurs through the resonating *Supply Cable*. A slight amplification also occur through the *Step-out Cable*. As the large 23rd harmonic current is injected into *Topside HV* and further into *Topside Main*, very large THD levels are generated. This explains the left-most THD peak in Figure 7.5, as well as the large THD content in variations 0 through 3888, in Figure 7.3 and 7.4.

As the length of the *Step-out Cable* is increased, Top 1 is shifted to lower frequencies, away from harmonic order 23. The *Topside Main* THD therefore temporarily decreases. When the *Step-out Cable* reaches a length of 9.7 km, Top 1 is shifted down to harmonic order 13 with an amplitude of 44 Ω (can be seen from Figure 7.7). An extreme amplification of the 13th harmonic current occurs in the *Supply Cable* and the *Step-out Cable*, causing high THD levels. A further increase of the *Step-out Cable* length, shifts Top 1 down to harmonic order 11. The cable length is now equal to 14 km. A new current amplification occurs in the *Supply Cable* and the *Step-out Cable*, which once more causes very high topside THD levels. This explains the two remaining THD tops in Figure 7.5. A further increase in the *Step-out Cable* length, shifts Top 1 to frequencies lower than the 11th harmonic. Since no harmonic current exist for these frequencies, the THD level declines.

In addition to Top 1, two other parallel resonances (Top 2 and Top 3) enters the 1 - 50 harmonic order range, as can be seen from the lower plot of Figure 7.6. However, as we can see from the upper plot of Figure 7.7, their amplitudes are very low. The magnitude of possible generated harmonic voltages therefore becomes lower. As the length of the *Step-out Cable* is increased from 25 to 30 km, Top 2 swipes across harmonic orders 37 and 35. Due to the presence of harmonic currents at these harmonic orders, the system experiences a slight THD increase at these *Step-out Cable* lengths, as can be seen in Figure 7.5. When the length of *Step-out Cable* is increased from 40 to 50 km, Top 2 swipes across harmonic order 25 and 23. Likewise, slight THD increases are visible at these lengths due to the presence of 25th and 23rd harmonic currents.

From Figure 7.7 we can see that the amplitudes of the parallel resonance tops quickly decreases, as the length of *Step-out Cable* increases. In addition, the resonance tops' harmonic order (the resonance frequencies) becomes increasingly static for increasing *Step-out Cable* lengths. When the *Step-out Cable* is long, the relative change in its impedance and admittance becomes smaller for a, let's say, 1 km length change. A long cable's impedance and admittance are dominating the network impedance, making the contribution and influence of other shorter cables, vanishingly small. Since all busbars are closely coupled, the *Step-out Cable*'s impedance dominates the network impedance characteristics of all the other busbars, since it normally is much longer than the other cables.

From the analysis above, we know that the two THD spikes for cable lengths 9.7 km and 14 km in Figure 7.5, are caused by amplification of the 13th and 11th harmonic currents, respectively. By utilizing 24-pulse rectifiers (with no injected 11th or 13th harmonic currents), the THD levels in the entire system should be considerably reduced. However, the very high THD level at a *Step-out Cable* length of 1 km is caused by the 23rd harmonic current, and would therefore still be problematic in a system utilizing 24-pulse rectifiers.

Figure 7.8 presents contour plots of the *Topside Main* THD levels as the lengths of *Load Cable 1* and *Supply Cable* are varied. In the plot to the left, all other cables (*Step-out Cable*, *Load Cable 2*, *Load Cable 3* and *Load Cable 4*) are kept constant at their minimum length. In the plot to the right, all other cables are kept constant at their maximum length.

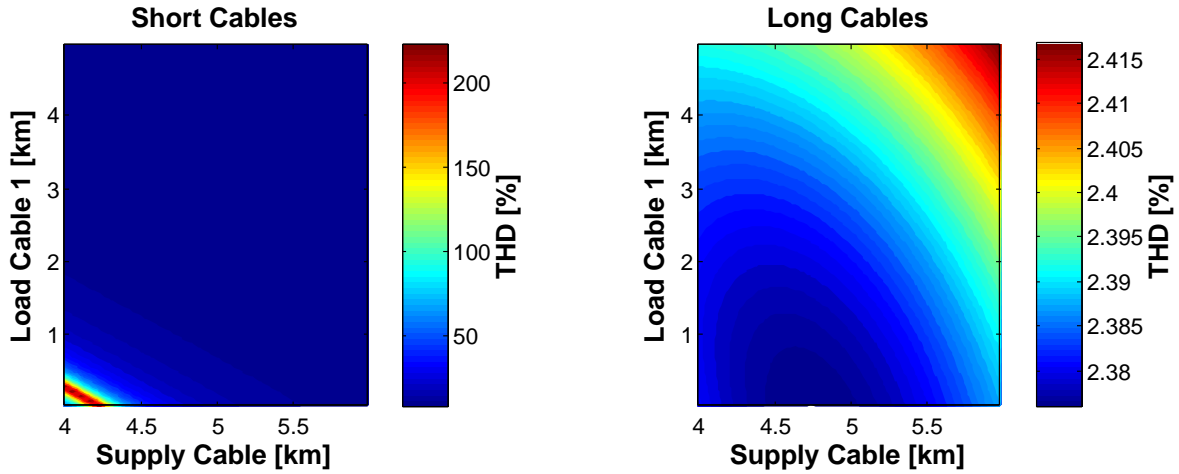


Figure 7.8: *Short Step-out* contour plots of *Topside Main* THD levels when remaining cables are kept short and long

Especially as the *Step-out Cable* becomes longer, the influence of the remaining cables decreases dramatically, as discussed earlier. Noticing the color scaling of the plots in Figure 7.8, it is clear that the THD level influence of *Load Cable 1* and *Supply Cable* are nearly absent as the *Step-out Cable* is at its longest. This confirms the findings of Section 7.1. The same trend as in Figure 7.8 is observed for all busbars, when varying the lengths of *Load Cable 1* through *4* or the *Supply Cable*.

7.3 Case Study 3: *Short Step-out* Worst-Case THD Scenario

In this section, a worst-case topology variant of the *Short Step-out*, when it comes to voltage THD levels, has been identified, simulated and analyzed. This, to illustrate the potential problems and consequences when not taking resonances and harmonics properly into account in the designing a subsea power system. The cable lengths defining the topology variant are presented in Table 7.2.

Cable	Length [km]
Step-out Cable	8.0
Supply Cable	6.0
Load Cable 1	0.18
Load Cable 2	0.34
Load Cable 3	0.1
Load Cable 4	0.26

Table 7.2: Cable lengths for Case Study 3

Figure 7.10 presents the current spectra in both ends of *Load Cable 1*. In addition, the network impedance characteristic at *Switchboard A* is included to highlight the relationship between currents in the cable and the network impedance. Figure 7.9 shows a principle sketch of the *Short Step-out* to explain the current spectra in Figure 7.10.

A parallel resonance, mainly caused by resonance between the capacitances of the *Supply Cable* and the *Step-out Cable*, and the short-circuit impedance of the topside *T5_step-up* transformer, is located at harmonic order 13 in the network impedance characteristic in Figure 7.10. As we can see, this causes an amplification of the 13th harmonic current flowing through *Load Cable 1*. Similar current amplification occurs in *Load Cable 2*.

At *Switchboard B* the harmonic behavior is very similar. Due to the strong coupling between *Switchboard A* and *Switchboard B*, the parallel resonance present in the network impedance characteristic of *Switchboard A* (seen in Figure 7.10) is also present at *Switchboard B*. This further causes current amplifications of the 13th harmonic currents flowing through *Load Cable 3* and *Load Cable 4*. The resulting harmonic voltage spectrum at *Switchboard B* can be found in Appendix C.2.1 (Figure C.8).

From *Switchboard B*, the harmonic currents from *Load Cable 3* and *Load Cable 4* are injected into the *Supply Cable*. Figure 7.12 presents the harmonic current spectra in both

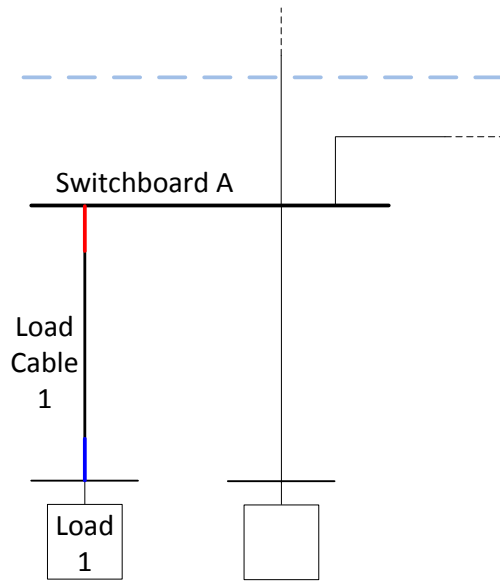


Figure 7.9: Explanatory sketch for Figure 7.10

ends of the *Supply Cable* along with the network impedance characteristic of *Switchboard A*.

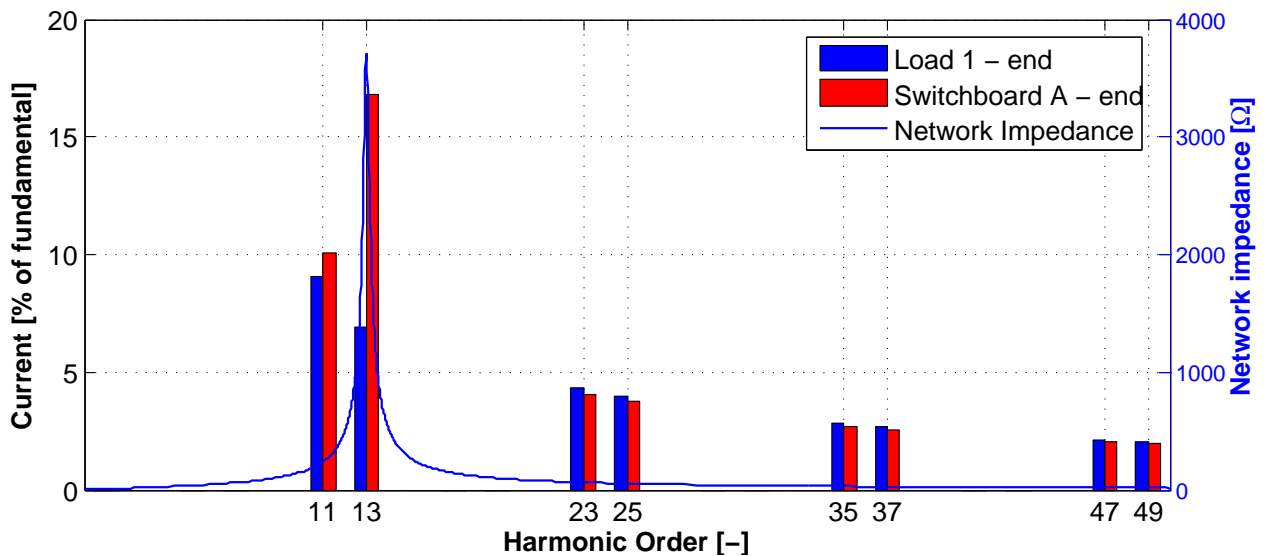


Figure 7.10: Case Study 3: Harmonic currents in *Load Cable 1* with network impedance characteristic seen from *Switchboard A*

Figure 7.11 is added as an explanatory sketch to Figure 7.12. Due to the resonance, a very powerful current amplification occur in the *Supply Cable*. The 13th harmonic current has an amplitude of over 400 Amperes as it is injected into *Switchboard A*.

Very large 13th harmonic current are now injected into *Switchboard A* from *Load Cable 1*, *Load Cable 2* and *Supply Cable*. This results in an extreme 13th harmonic voltage at *Switchboard A*.

Figure 7.13 shows the harmonic voltage spectrum and the network impedance characteristic at *Switchboard A*, along with the individual IEC harmonic voltage limits. The 13th harmonic voltage with a ~ 4.5 pu amplitude, causes a THD of several hundred percent at *Switchboard A*.

The harmonic currents are now fed into the *Step-out Cable*. Since also the capacitance of the *Step-out Cable* is a part of the parallel resonance at harmonic order 13, further amplification occur. The *Step-out Cable* is now relatively short, and its filtering ability of high frequencies, are limited. However, the topside *T5-step-up* transformer, acting as a low-pass filter, dampens the amplitude of high frequency voltage harmonics. The harmonic voltage spectrum at *Topside Main* is presented in Figure 7.14. The resulting

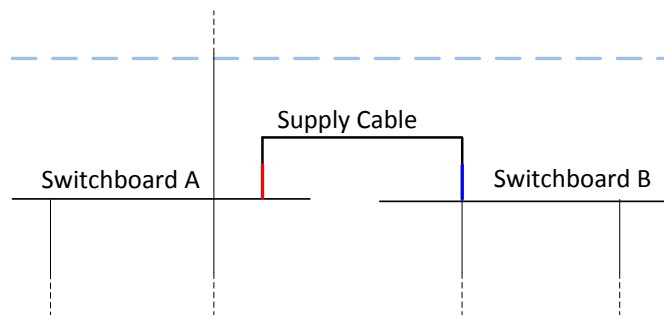


Figure 7.11: Explanatory sketch for Figure 7.12

THD level at *Topside Main* is 127.9 %.

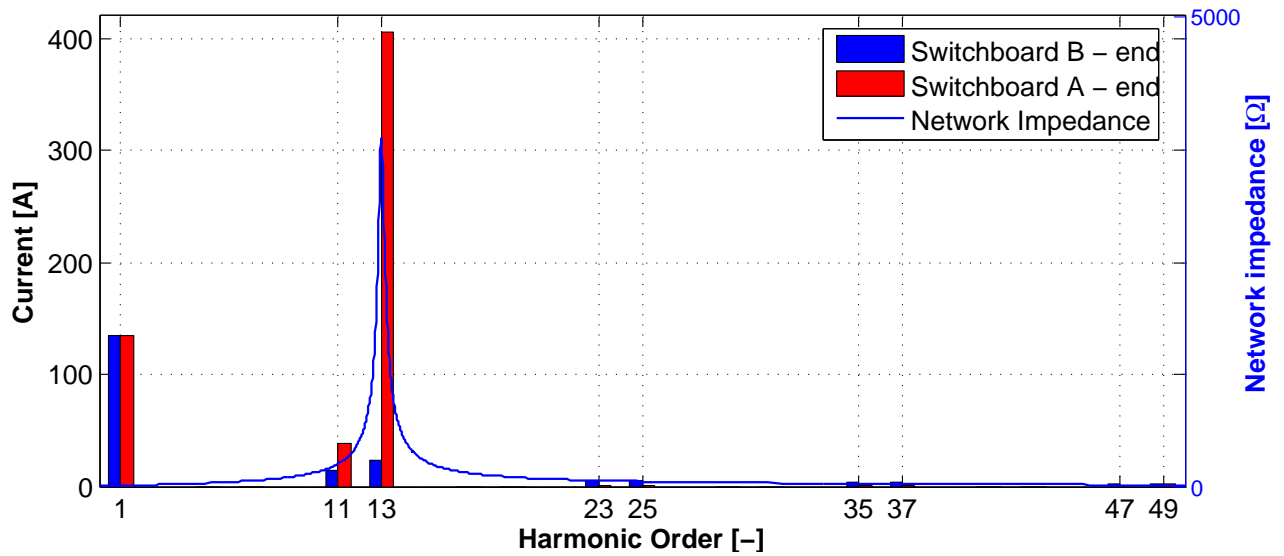


Figure 7.12: Case Study 3: Harmonic currents in *Supply Cable* with network impedance characteristic seen from *Switchboard A*

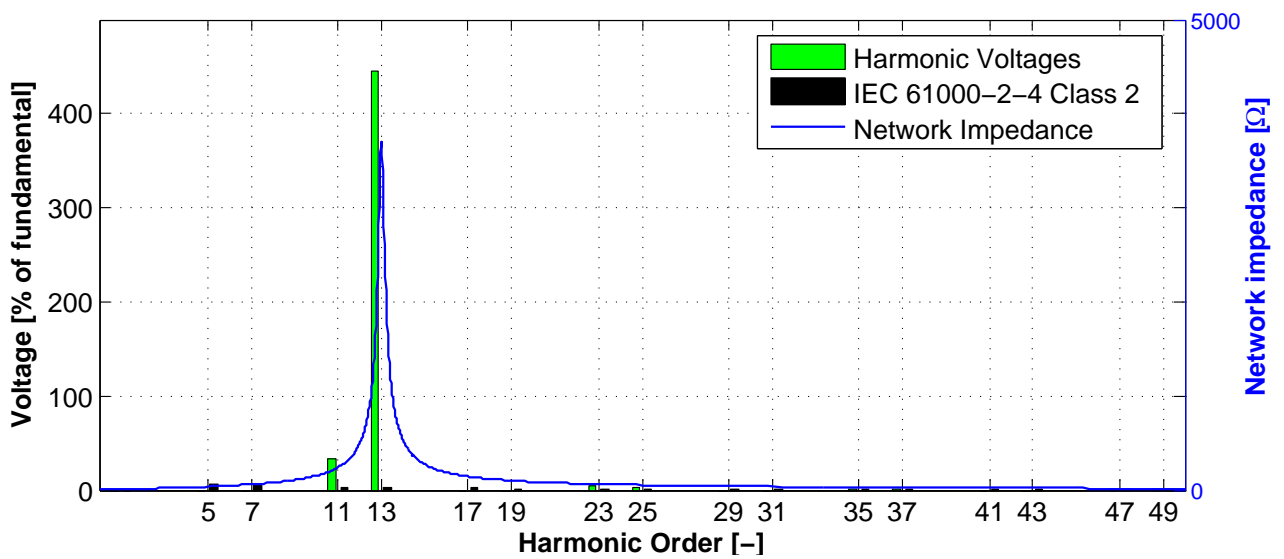


Figure 7.13: Case Study 3: Harmonic voltages and network impedance characteristic seen from *Switchboard A*

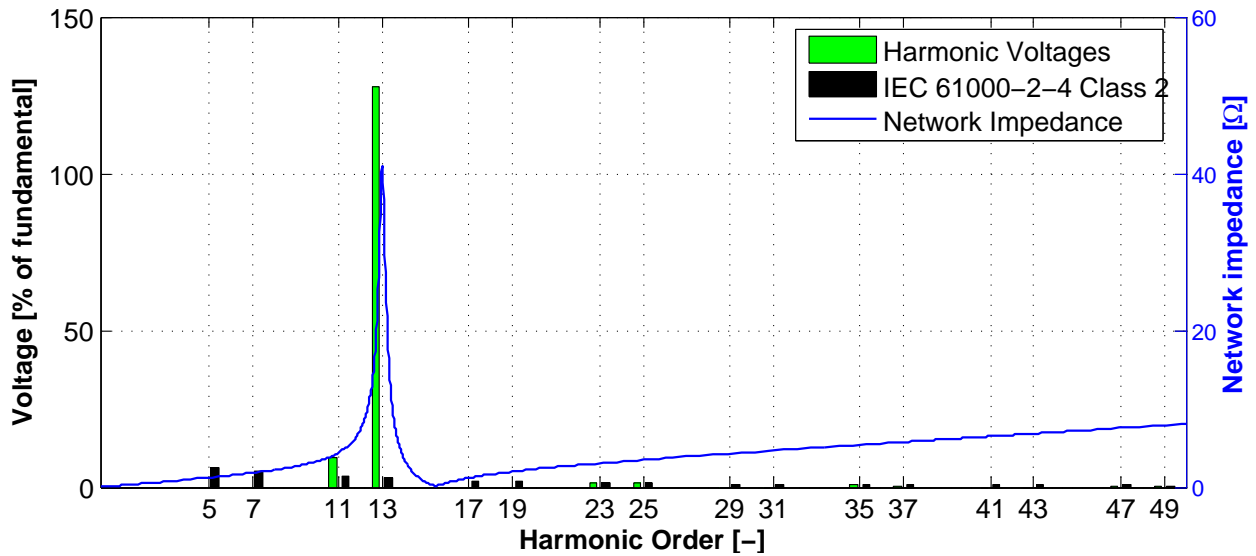


Figure 7.14: Case Study 3: Harmonic voltages and network impedance characteristic seen from *Topside Main*

Although the 13th harmonic voltage is considerably dampened from *Switchboard A* to *Topside Main*, its amplitude is still larger than the fundamental. It is clear that the absence of a subsea step-down transformer, reduces the harmonic filtering considerably.

The inductance of the resonating circuits in this case study, is the short-circuit impedance (leakage inductance) of the topside *T5_step-up* transformer. Currently, this impedance is set to 8 %. However, by slightly changing this impedance, the entire power system’s harmonic behavior changes substantially. Figure 7.15 shows plots of the total amplification of the 11th and 13th harmonic currents, and the *Topside Main* THD level for a varying short-circuit impedance of the *T5_step-up* transformer. With a short-circuit impedance of 8 %, the 13th harmonic current is amplified over 45 times, compared to what is injected by the subsea VSDs. But by only decreasing the short-circuit impedance to 7 %, the total amplification is reduced to under 15 times the injected. Since the resonance occur for a relatively low harmonic order (the 13th) and a short cable (8 km), the parallel resonance top is extremely tall and sharp in its shape. The slightest shift in either direction will therefore have an enormous impact on the network impedance, at frequency close to the resonance frequency.

As the short-circuit impedance increases, the amplification of the 11th harmonic current increases as well. With Equation 3.15 in mind, it is obvious that an increased inductance in a resonating circuit, lowers the circuit’s resonance frequency. The parallel resonance is therefore shifted toward the 11th harmonic, causing an increase of its amplification.

The above illustrates the extreme ”tuning” of a resonating power system. Only a small change in one of the system’s parameters may change the behavior completely, for both the better or worse. A system as the one discussed in this case study would never be built in real life, and THD levels of several hundred percent is also rather unrealistic. The design would be changed long before leaving the drawing board. However, Case Study 3

emphasizes the importance of a thorough and detailed harmonic and resonance analysis early in the designing process of a subsea power system.

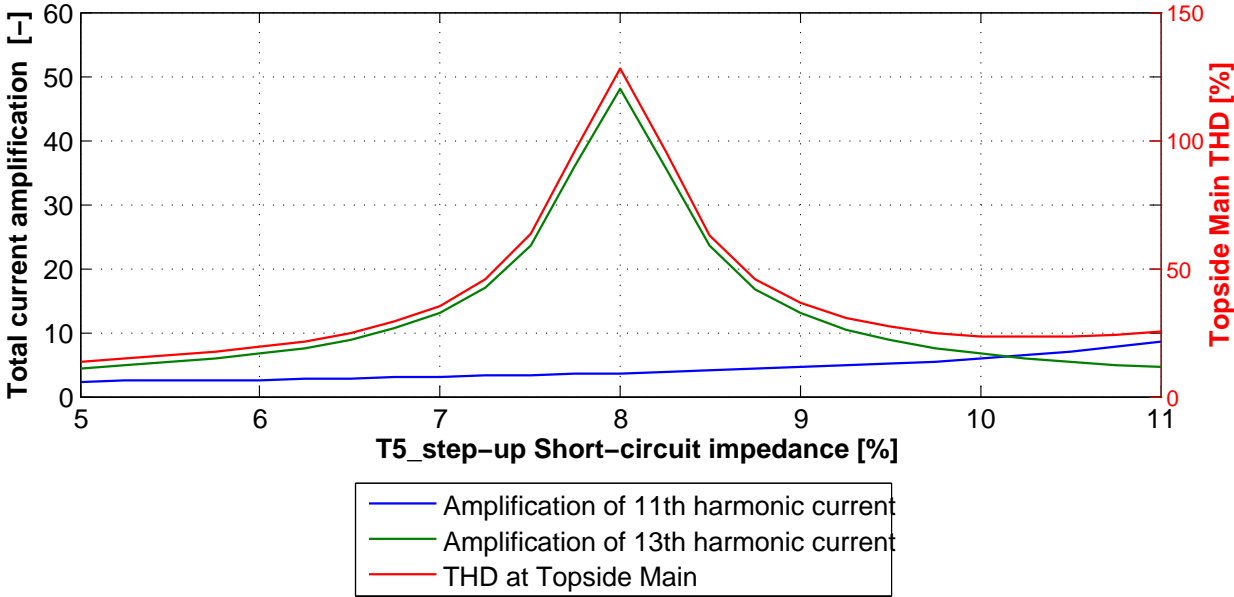


Figure 7.15: Harmonic current amplification for varying *T5_step-up* transformer short-circuit impedance

7.4 Case Study 4: *Short Step-out* Lower THD Scenario

This section will investigate the harmonic content of a *Short Step-out* variant with relatively low levels of harmonic disturbance. In addition, measures to obtain acceptable THD levels will be discussed and tested, if needed. Table 7.3 presents the cable lengths describing the variant under consideration. Note that the length of the *Supply Cable* is set to zero. This means that all four pump loads are connected to the same subsea busbar. The network model has therefore been slightly altered. All four loads are now connected to *Switchboard A*. *Supply Cable* and *Switchboard B* have been removed from the system.

Cable	Length [km]
Step-out Cable	25
Supply Cable	0
Load Cable 1	0.06
Load Cable 2	0.06
Load Cable 3	0.06
Load Cable 4	0.06

Table 7.3: Cable lengths for Case Study 4

Since the four subsea pump loads now are connected to one common busbar, have equal load cable lengths, cable types and load characteristics, the current spectra are equal for all four load cables. Figure 7.17 shows the current spectra of both ends of *Load Cable 1* through *Load Cable 4*, in addition to the network impedance characteristic of *Switchboard A*. An explanatory sketch is presented in Figure 7.16.

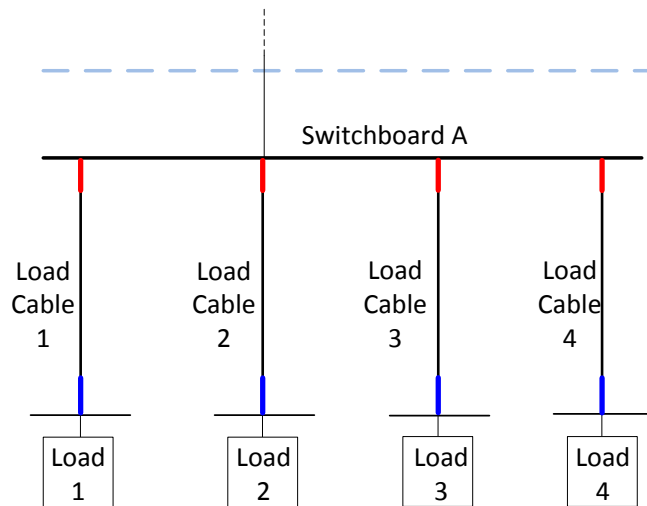


Figure 7.16: Explanatory sketch for Figure 7.17

Nearly no harmonic current amplification occurs through the load cables. Since the *Step-out Cable* is 25 km long, its resonance frequency is lower than the 11th harmonic which can be seen in the plot of the network impedance characteristic, which now is dominated by the *Step-out Cable*'s impedance. Further, Figure 7.18 shows the harmonic voltage spectrum and network impedance characteristic at *Switchboard A*, along with the individual IEC 61000-2-4 Class 2 limits. Here, the relation between network impedances and generated harmonic voltages are particularly visible. The 23rd and 25th harmonic currents experiences a very low network impedance at *Switchboard A*, and very low harmonic voltages are generated at these harmonic orders. On the other hand, the 11th, 13th, 47th and 49th harmonic currents experiences a much larger network impedance at *Switchboard A*, due to their

vicinity to parallel resonances. The generated harmonic voltages are therefore far larger at these harmonic orders.

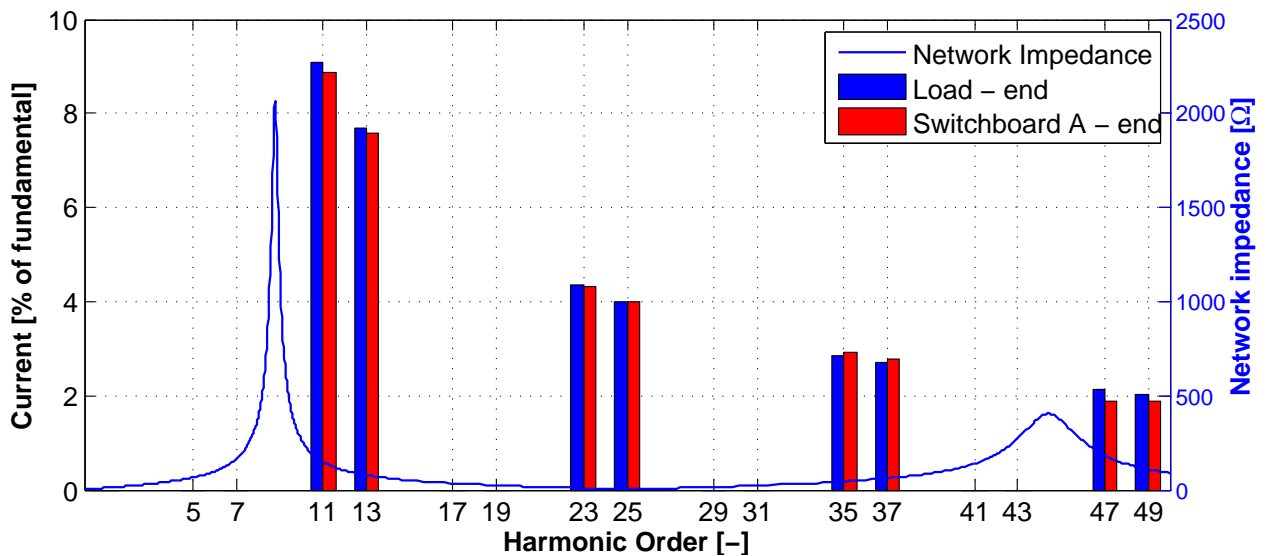


Figure 7.17: Case Study 4: Harmonic currents in *Load Cable 1* through *Load Cable 4* with network impedance characteristic seen from *Switchboard A*

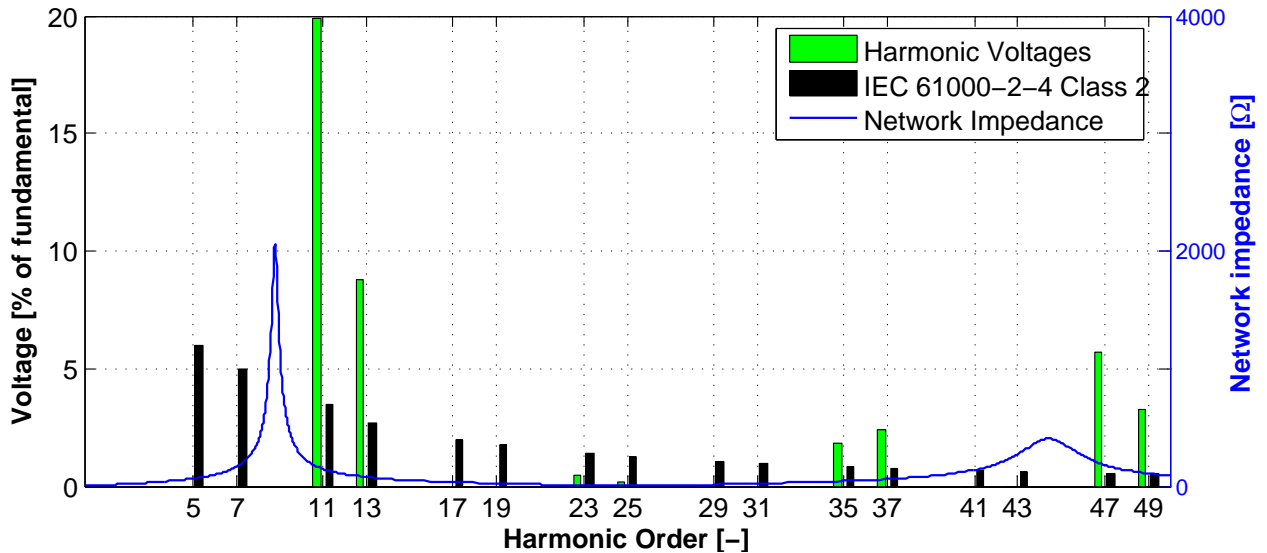


Figure 7.18: Case Study 4: Harmonic voltage spectrum and network impedance characteristic seen from *Switchboard A*

Although no harmonic current amplification occur, the voltage harmonic content at *Switchboard A* is too high. The 11th, 13th, 35th, 37th, 47th and 49th harmonic voltages are all above their individual IEC limits, and the resulting THD level is 22.7 %.

The harmonic current contribution from *Load Cable 1* through *Load Cable 4* are further injected into the *Step-out Cable*. Figure 7.20 presents the harmonic current spectra

in both ends of the *Step-out Cable*, in addition to the network impedance characteristic of the *Topside HV* busbar. Figure 7.19 offers an explanatory sketch for the spectra in Figure 7.20.

Due to the vicinity to a parallel resonance between the capacitance of the *Step-out Cable* and the inductance of *T5_step-up* transformer, a quite large current amplification of the 11th harmonic current occurs through the *Step-out Cable*. The remaining current harmonics are considerably dampened through the same cable, due to its filtering effect of higher frequencies.

Figure 7.21 shows the harmonic voltage spectrum and network impedance characteristic at *Topside Main*. The harmonic voltage filtering ability of a transformer now becomes clear. All harmonic voltages except the 11th, 37th, 47th and 49th are reduced in magnitude to levels equal or below the IEC 61000-2-4 Class 2 limit. The *Topside Main* THD level is now only 6.5 %.

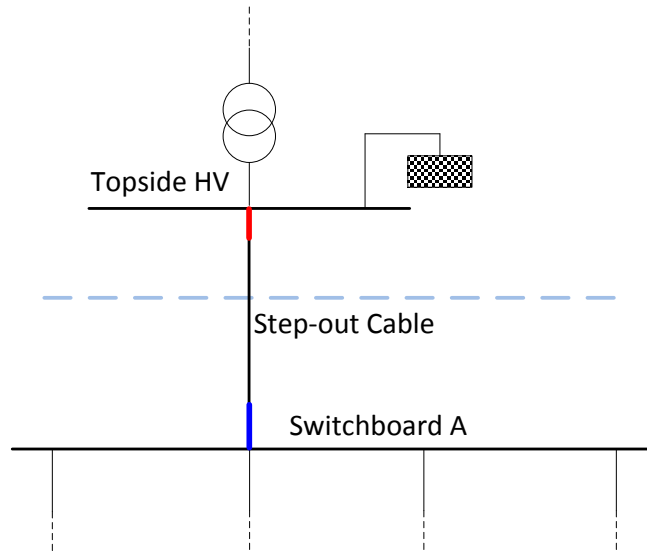


Figure 7.19: Explanatory sketch for Figure 7.20

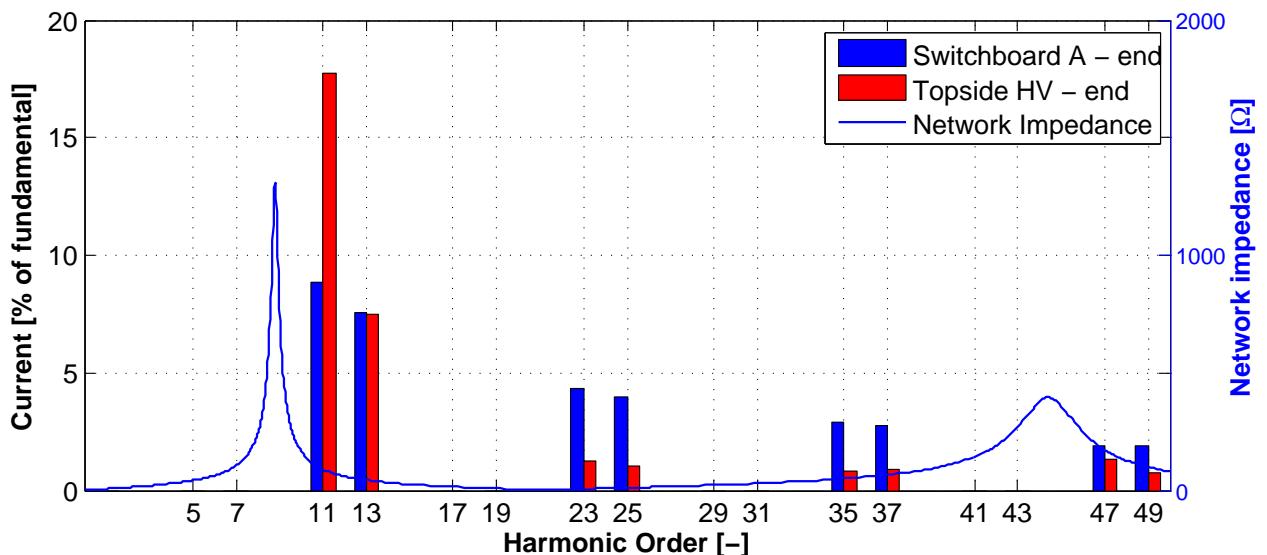


Figure 7.20: Case Study 4: Harmonic currents in *Step-out Cable* with network impedance characteristic seen from *Topside HV*

Even though the *Topside Main* THD level in the case described above is within the

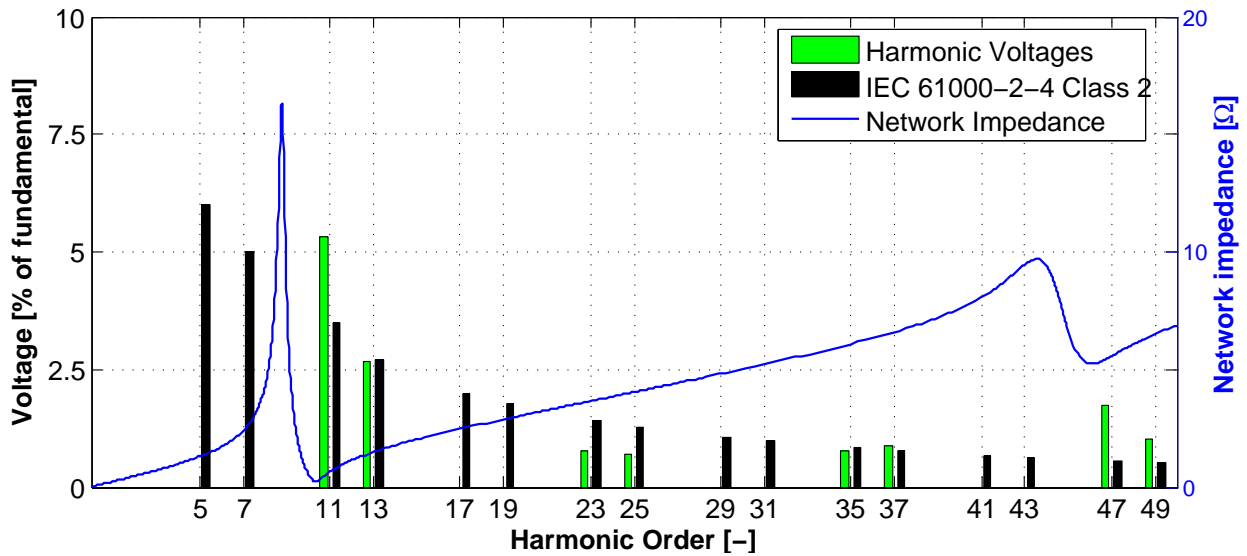


Figure 7.21: Case Study 4: Harmonic voltage spectrum and network impedance characteristic seen from *Topside Main*

IEC limit, the harmonic content at *Topside HV* and *Switchboard A* are too high, with THD levels of 20.1 and 22.7 %, respectively. Since the 11th and 13th harmonic voltages are the most responsible for the large THD levels, a natural way to reduce the harmonic content would be to change the 12-pulse rectifiers with 24-pulse rectifiers. Ideally, no currents of harmonic orders 11, 13, 35 and 37 would then be injected into the power system, thus lowering the busbars' THD levels.

By modifying the 12-pulse rectifiers to inject 24-pulse current spectra, as was done in the analysis of the *Long Step-out*, new THD levels and voltage spectra have been calculated. The harmonic voltage spectra of such a system are identical to those presented above (Figure 7.18 and 7.21), only without the presence of the 11th, 13th, 35th and 37th harmonics. The THD levels for a system utilizing 24-pulse rectifiers instead of 12-pulse rectifiers have been calculated to be 6.5 % at *Switchboard A*, 7.0 % at *Topside HV* and 2.3 % at *Topside Main* which are all below the IEC limit. So far, the situation seems fine. However, from the voltage spectra presented above, we know that the 47th and 49th harmonic voltages violates the individual harmonics' limits at all busbars. At *Topside HV*, the 23rd and 25th harmonic voltages are above the limit, as well.

Such a problem where the THD level is acceptable, but certain harmonics are too large (with respect to the utilized standard), may happen in the designing process of any electrical power system. One must then decide if the situation is acceptable, or if measures should be taken to reduce the harmonics further. Increasing the number of pulses or installing harmonic filter may be relevant. This would depend on the power system itself (e.g. presence of possible sensitive equipment), the possibility of harmonic mitigation measures, and of course the cost of further harmonic reduction.

7.5 General Observations for the *Short Step-out*

From the Series Scan simulations in Section 7.1, it was found that short lengths of the *Step-out Cable* caused the highest THD levels. The high THD levels were mainly caused by harmonic orders 11, 13 and 23. However, as the length of the *Step-out Cable* increases the amplitudes of the parallel resonance tops are reduced to more or less harmless magnitudes.

Without a subsea step-down transformer, the branches of the *Short Step-out* are electrically much stronger connected, than was the case for the *Long Step-out*. A parallel resonance in one part of the system therefore infects the entire system, causing the risk of getting current amplification several places simultaneously, for the same harmonic order. Case Study 2 investigated such a scenario, where the 13th harmonic current was amplified through several cables. On the other hand, the lack of a large subsea series impedance causes a long *Step-out Cable* to become very dominant in determining the network impedance characteristics of the system. When the *Step-out Cable* is set to 60 km, the remaining cables have very little influence on the network impedance characteristics, and the system's THD levels.

The above analysis of the *Short Step-out* has only been done with 12-pulse rectifiers. To understand the influence of the different harmonic, Series Scan simulations have been conducted with specified harmonic current injections. Figure 7.22 and 7.23 shows the THD plots of the topside and subsea busbars, along with the corresponding cable length variation order. Here, the injected harmonic current spectra of the subsea VSD only contains the 11th and 13th harmonic current (along with the fundamental). The harmonic contribution of the *Topside SVC* is also removed.

These THD plots are very similar to those of Figure 7.3 and 7.4, implying that the 11th and 13th harmonic currents are the main cause of the high THD levels found earlier. Figure C.10, C.11 and C.12 in Appendix C.2.2 presents similar simulations, where only the 23rd and 25th, 35th and 37th, 47th and 49th harmonic currents are injected by the VSDs. From these results, the 11th and 13th harmonic currents clearly causes the most problematic harmonic conditions, whereas the 35th, 37th, 47th and 49th causes the least problems. By simply changing the 12-pulse rectifier with 24-pulse rectifier will reduce the harmonic problems considerably.

By identifying the importance and influence of the different harmonic for a specific topology variant, the system designer can choose the best fitting rectifier type. A 12- or 24-pulse rectifier might be enough to keep the harmonic low, instead of installing a more complex and expensive 36-pulse rectifier.

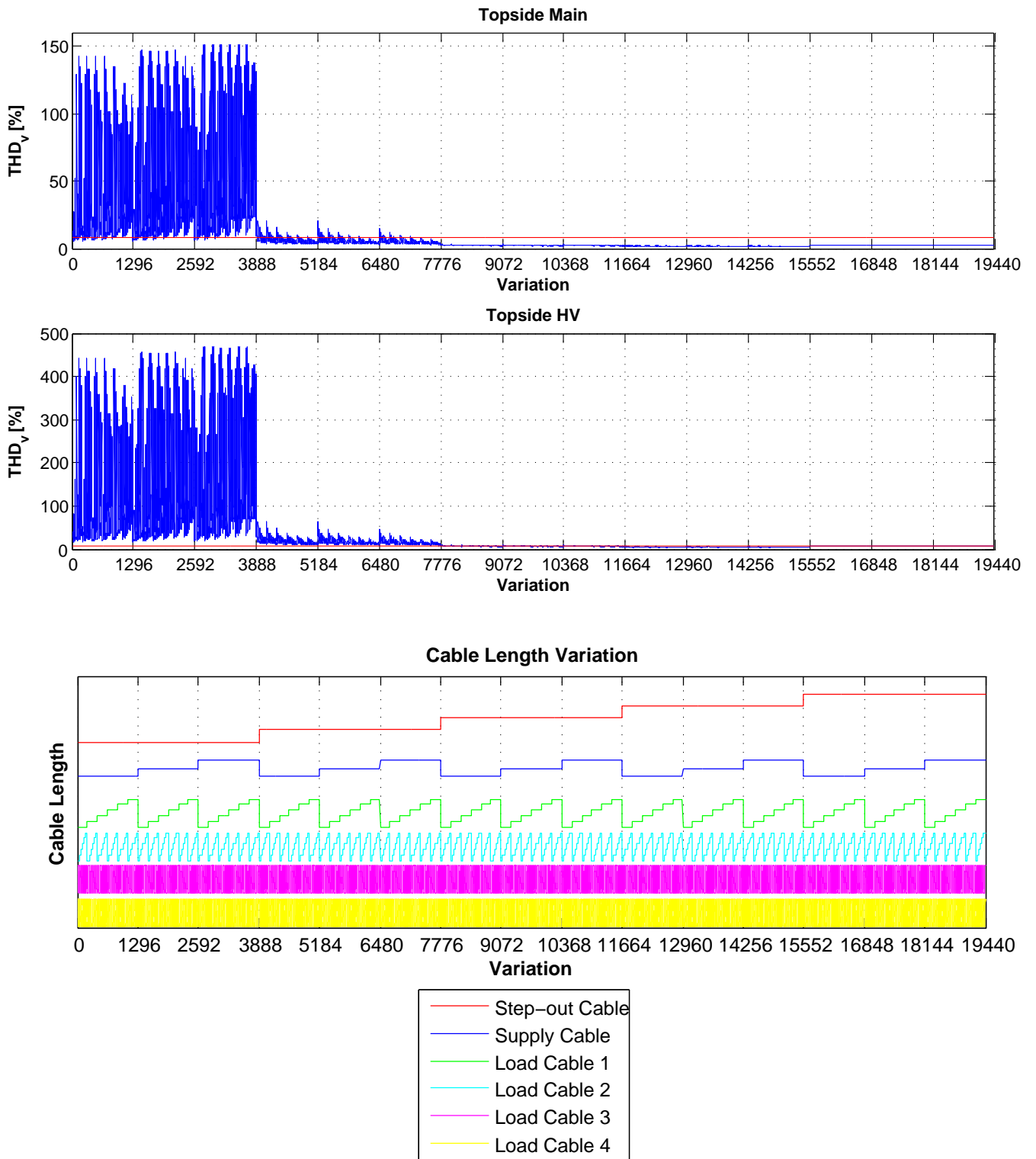


Figure 7.22: Topside busbars' THD levels caused by the 11th and 13th harmonic current, only

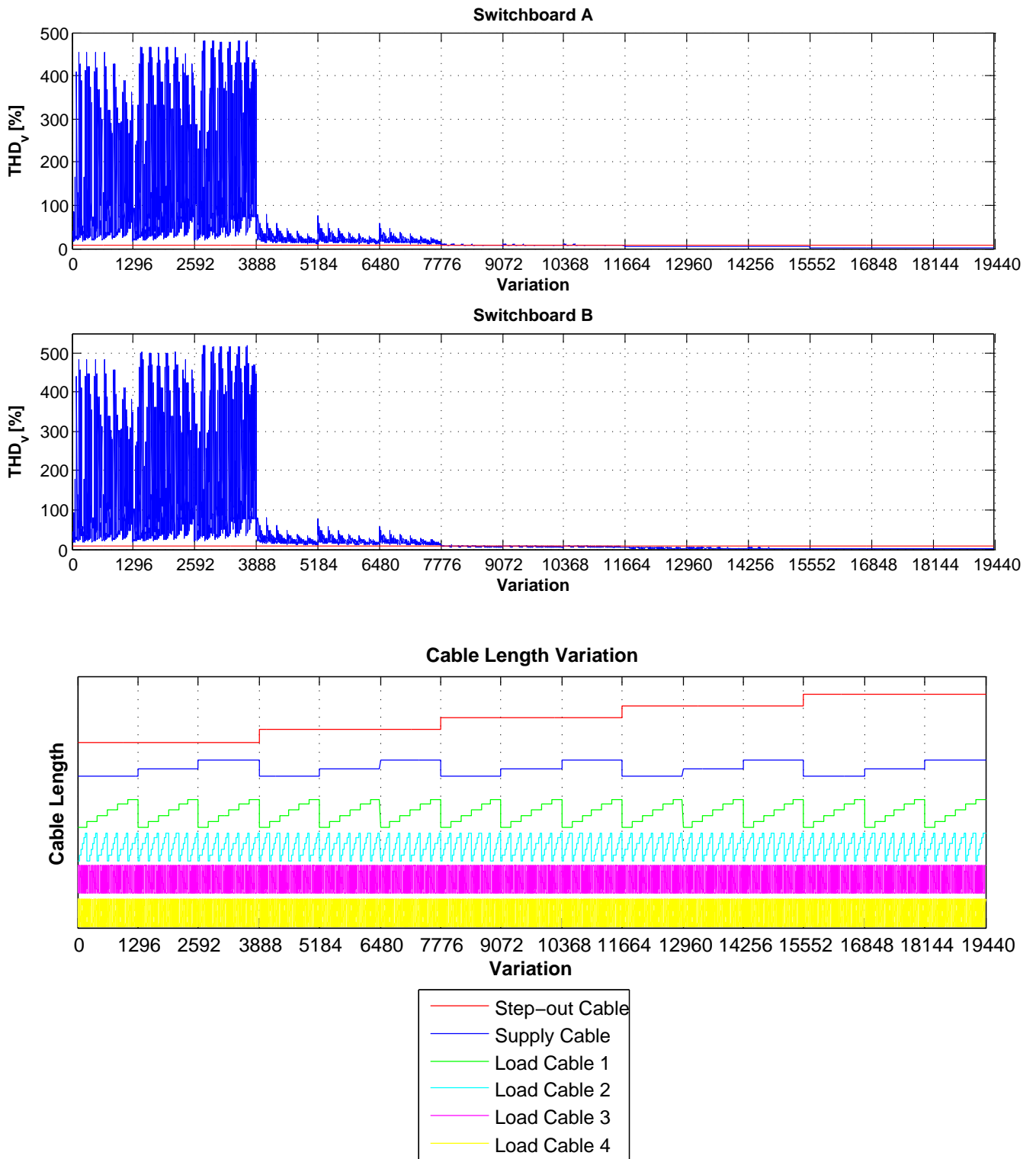


Figure 7.23: Subsea busbars' THD levels caused by the 11th and 13th harmonic current, only

8 Discussion

The models constructed in this thesis are further developed and refined versions of those constructed and analyzed in the specialization project, fall 2014. As found in Section 6.1, frequency-dependent cable resistances have very large influence on the systems THD levels, and are therefore required to obtain quantitatively trustworthy results. To further increase accuracy, frequency-dependent inductances should be included in the cable model.

Throughout the simulations and case studies conducted in this thesis, very high levels of harmonics have been observed. In many cases, unrealistically high. It is therefore important to reveal the possible modeling weaknesses, and to get a grasp on how conservative the results really are.

In the studies conducted, the theoretical harmonic current spectra of 6- and 12-pulse rectifiers have been utilized. The EMT-simulation test in Section 3.1.1 showed that the AC-side current of a 6-pulse rectifier, is not equal to the current resulting from the ideal-rectifier simplification. By conducting an EMT-simulation test on a 12-pulse rectifier setup, an alternative harmonic current injection has been found. This gives an indication of how conservative the simplification on theoretical rectifiers are. The test-configuration was done as follows;

A long cable connects a grid element to a 12-pulse rectifier with accompanying DC-load. The cable, rectifier and load are identical to those supplying the gas compressor load from *Switchboard A*, in the *Long Step-out*. The cable length has in this case been increased to 50 km to weaken the power system at the rectifier - end of the cable. A 2 mF smoothing capacitor is included at the rectifier's DC-bus. An EMT-simulation has been conducted. The rectifiers are now modeled by their diodes, as depicted in Figure 3.5. A harmonic current spectrum has been calculated from Fourier analysis, based on the current waveform. Figure 8.1 shows both the theoretical 12-pulse rectifier spectrum, and the harmonic current spectrum found from the EMT-test.

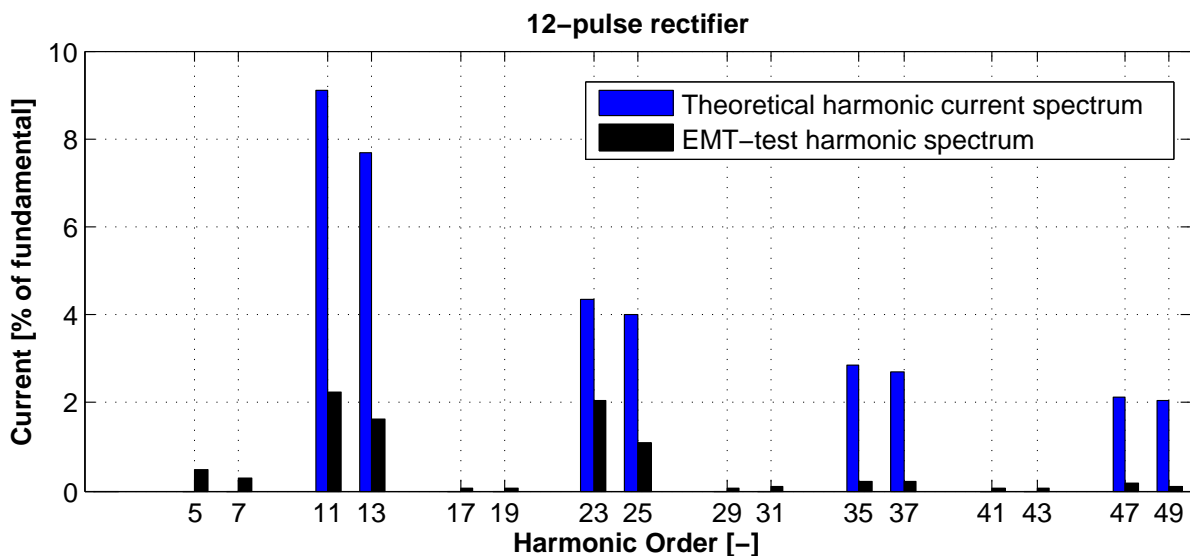


Figure 8.1: Comparison of theoretical- and EMT-test's harmonic current spectra

Although the accuracy of the simplified EMT-simulations test can be questioned, Figure 8.1 indicates that the use of theoretical harmonic current injections possibly is a *too* conservative simplification to obtain quantitatively trustworthy results. To illustrate the impact the change on injected current spectra may have on the results, the THD levels of Case Study 1 and 2 (the two study cases of the *Long Step-out*) have been re-calculated, utilizing the EMT-test’s harmonic current spectra (black current spectrum in Figure 8.1). Table 8.1 shows the results.

Busbar	Case Study 1		Case Study 2	
	Theoretical spectrum, THD [%]	EMT-test spectrum, THD [%]	Theoretical spectrum, THD [%]	EMT-test spectrum, THD [%]
Topside Main	14.9	5.8	0.9	0.4
Topside HV	34.0	13.2	2.2	0.9
Switchboard A	221.6	22.7	20.0	4.1
Switchboard B	147.9	67.2	19.9	4.1

Table 8.1: THD levels in Case Study 1 and 2 with the EMT-test’s harmonic current spectra

Especially as the THD levels are very large, the use of the EMT-test harmonic current spectra gives more realistic and trustworthy results. Mohan, Undeland and Robbins [9] proposes a typical 6-pulse rectifier spectrum which is considerably lower than the theoretical. From the industry, alternative harmonic current spectra are proposed by ABB and Siemens as typical for AC drives [23, 24]. Also these, with considerably lower amplitudes than the theoretical spectrum. Common to the spectra of Mohan, Undeland and Robbins, ABB, Siemens as well as the EMT-test’s spectrum, are lowered amplitudes of the higher harmonic currents. This would lead to lowered harmonic voltages throughout the systems. Although the results found in this thesis might be questionable from a quantitatively point of view, the results should still be of some qualitative value.

Both the DC-loads representing the compressor- and pump loads, and the VSD rectifiers were modeled as harmonics current sources during the network modeling in this thesis. When utilizing the built in rectifier model, it is automatically modeled as a harmonic current source under Harmonic Load Flow calculations. The user has therefore no choice but to use the current source model. The DC-loads on the other hand, have been modeled as current source due to its behavior corresponds best to the real components’ behavior. Alternatively, the load could be modeled using an impedance model. When the system impedance matrix is calculated, current sources are set to zero Ampere (open-circuit) and voltage sources are set to zero Volt (short-circuit), as discussed in Section 5.1.3. As the current sources in the rectifier models are set to zero, the DC-loads are isolated from the system, therefore not affecting the impedances when viewed from the cable system (e.g. *Switchboard A* or *Switchboards B*). With the rectifier current sources always determining the current spectra, the modeling of the DC-loads have very little influence on the Harmonic Load Flow calculation. Its only task would be to assure a correct fundamental load current. Tests, where the current source DC-loads have been substituted with impedance model DC-loads, have been conducted with clear results. Neither the network impedance characteristics nor the THD levels were influenced by the load model change.

Especially in the simulations of the worst-case scenarios, extreme harmonic current amplifications were found. Leading to THD levels of several hundred percent, the results are quantitatively not trustworthy. Whenever the very large THD levels occurred, harmonic current amplification was present in the system. In Section 3.3 the mechanisms causing current amplification, was discussed. The enormous influence of the systems resistances were illustrated through an example (Figure 3.15). By changing the resistance of the network equivalent $Z_{network}$ from 1 to 20 Ω , the current amplification at resonance was reduced from ~ 9 times to below 2 times the injected current. It is therefore natural to question the resistances of the system, due to the extreme current amplification observed in the results.

With both frequency-dependent and temperature corrected resistances, the subsea cables' conductor resistances should be fairly accurate. The transformers' copper- and no-load losses on the other hand, are mostly based on estimates from traditional topside transformers of similar power ratings. With the extreme influence of certain parameters, illustrated by changing the topside transformer's short-circuit impedance in Section 7.3, it is clear that an accurate transformer model is essential. To increase the credibility of the results, the transformer copper- and core losses should be revisited.

Since the type of network topologies considered in this thesis (systems with subsea VSDs) are mainly on the drawing board- and pilot project stage, openly accessible literature are hardly available. Data sheets of subsea power components (as transformers and VSDs) are also not easily available. Some of the system's electrical component parameters are therefore estimates or approximations based on traditional electrical components for on-shore/topside applications. Ideally, with full access to component parameters, it should be possible to make the models more accurate. However, considering the preconditions and time constraint of this thesis, reasonably acceptable network models have been constructed.

It should be mentioned that utilizing 12-pulse rectifiers in the subsea VSDs, as has been done in this thesis, is not very realistic. Especially for the larger loads, a 24- or 36-pulse would be more relevant. However, by conducting the simulations with 12-pulse rectifiers, the thesis also becomes a feasibility study for usage of 12-pulse VSD rectifiers. In addition, it reveals which harmonics that *really* are the cause of the problems, which could simplify the process of harmonic mitigation.

9 Conclusion

The results from the simulations and analysis' done in this thesis have emphasized the importance of a detailed and thorough harmonic and resonance analysis of subsea electrical power systems. To avoid ending up with a malfunctioning power system, the harmonic study should be conducted early in the designing process of the power system. Section 6.1 clarified the importance of utilizing frequency-dependent cable resistances in the network model. As was discussed in Section 7.3, the smallest change in a system parameter, may change the entire system's harmonic behavior. An accurate network model is therefore *very* important to obtain trustworthy results.

Based on the EMT-simulation test conducted in the Discussion (Section 8), it was found that the theoretical harmonic current injections utilized in this thesis, most likely generated *too* conservative results. The harmonic content becomes unnaturally high, and the results are not completely trustworthy, from a quantitative point of view. By utilizing more realistic harmonic current injections, the results would become increasingly realistic. Such a simplification should therefore be used with caution, and preferably avoided when the harmonic sources/loads are of large current ratings and dominating in the power system. However, the analysis' conducted above still offers some qualitatively trustworthy results.

In the analysis of the *Long Step-out* topology, it became clear that parallel resonances between the load- and supply cables, and the subsea step-down transformer, were the most problematic harmonic and resonance phenomena. Due to the large short-circuit impedances of the transformer, these resonances appear more or less "local" in the system, not spreading to other busbars. However, heavily amplified harmonic currents could spread throughout the system, causing very large harmonic voltages at the other busbars. Case Study 1 in Section 6.3, illustrated this phenomenon clearly. On the other hand, the presence of a subsea transformer leads to a very efficient LCL low-pass filter in the system, keeping especially the *Topside Main* THD levels low. Viewed from topside, the system performance could therefore seem acceptable, while the subsea voltages could be heavily distorted, and exceed the IEC requirements. Due to its very long length, the Step-out Cable of the *Long Step-out* have a very low resonance frequency (lower than the lowest injected current's harmonic order). Resonance phenomena in the Step-out Cable is therefore *not* the main concern of the *Long Step-out* topology.

Based on the above, it is clear that under analysis of subsea power systems of the same principle construction as the *Long Step-out*, the *subsea* busbars are the main concern with respect to harmonic content. If the harmonic orders of interest is limited to, let us say, harmonic order 50, the load- and supply cables may be disregarded, but *only* if their lengths are *very* short. In this case, the cables resonance frequency will become higher than the frequency-range of interest. However, as a rule, *all cables* should be included in a simulation model with the presence of a subsea step-down or distribution transformer.

In contrary to the *Long Step-out*, there is no subsea step-down transformer in the *Short Step-out* topology, which changes the harmonic behavior substantially. Due to the strong coupling between the system busbars, a possible parallel resonance infects the network impedance characteristic at all system busbars. With the Step-out Cable usually being

the longest, and therefore the most influential on the network impedance characteristics, resonance in the Step-out Cable is the most serious concern in the *Short Step-out* topology. With less harmonic filtering (no subsea step-down transformer), the topside harmonic voltages may become very large. The topside THD levels for the *Short Step-out* are therefore relatively representative for the THD levels subsea, compared to what was the case for the *Long Step-out*.

Due to the strong connection between the busbars and the lack of a subsea step-down transformer, the harmonic behavior is more predictable for the *Short Step-out*, than for the *Long Step-out*. As long as one cable is considerably longer than the others, this cable determines possible parallel resonances. The load- and supply cables may therefore be disregarded in an introductory analysis, simplifying the system modeling. However, it must be emphasized that this only applies as long as the Step-out Cable is very long and the remaining cables are very short.

For both the *Long Step-out* and the *Short Step-out*, a very long step-out cable and very short subsea supply- and load cables are preferable to minimize the harmonic voltage content. Consequently, shifting the step-out cable's resonance frequency to a lower frequency than the lowest injected harmonic current, and shifting the supply- and load cables' resonance frequencies as high as possible.

Further Work

In the Discussion section it was revealed that the theoretical harmonic current injections used, most likely are too deviant from the actual harmonic current. The simplification led to too conservative results. By conducting detailed analysis' on 6- and 12-pulse rectifiers, more realistic injected harmonic current spectra could be derived and used in calculations. The modeling possibilities of rectifiers during Harmonic Load Flow calculations in PowerFactory, are quite limited. Either EMT-simulations in PowerFactory or other simulation software should be utilized to increase the accuracy of the harmonic current injections. This would lead to more trustworthy results and would be very important in the continuation of studying such networks.

This thesis has focused on a wide range of topology variants, and only analyzed a few of them in detail. The harmonic current injections caused by the subsea VSDs have been in focus. However, a large part of the topside loads on a oil platform are in fact VSD driven electrical machines. Studying the entire system as a whole and investigating the interaction between the topside and subsea power system could be a direction for further work.

In the designing process of a subsea power system as those discussed in this thesis, the designer will be bound by some constraints. For instance, the cable lengths might have an absolute minimum length due to the physical distance between the utility and the loads. Further, upper cable length limits could possibly be determined from economical (or technical) constraints. In the same way, the designer might have the possibility to alter the short-circuit impedances of transformers by, let's say, $\pm 1\%$. With the definition of such designing constraints, modified versions of the series scan simulation scripts developed in this thesis could be utilized to find the optimal design to assure minimal levels of harmonics. The script could be modified to also include change in short-circuit impedances, cable

types, pulse number of the rectifiers etc.. By also including the economical perspective with additional cost of e.g. a slightly longer cable, a cost-benefit analysis would become possible. Such a tool could be developed, and might be useful in the designing process of a subsea power system.

The topic of this thesis is highly relevant for the offshore petroleum industry, especially in Norway where all the oil and gas reservoirs are located offshore. Companies as ABB, Siemens, GE and Schneider Electric are constantly working to improve the subsea power components and networks, in close cooperation with operator companies such as Statoil. Having a partner from the industry or a manufacturer is very valuable, and contributes to being updated on the latest technical developments, known issues and relevant challenges.

References

- [1] Ø. Garvik, “Oil & Gas Subsea Transmission and Distribution Networks,” Specialization project at NTNU, December 2014.
- [2] *NEK IEC 61000-2-4, Electromagnetic Compatibility (EMC) - Part 2-4: Environment Compatibility levels in industrial plants for low-frequency conducted disturbances*, 2.0 ed., Norsk Elektroteknisk Komité, 2002.
- [3] Baerd, Normann, Hazel, “Ormen Lange Subsea Compression Station Pilot,” PCIC Europe 2010 Conference Record, 2010.
- [4] S. Midttveit et al, “Subsea Electrical Power Standardization,” PCIC Europe IS-50, 2013.
- [5] X. Liang, W. Jackson, “Influence of Subsea Cables on Offshore Power Distribution Systems,” Industry Applications Society Annual Meeting, IEEE, 2008.
- [6] C. Chien, R.W.G. Bucknall, “Theoretical aspect of the harmonic performance of subsea AC transmission systems for offshore power generation schemes,” *IEE Proceedings - Generation, Transmission and Distribution*, vol. 153, no. 5, September 2006.
- [7] R. Råd, “Converter Fed Subsea Motor Drives,” Ph.D. dissertation, Norges Tekniske Høgskole, 1995, Institutt for Elkraftteknikk.
- [8] B. Monsen et al, “Åsgard Subsea Gas Compression - Technology Qualification Testing With High-Speed VSD and Very Long Step-Out Cable,” *IEEE Transactions on Industry Applications*, vol. 50, no. 2, March/April 2014.
- [9] Mohan, Undeland, Robbins, *Power Electronics*, 3rd ed. John Wiley & Sons, Inc., 2003.
- [10] *SVS - Static Var System, ElmSvs*, DIgSILENT PowerFactory, Technical Reference Documentation.
- [11] K. D. Patil, W. Z. Gandhare, “Effects of Harmonics in Distribution Systems on Temperature Rise and Life of XPLE Power Cables,” 2011 International Conference on Power and Energy Systems, ICPS, December 2011.
- [12] *IEEE 519-2014, IEEE Recommended Practice and Requirements for Harmonic Control in Electrical Power Systems*, Institute of Electrical and Electronics Engineers, 2014.
- [13] *Two-Winding Transformer (3-phase), ElmTr2*, DIgSILENT PowerFactory, Technical Reference Documentation.
- [14] *Overhead Line Models, TypLne, TypGeo, TypTow*, DIgSILENT PowerFactory, Technical Reference Documentation.
- [15] *NEK IEC 60287-1-1, Electric cables, Calculation of the current rating, Part 1-1: Current rating equations and calculation of losses*, 2.1 ed., Norsk Elektroteknisk Komité, 2014.

- [16] *NEK IEC 60228, Conductors of insulated cables*, 3.0 ed., Norsk Elektroteknisk Komité, 2004.
- [17] D. Locke, *Guide to the Wiring Regulations: 17th Edition IEE Wiring Regulations (BS 7671:2008)*. John Wiley & Sons Ltd, 2008, Electrical Contractors' Association.
- [18] *Rectifier/ Inverter, ElmRec, ElmRecmono, TypRec*, DIgSILENT PowerFactory, Technical Reference Documentation.
- [19] *NEK IEC 60076-5, Power transformers - Part 5: Ability to withstand short-circuit*, 3.0 ed., Norsk Elektroteknisk Komité, 2006.
- [20] J. Song-Manguelle et al, "Power Transfer Capability of HVAC Cables for Subsea Transmission and Distribution Systems," *IEEE Transactions on Industry Applications*, vol. 50, no. 4, July/August 2014.
- [21] *AC - Voltage Source, ElmVac*, DIgSILENT PowerFactory, Technical Reference Documentation.
- [22] *AC - Current Source, ElmIac*, DIgSILENT PowerFactory, Technical Reference Documentation.
- [23] *Technical guide No 6, Guide to harmonics with AC drives*, ABB, 2013.
- [24] *Harmonics in power systems, Causes, effects and control*, Siemens, May 2013.
- [25] *XLPE Submarine Cable Systems, Attachment to XLPE Land Cable Systems - User's Guide*, 5th ed., ABB, March 2010.
- [26] *Submarine Power Cables*, Nexans, June 2013.

A General

A.1 Frequency-Dependent Cable Resistances

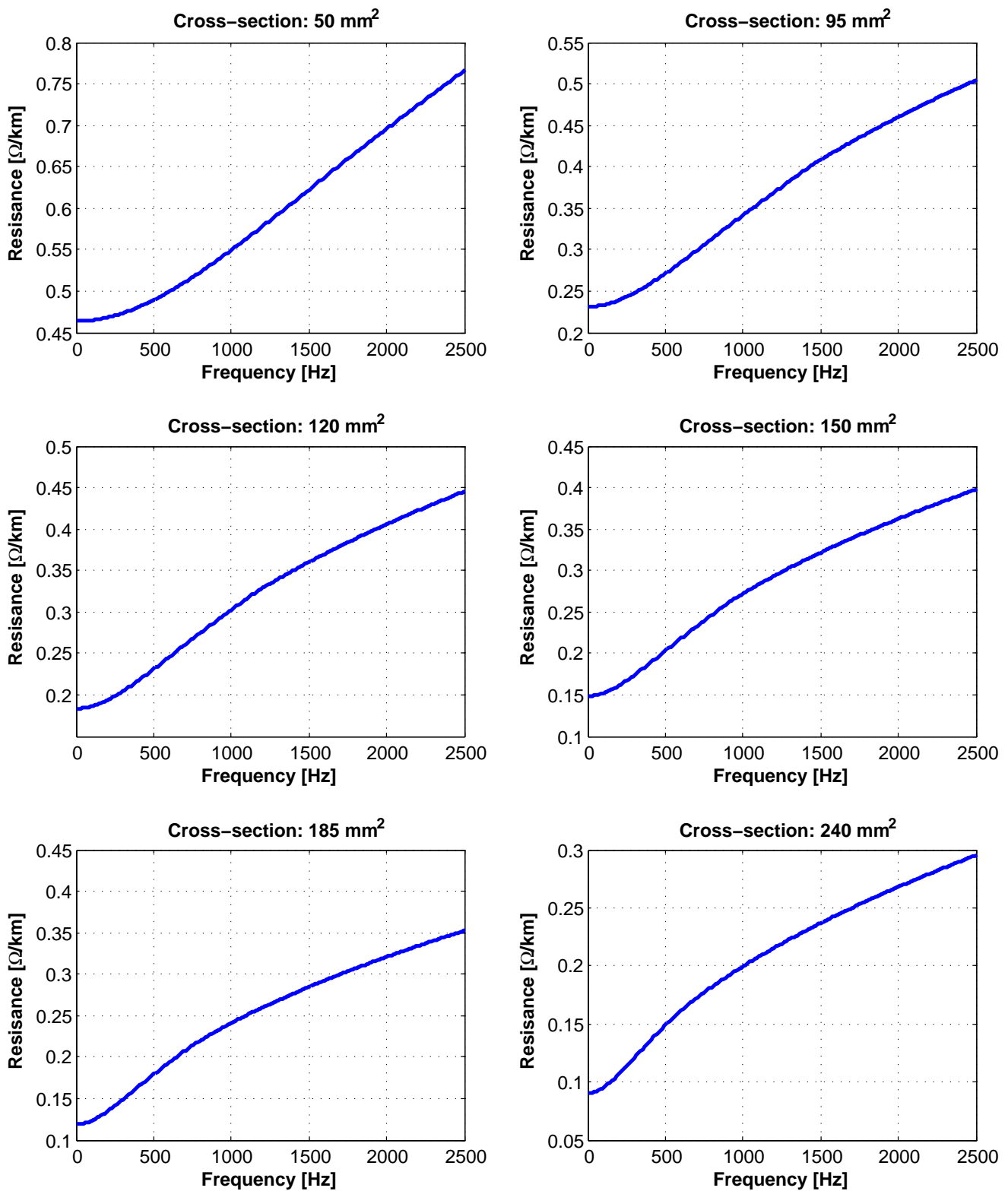


Figure A.1: Frequency-dependency of cable conductor resistances

B Network Component Parameters

B.1 Long Step-out Topology

B.1.1 Cable Parameters

Cable	$U_m[kV]$	$I_{rated}[A]$	$A[mm^2]$	$L[\frac{mH}{km}]$	$C[\frac{\mu F}{km}]$	$R_{cond}^*[\frac{\Omega}{km}]$
Step-out Cable	123	480	240	0.43	0.15	0.090
Supply Cable A	36	384	150	0.40	0.22	0.148
Supply Cable B	36	384	150	0.40	0.22	0.148
Load Cable 1	36	346	120	0.41	0.20	0.153
Load Cable 2	36	195	50	0.42	0.17	0.463
Load Cable 3	36	346	120	0.41	0.20	0.153
Load Cable 4	36	195	50	0.42	0.17	0.463

Cable	$I_{SC(1s)}[kA]$	Length [km]	Manufacturer	Insulation	Ref
Step-out Cable	34.5	50.0 - 200	ABB	XLPE	[25]
Supply Cable A	21.4	0.02 - 0.7	Nexans	XLPE	[26]
Supply Cable B	21.4	0.02 - 5.0	Nexans	XLPE	[26]
Load Cable 1	17.1	0.02 - 0.7	Nexans	XLPE	[26]
Load Cable 2	7.1	0.02 - 0.7	Nexans	EPR	[26]
Load Cable 3	17.1	0.02 - 0.7	Nexans	XLPE	[26]
Load Cable 4	7.1	0.02 - 0.7	Nexans	EPR	[26]

Table B.1: Long Step-out cable parameters

*The conductor core resistances in the table above are for the fundamental frequency (50 Hz) at an operational temperature of $70^\circ C$.

Cable	$U[kV]$
Step-out Cable	75
Supply Cable A	30
Supply Cable B	30
Load Cable 1	30
Load Cable 2	30
Load Cable 3	30
Load Cable 4	30

Table B.2: Long Step-out cable operational voltages

B.1.2 Transformer Parameters

Transformer type	$U_{HV}[kV]$	$U_{MV}[kV]$	$U_{LV}[kV]$	$S[MVA]$	$u_{k1}^*[\%]$	$u_{k2}^{**}[\%]$
T1_vsd	30	3.6	3.6	20	8	16
T2_vsd	30	2.3	2.3	1	8	16
T3_vsd	30	3.6	3.6	20	8	16
T4_vsd	30	2.3	2.3	1	8	16
T5_step-up	75	-	11	40	10	-
T6_step-down	75	30	30	40	10	20

Transformer type	$P_{copper}[kW]$	$P_0[kW]$	$I_0[\%]$	Vector group
T1_vsd	120	17	0.4	Y0y0d1
T2_vsd	11.5	3.1	0.7	Y0y0d1
T3_vsd	120	17	0.4	Y0y0d1
T4_vsd	11.5	3.1	0.7	Y0y0d1
T5_step-up	195	32	0.35	YNd1
T6_step-down	195	32	0.35	Y0y0d0.50

Table B.3: Long Step-out transformer parameters

*Short-circuit voltage between primary-secondary winding and primary-tertiary winding.

**Short-circuit voltage between secondary-tertiary winding.

B.1.3 Load Parameters

Load	System	Load Model (Harmonics)	P*** [MW]	Q [MVar]	Voltage [pu]
Load 1	DC	Current Source	13.3	0	1
Load 2	DC	Current Source	0.55	0	1
Load 3	DC	Current Source	13.3	0	1
Load 4	DC	Current Source	0.55	0	1

Table B.4: Long Step-out load parameters

***Efficiencies of 90 % are assumed for all loads. The compressor loads (Load 1 and Load 3) have mechanical shaft power ratings of 12 MW, while the condensate pump loads (Load 2 and Load 4) have mechanical shaft power ratings of 500 kW.

B.1.4 Rectifier Parameters

Rectifier	$U_{rated,AC}$ [kV]	P_{rated} [MW]	U_{DC} [kV]	Technology
Rectifier A	3.6	2 x 7.5	9.72	Diode
Rectifier B	2.3	2 x 0.35	6.21	Diode
Rectifier C	3.6	2 x 7.5	9.72	Diode
Rectifier D	2.3	2 x 0.35	6.21	Diode

Table B.5: Long Step-out rectifier parameters

B.1.5 SVC Parameters

Q Reactance [MVar]	TCR Limit [MVar]	Q setpoint [MVar]
35	35	5

Table B.6: Long Step-out SVC specifications

B.1.6 Topside Grid Parameters

Short-circuit power [MVA]	Short-circuit current [kA]	R/X [-]
570	30	0.1

Table B.7: Long Step-out topside grid specifications

B.2 Short Step-out Topology

B.2.1 Cable Parameters

Cable	U_m [kV]	I_{rated} [A]	A [mm ²]	L [$\frac{mH}{km}$]	C [$\frac{\mu F}{km}$]	R_{cond}^* [$\frac{\Omega}{km}$]
Step-out Cable	36	430	185	0.38	0.23	0.119
Supply Cable	36	346	120	0.41	0.20	0.153
Load Cable 1	36	306	95	0.43	0.19	0.231
Load Cable 2	36	306	95	0.43	0.19	0.231
Load Cable 3	36	306	95	0.43	0.19	0.231
Load Cable 4	36	306	95	0.43	0.19	0.231

Cable	$I_{SC(1s)}$ [kA]	Length [km]	Manufacturer	Insulation	Ref
Step-out Cable	26.5	1.0 - 60	Nexans	XLPE	[26]
Supply Cable	17.1	4.0 - 6.0	Nexans	XLPE	[26]
Load Cable 1	13.6	0.02 - 5.0	Nexans	XLPE	[26]
Load Cable 2	13.6	0.02 - 5.0	Nexans	XLPE	[26]
Load Cable 3	13.6	0.02 - 5.0	Nexans	XLPE	[26]
Load Cable 4	13.6	0.02 - 5.0	Nexans	XLPE	[26]

Table B.8: Short Step-out cable parameters

*The conductor core resistances in the table above are for the fundamental frequency (50 Hz) at an operational temperature of 70°C.

Cable	U [kV]
Step-out Cable	30
Supply Cable	30
Load Cable 1	30
Load Cable 2	30
Load Cable 3	30
Load Cable 4	30

Table B.9: Short Step-out cable operational voltages

B.2.2 Transformer Parameters

Transformer type	$U_{HV}[kV]$	$U_{MV}[kV]$	$U_{LV}[kV]$	$S[MVA]$	$u_{k1}^*[\%]$	$u_{k2}^{**}[\%]$
T1_vsd	30	3.6	3.6	5	8	16
T2_vsd	30	3.6	3.6	5	8	16
T3_vsd	30	3.6	3.6	5	8	16
T4_vsd	30	3.6	3.6	5	8	16
T5_step-up	30	-	11	20	8	-

Transformer type	$P_{copper}[kW]$	$P_0[kW]$	$I_0[\%]$	Vector group
T1_vsd	43	6	0.47	Y0y0d1
T2_vsd	43	6	0.47	Y0y0d1
T3_vsd	43	6	0.47	Y0y0d1
T4_vsd	43	6	0.47	Y0y0d1
T5_step-up	120	17	0.4	YNd1

Table B.10: *Short Step-out* transformer parameters

*Short-circuit voltage between primary-secondary winding and primary-tertiary winding.

**Short-circuit voltage between secondary-tertiary winding.

B.2.3 Load Parameters

Load	System	Load Model (Harmonics)	P*** [MW]	Q [MVA _r]	Voltage [pu]
Load 1	DC	Current Source	3.3	0	1
Load 2	DC	Current Source	3.3	0	1
Load 3	DC	Current Source	3.3	0	1
Load 4	DC	Current Source	3.3	0	1

Table B.11: *Short Step-out* load parameters

***Efficiencies of 90 % are assumed for all loads. The pump loads (Load 1 through Load 4) have mechanical shaft power ratings of 3 MW.

B.2.4 Rectifier Parameters

Rectifier	$U_{rated,AC}$ [kV]	P_{rated} [MW]	U_{DC} [kV]	Technology
Rectifier A	3.6	2 x 2	9.72	Diode
Rectifier B	3.6	2 x 2	9.72	Diode
Rectifier C	3.6	2 x 2	9.72	Diode
Rectifier D	3.6	2 x 2	9.72	Diode

Table B.12: *Short Step-out* rectifier parameters

B.2.5 SVC Parameters

Q Reactance [MVar]	TCR Limit [MVar]	Q setpoint [MVar]
25	25	1.5

Table B.13: *Short Step-out* SVC specifications

B.2.6 Topside Grid Parameters

Short-circuit power [MVA]	Short-circuit current [kA]	R/X [-]
570	30	0.1

Table B.14: *Short Step-out* topside grid specifications

C Harmonic and Resonance Analysis - Extras

C.1 Long Step-out

C.1.1 Case Study 1

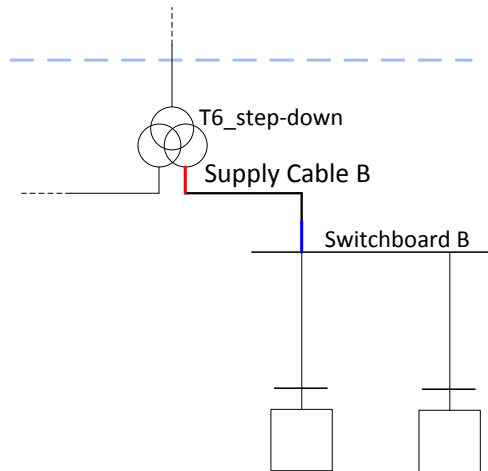


Figure C.1: Case Study 1: Explanatory sketch for Figure C.2

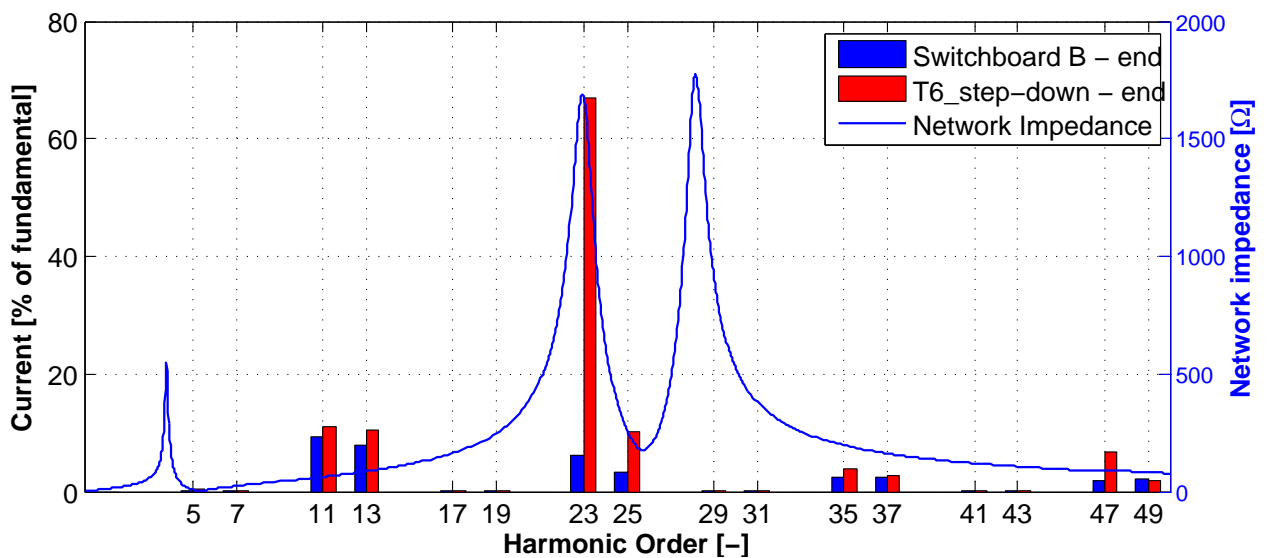


Figure C.2: Case Study 1: Harmonic current spectra of *Supply Cable B*, network impedance characteristic at *Switchboard B*

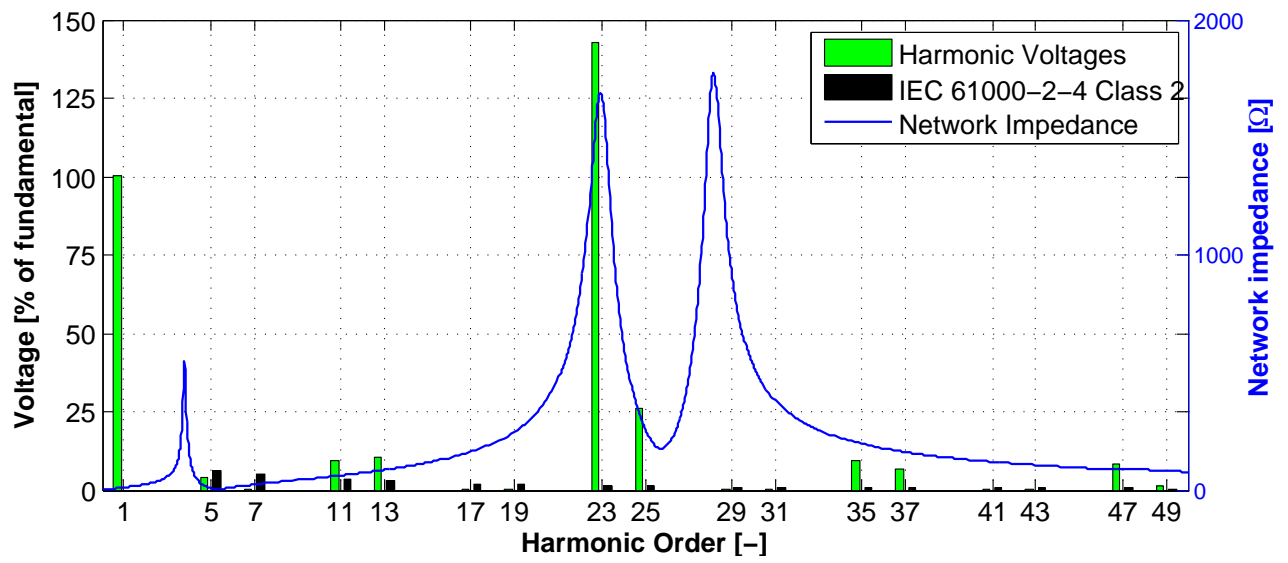


Figure C.3: Case Study 1: Harmonic voltage spectrum and network impedance characteristic at *Switchboard B*

C.1.2 General Observations for the *Long Step-out*

The cable length variation in Figure C.4 through C.6 are done according to Figure C.7.

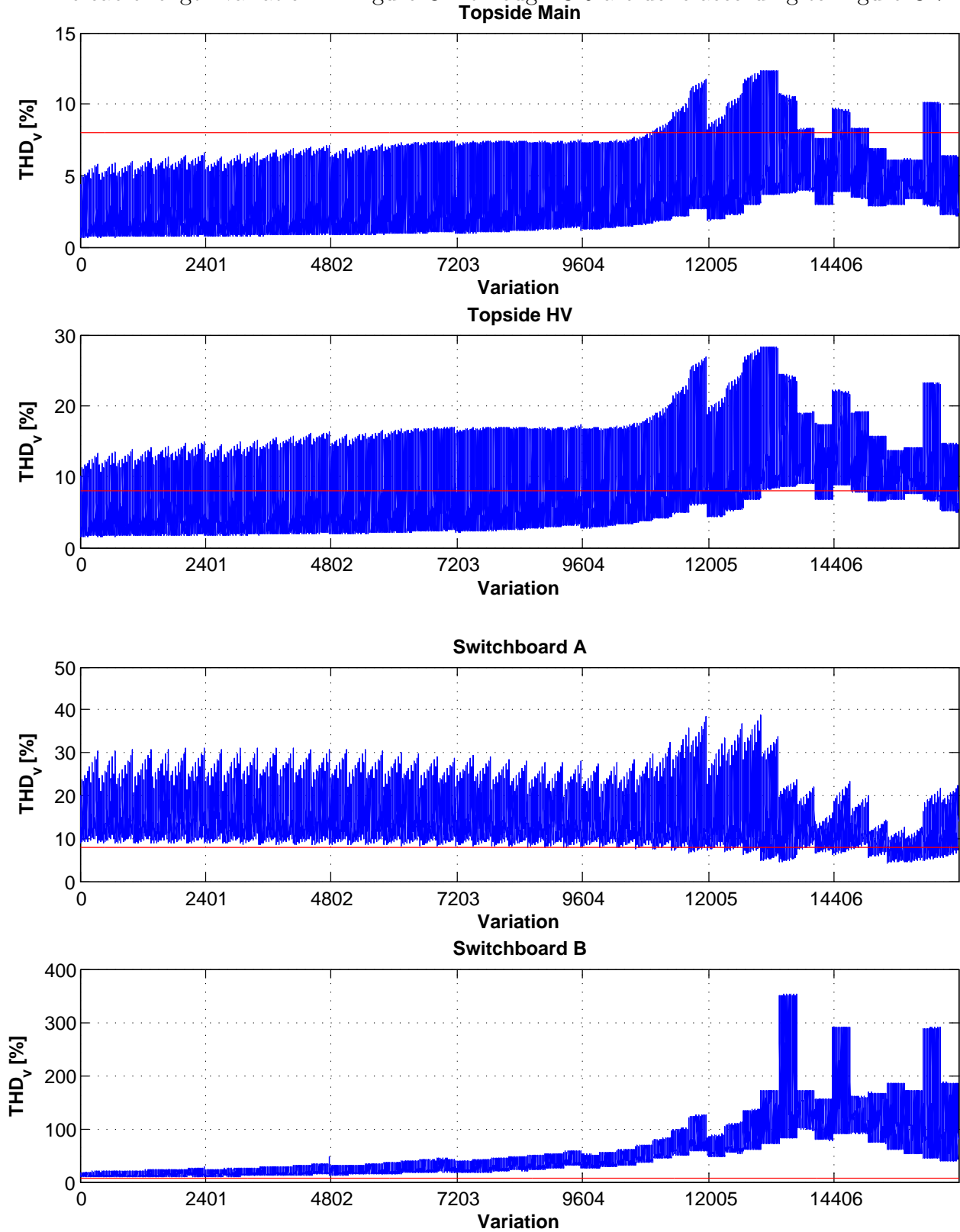


Figure C.4: Busbars' THD levels caused by 23th and 25th harmonics, only

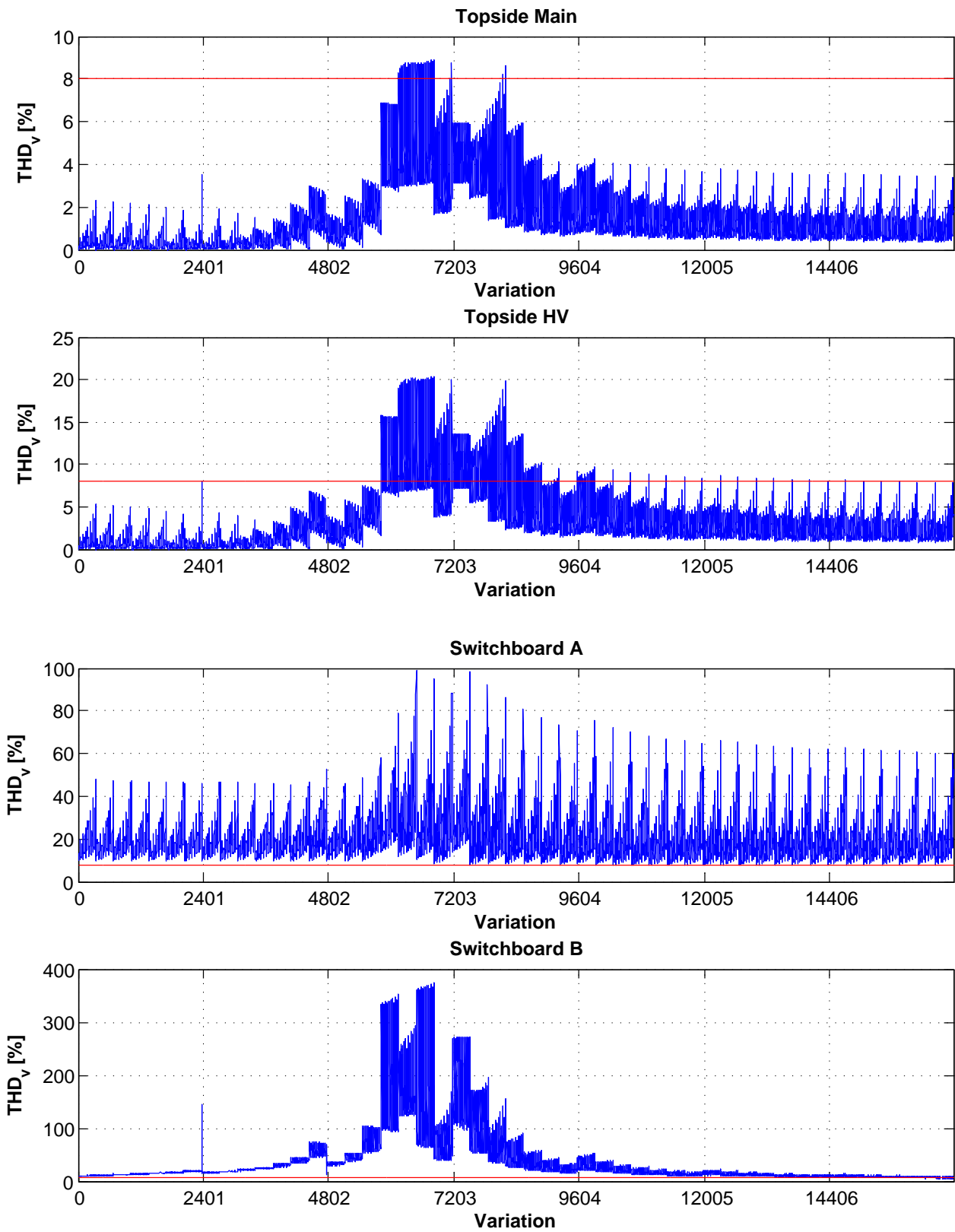


Figure C.5: Busbars' THD levels caused by 35th and 37th harmonics, only

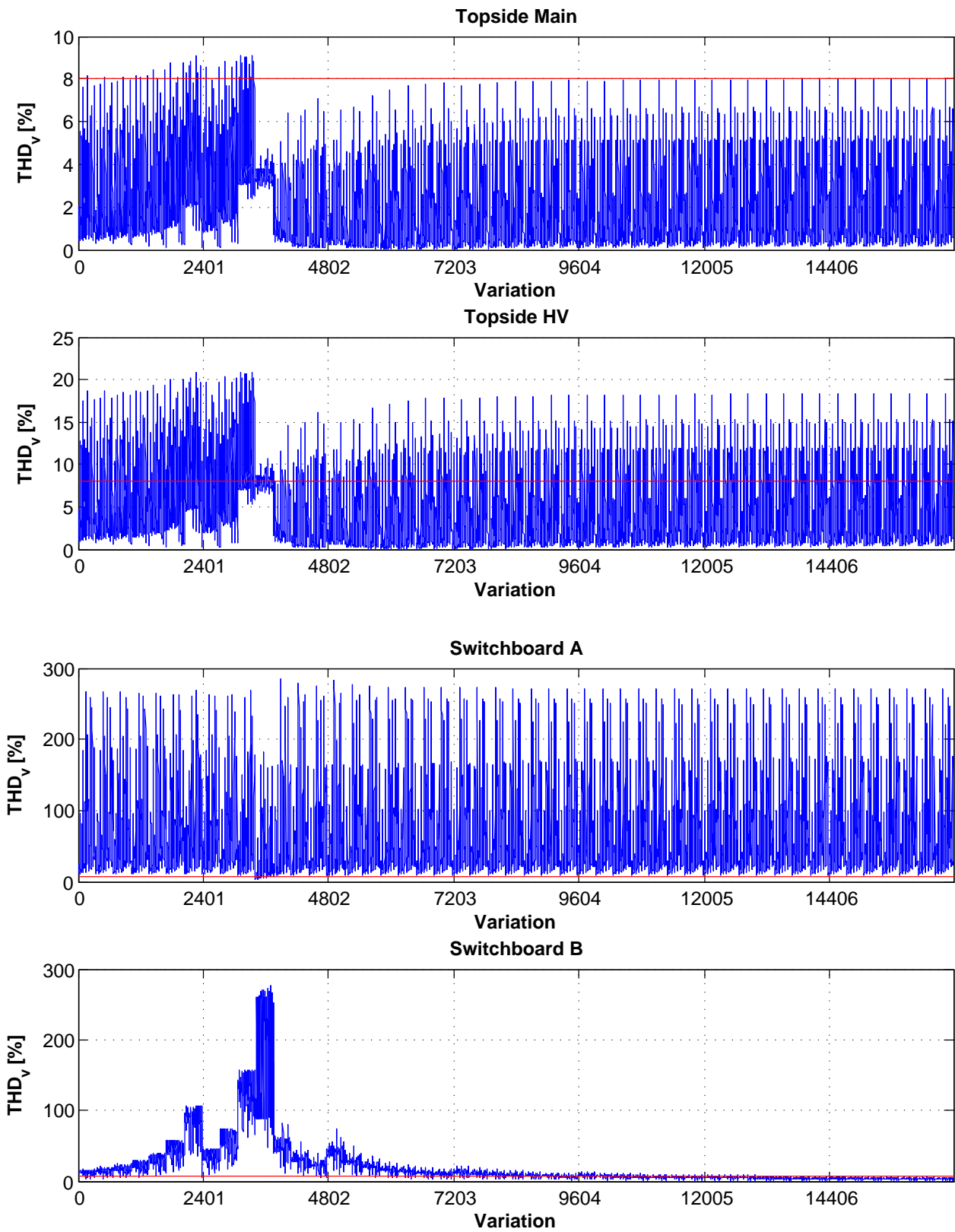


Figure C.6: Busbars' THD levels caused by 47th and 49th harmonics only

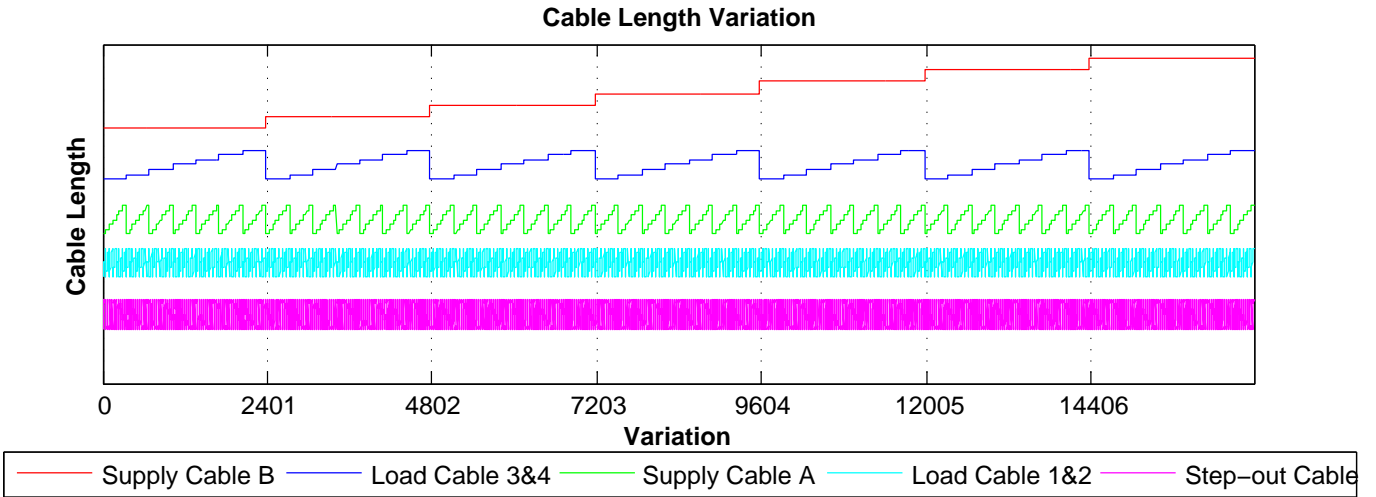


Figure C.7: Cable length variation order for Figure C.4, C.5 and C.6

C.2 Short Step-out

C.2.1 Case Study 3

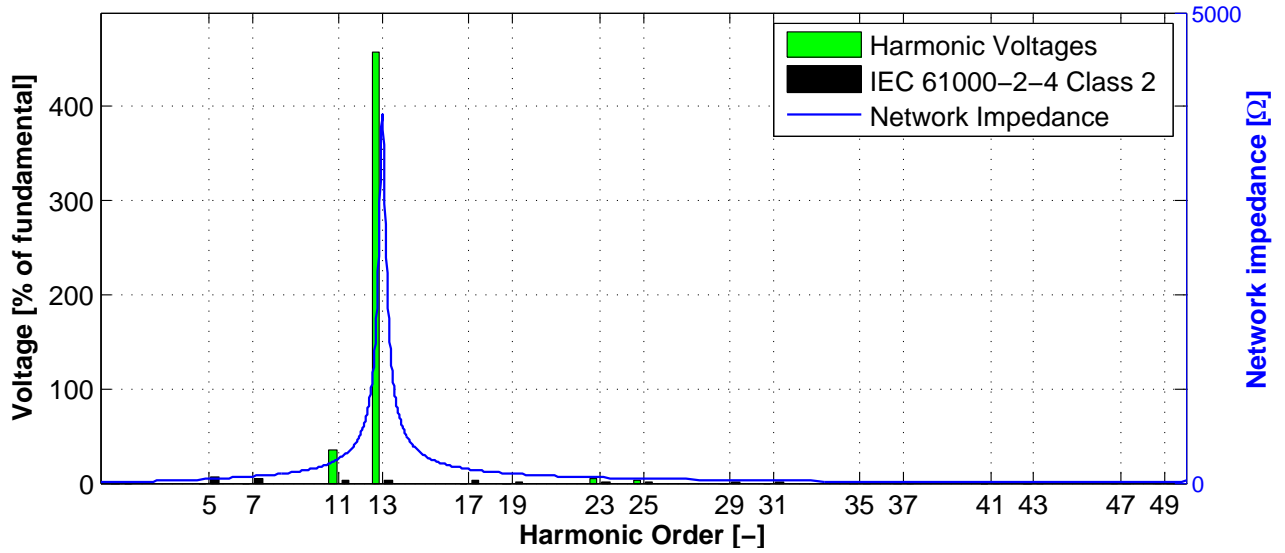


Figure C.8: Case Study 3: Harmonic voltage spectrum and network impedance characteristic at *Switchboard B*

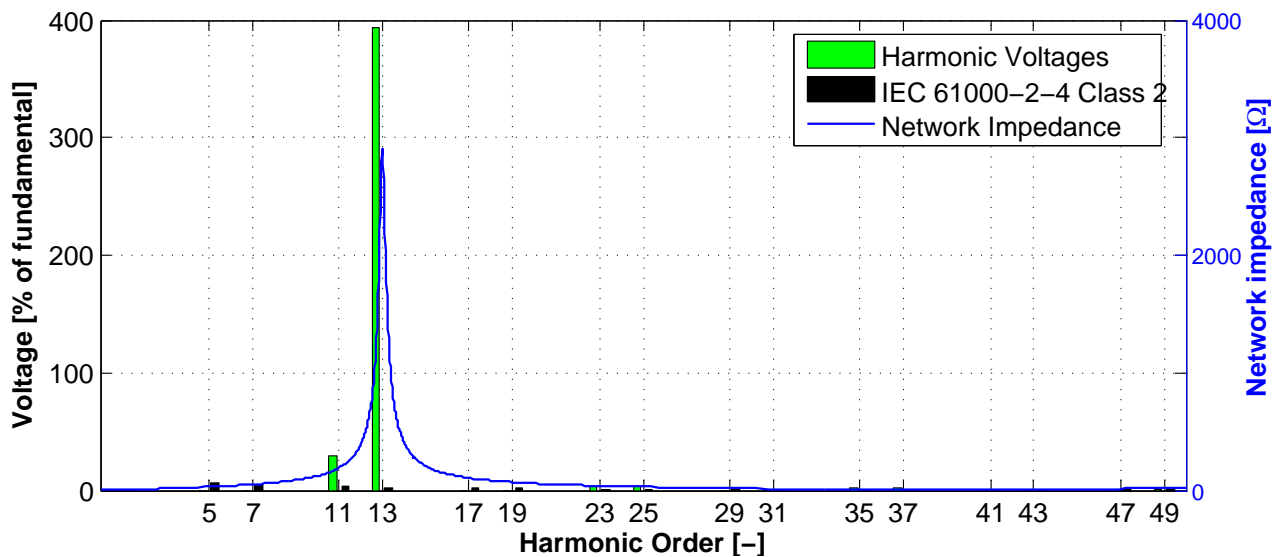


Figure C.9: Case Study 3: Harmonic voltage spectrum and network impedance characteristic at *Topside HV*

C.2.2 General Observations for the *Short Step-out*

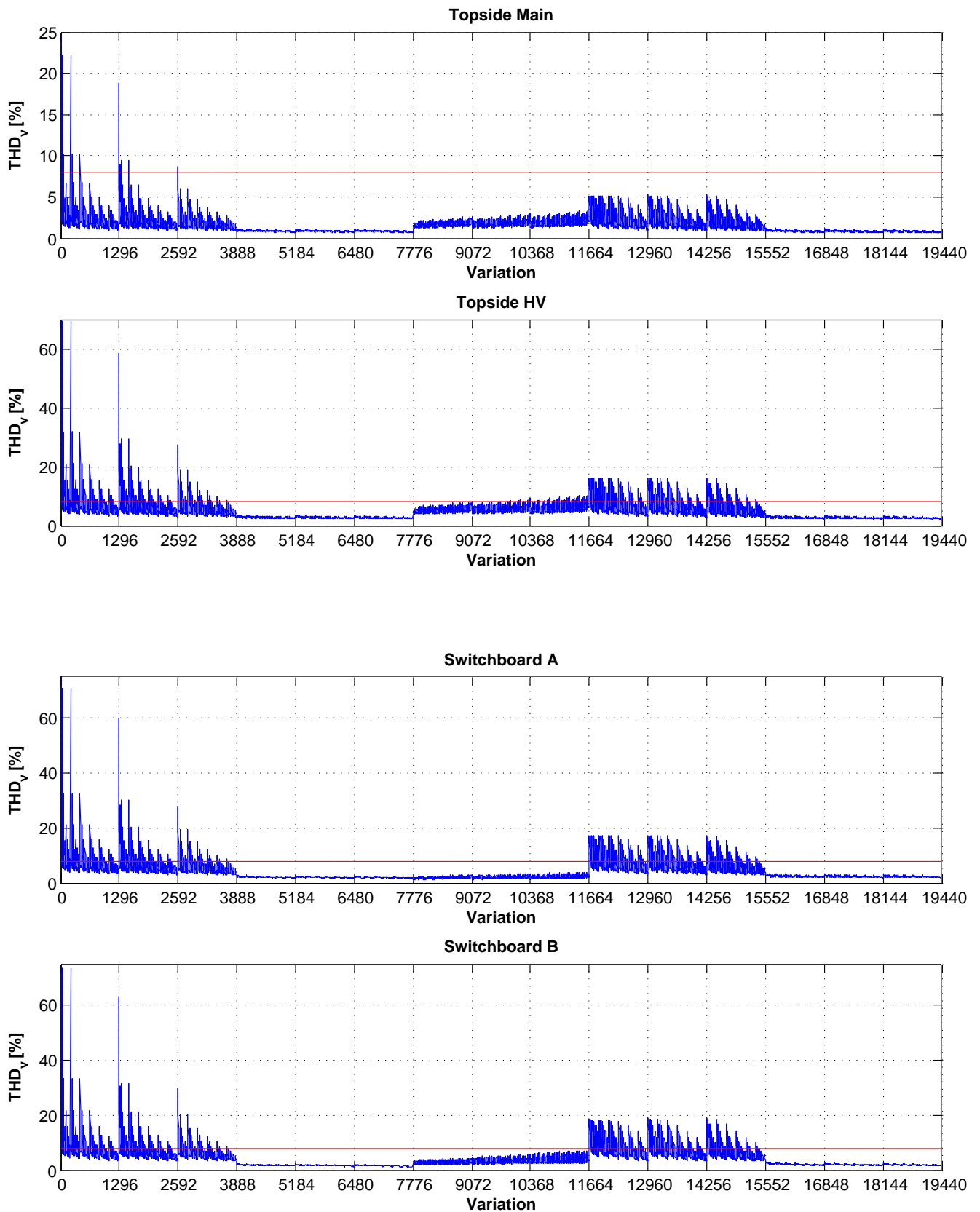


Figure C.10: Busbars' THD levels caused by 23rd and 25th harmonic currents, only

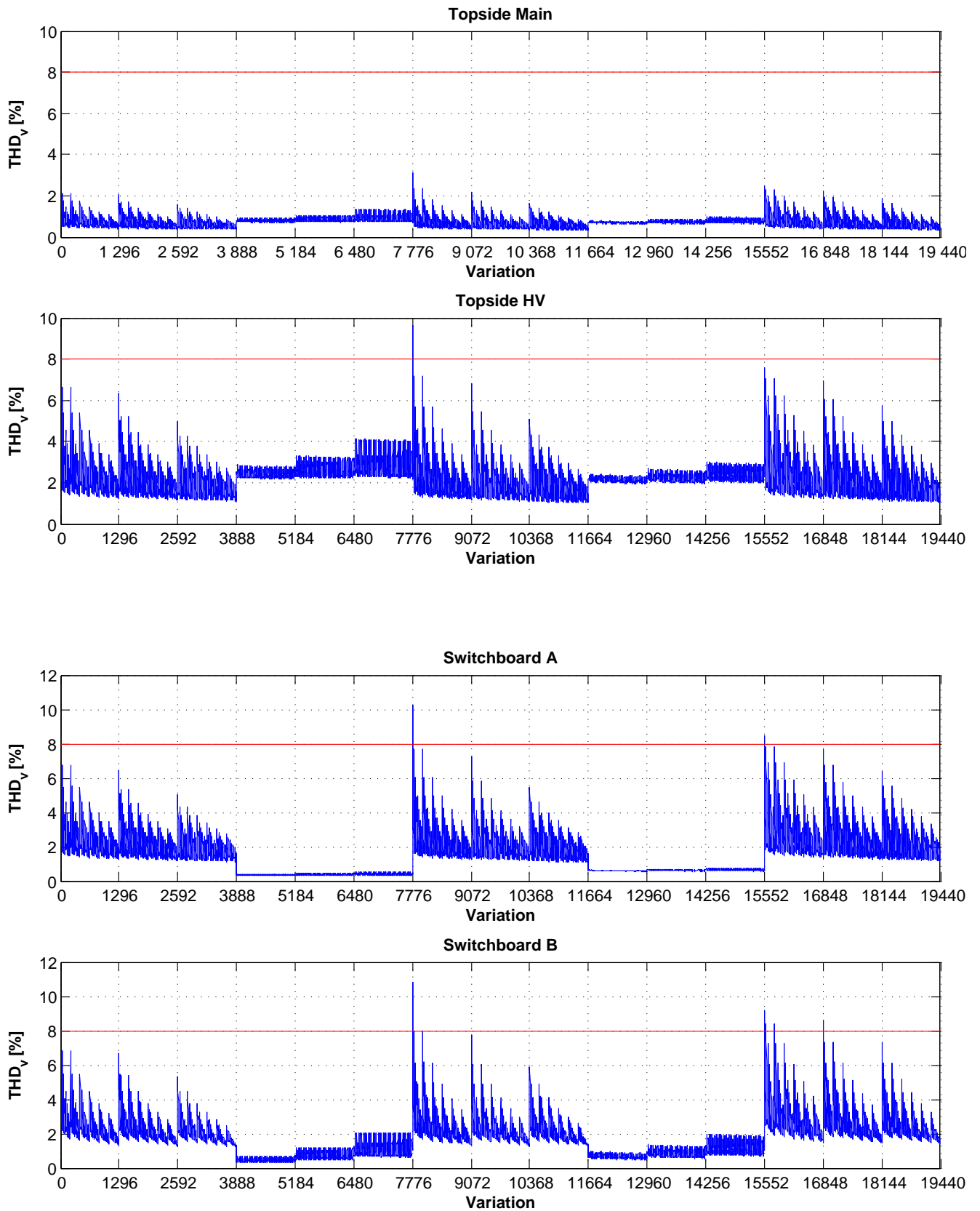


Figure C.11: Busbars' THD levels caused by 35th and 37th harmonic currents, only

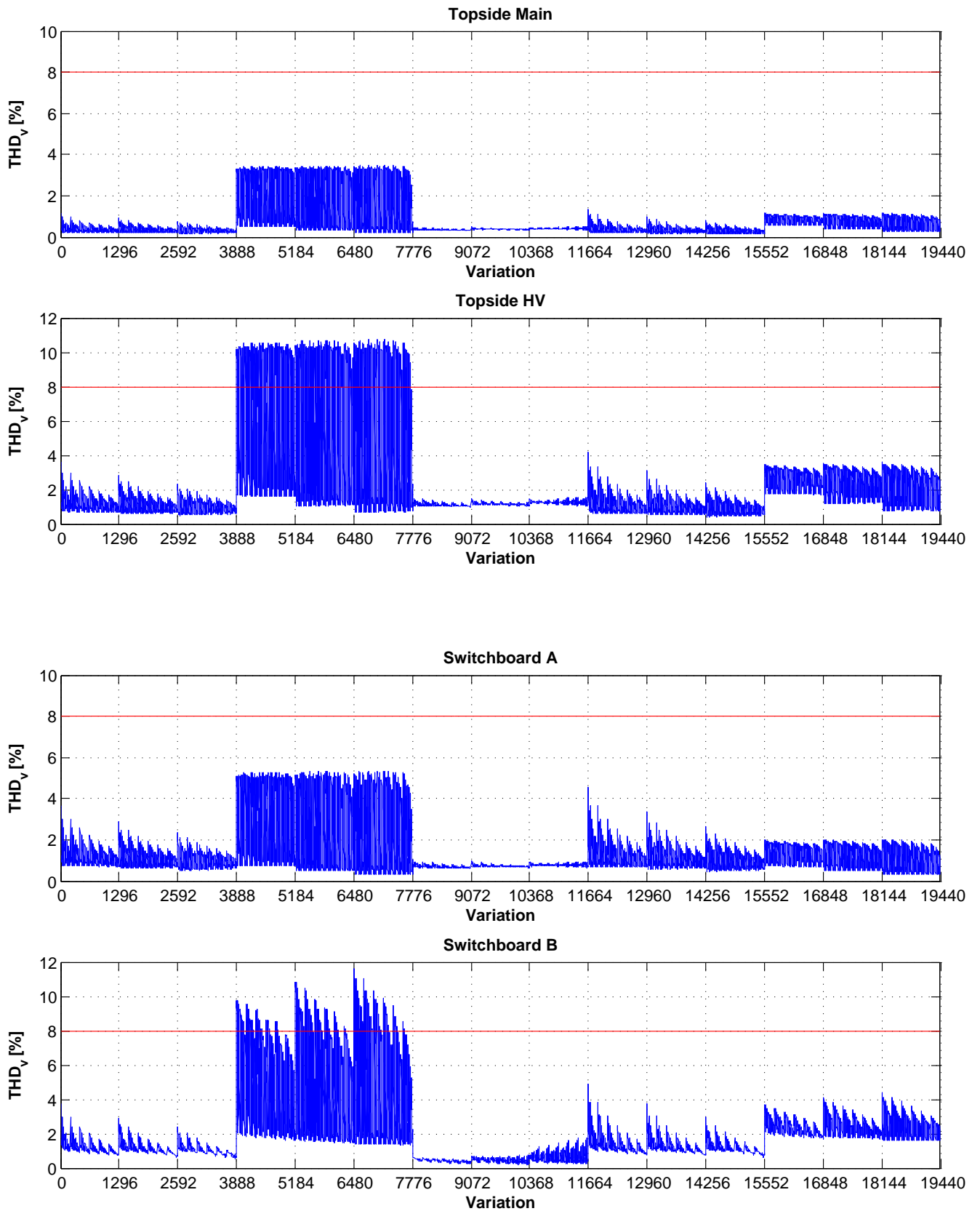


Figure C.12: Busbars' THD levels caused by 47th and 49th harmonic currents, only

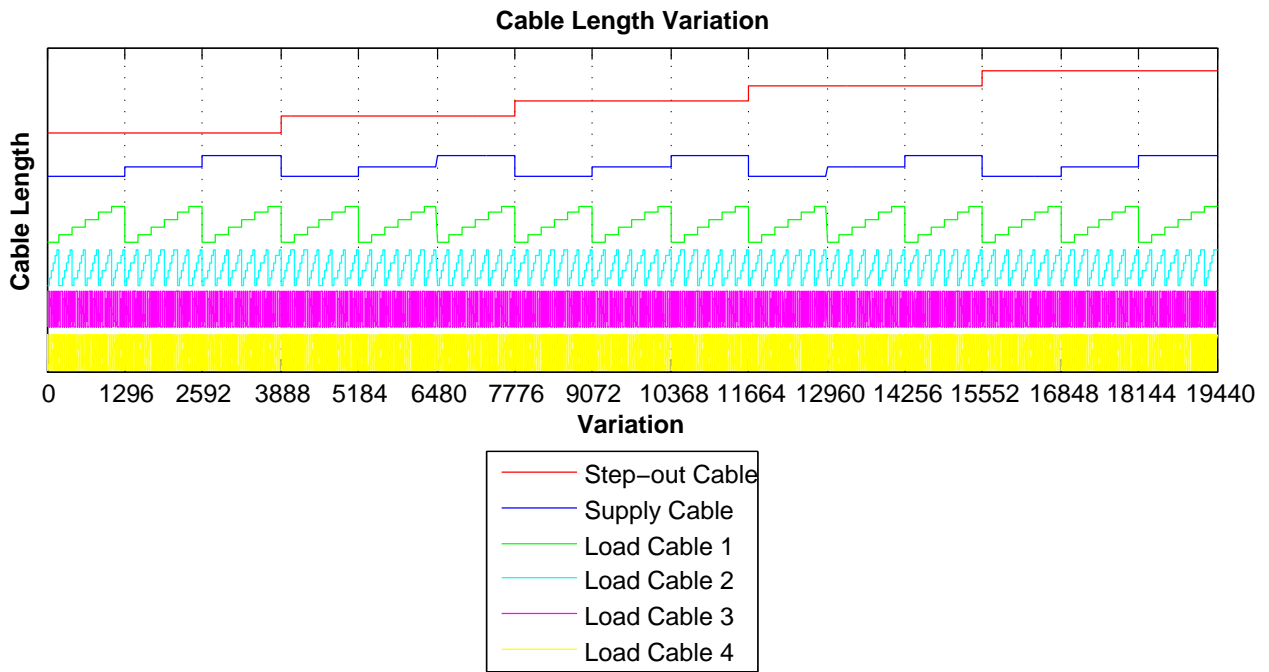


Figure C.13: Cable length variation order for Figure C.10, C.11 and C.12

D DPL Scripts

This appendix presents the DPL scripts used in the Initial Simulations. In Section 5.2.3, a simplified pseudo-code based on the following scripts, is presented.

D.1 *Long Step-out* Topology DPL Script

```
!SUBSEA COMPRESSOR TRAIN TOPOLOGY, Simulation script                                !
!                                                                                  !
!Oeyvind Garvik                                                                    !
!Master thesis, Energy and Environmental Engineering, Electrical Power Engineering    !
!NTNU, spring 2015                                                                  !
!                                                                                  !
! Script function:                                                                  !
!   Load Flow                                                                      !
!   Harmonic Load Flow                                                             !
!   Short Circuit                                                                  !
!-----!
! Variable declarations
set sAllObjs;
object Ldf,HrmLdf, SC_Sim,oStepOut_C, oSupA_C,
      oSupB_C, oLd1_C,
      oLd2_C, oLd3_C, oLd4_C,
      oTS_Main, oTS_HV,
      oSwA, oSwB,oLd1_t,oLd2_t,
      oLd3_t, oLd4_t, oT6term, oT5;
int nRow, completed, stop, n1, n2, n3, n4, n5, SimNum, LoadFlow, SC_1,
    SC_2;
double THD_TS_main, THD_TS_HV,
       THD_SwA, THD_SwB,v_TS_main,
       v_TS_HV, v_SwA,
       v_SwB, v_T5_HV,
       v_Ld1_t, v_Ld2_t, v_Ld3_t,v_Ld4_t,
       ip_SwA, ip_SwB, estimate, v_T6term, vDrop;

ClearOutput();
EchoOff(); ! suppress output windows and graphics updates

! Get the set of all objects
sAllObjs = AllRelevant();

!=====Identifying all network object needed=====
! Step-out cable
oStepOut_C = sAllObjs.FirstFilt('SCTT_Step-out Cable.ElmLne');
if (oStepOut_C)
  Info('Step-out Cable found: \ce%s',oStepOut_C:loc_name);
else {
  Error('No Step-out Cable found');
  exit();
}

! Supply Cable A
oSupA_C = sAllObjs.FirstFilt('SCTT_Supply Cable A.ElmLne');
if (oSupA_C)
  Info('Supply Cable A found: \ce%s',oSupA_C:loc_name);
```



```

else {
    Error('No Supply Cable A cable found');
    exit();
}

! Supply Cable B
oSupB_C = sAllObjs.FirstFilt('SCTT_Supply Cable B.ElmLne');
if (oSupB_C)
    Info('Supply Cable B found: \ce%s',oSupB_C:loc_name);
else {
    Error('No Supply Cable B cable found');
    exit();
}

! Load Cable 1
oLd1_C = sAllObjs.FirstFilt('SCTT_Load Cable 1.ElmLne');
if (oLd1_C)
    Info('Load Cable 1 found: \ce%s',oLd1_C:loc_name);
else {
    Error('No Load Cable 1 cable found');
    exit();
}

! Load Cable 2
oLd2_C = sAllObjs.FirstFilt('SCTT_Load Cable 2.ElmLne');
if (oLd2_C)
    Info('Load Cable 2 found: \ce%s',oLd2_C:loc_name);
else {
    Error('No Load Cable 2 cable found');
    exit();
}

! Load Cable 3
oLd3_C = sAllObjs.FirstFilt('SCTT_Load Cable 3.ElmLne');
if (oLd3_C)
    Info('Load Cable 3 found: \ce%s',oLd3_C:loc_name);
else {
    Error('No Load Cable 3 cable found');
    exit();
}

! Load Cable 4
oLd4_C = sAllObjs.FirstFilt('SCTT_Load Cable 4.ElmLne');
if (oLd4_C)
    Info('Load Cable 4 found: \ce%s',oLd4_C:loc_name);
else {
    Error('No Load Cable 4 cable found');
    exit();
}

! Load 1 terminal
oLd1_t = sAllObjs.FirstFilt('SCTT_SS_T1term_HV.ElmTerm');
if (oLd1_t)
    Info('Load 1 T1 terminal found: \ce%s',oLd1_t:loc_name);
else {
    Error('No Load 1 T1 terminal found');
}

```

```

    exit();
}

! Load 2 terminal
oLd2_t = sAllObjs.FirstFilt('SCTT_SS_T2term_HV.ElmTerm');
if (oLd2_t)
    Info('Load 2 T2 terminal found: \ce%s',oLd2_t:loc_name);
else {
    Error('No Load 2 T2 terminal found');
    exit();
}

! Load 3 terminal
oLd3_t = sAllObjs.FirstFilt('SCTT_SS_T3term_HV.ElmTerm');
if (oLd3_t)
    Info('Load 3 T3 terminal found: \ce%s',oLd3_t:loc_name);
else {
    Error('No Load 3 T3 terminal found');
    exit();
}

! Load 4 terminal
oLd4_t = sAllObjs.FirstFilt('SCTT_SS_T4term_HV.ElmTerm');
if (oLd4_t)
    Info('Load 4 T4 terminal found: \ce%s',oLd4_t:loc_name);
else {
    Error('No Load 4 T4 terminal found');
    exit();
}

! Switchboard A
oSwa = sAllObjs.FirstFilt('SCTT_SS_Switchboard A.ElmTerm');
if (oSwa)
    Info('Switchboard A found: \ce%s',oSwa:loc_name);
else {
    Error('No Switchboard A found');
    exit();
}

! SS T5 HV terminal
oT6term = sAllObjs.FirstFilt('SCTT_SS_T6term_HV.ElmTerm');
if (oT6term)
    Info('T6 terminal found: \ce%s',oT6term:loc_name);
else {
    Error('No T6 terminal found');
    exit();
}

! Switchboard B
oSwb = sAllObjs.FirstFilt('SCTT_SS_Switchboard B.ElmTerm');
if (oSwb)
    Info('Switchboard B found: \ce%s',oSwb:loc_name);
else {
    Error('No Switchboard B found');
    exit();
}

```

```

! Topside Main switchboard
oTS_Main = sAllObjs.FirstFilt('SCTT_TS_Main.ElmTerm');
if (oTS_Main)
    Info('TS Main found: \ce%s',oTS_Main:loc_name);
else {
    Error('No TS Main found');
    exit();
}

! Topside HV switchboard
oTS_HV = sAllObjs.FirstFilt('SCTT_TS_HV.ElmTerm');
if (oTS_HV)
    Info('TS HV found: \ce%s',oTS_HV:loc_name);
else {
    Error('No TS HV found');
    exit();
}

! T5
oT5 = sAllObjs.FirstFilt('SCTT_TS_T5_step-up.ElmTr2');
if (oT5)
    Info('T5 found: \ce%s',oT5:loc_name);
else {
    Error('No T5 found');
    exit();
}

!=====

! Initialize result matrix
SCTT_ResMat.Init(0,22,0);
SCTT_ResMat.ColLbl('Stp-o C [km]',1);
SCTT_ResMat.ColLbl('SupA C [km]',2);
SCTT_ResMat.ColLbl('SupB C [km]',3);
SCTT_ResMat.ColLbl('Ld1& 2 C [km]',4);
SCTT_ResMat.ColLbl('Ld3& 4 C [km]',5);
SCTT_ResMat.ColLbl('THD_TS_main [%]',6);
SCTT_ResMat.ColLbl('THD_TS_HV [%]',7);
SCTT_ResMat.ColLbl('THD_SwA [%]',8);
SCTT_ResMat.ColLbl('THD_SwB [%]',9);
SCTT_ResMat.ColLbl('T5 tap [-]',10);
SCTT_ResMat.ColLbl('Volt_TS_main [pu]',11);
SCTT_ResMat.ColLbl('Volt_TS_HV [pu]',12);
SCTT_ResMat.ColLbl('Volt_SS_T6term [pu]',13);
SCTT_ResMat.ColLbl('Step-out voltage drop [%]',14);
SCTT_ResMat.ColLbl('Volt_SwA [pu]',15);
SCTT_ResMat.ColLbl('Volt_SwB [pu]',16);
SCTT_ResMat.ColLbl('Volt_Ld1 [pu]',17);
SCTT_ResMat.ColLbl('Volt_Ld2 [pu]',18);
SCTT_ResMat.ColLbl('Volt_Ld3 [pu]',19);
SCTT_ResMat.ColLbl('Volt_Ld4 [pu]',20);
SCTT_ResMat.ColLbl('Ip Sw A [kA]',21);
SCTT_ResMat.ColLbl('Ip Sw B [kA]',22);

!Computes estimated duration
n1 = (floor((L_St0_max-L_St0_min)/L_St0_incr)+1);
n2 = (floor((L_SupA_max-L_SupA_min)/L_SupA_incr)+1);

```

```

n3 = (floor((L_SupB_max-L_SupB_min)/L_SupB_incr)+1);
n4 = (floor((L_Ld12_max-L_Ld12_min)/L_Ld12_incr)+1);
n5 = (floor((L_Ld34_max-L_Ld34_min)/L_Ld34_incr)+1);
SimNum = n1*n2*n3*n4*n5;
estimate = (SimNum*0.154)/60;
output('Number of simulations to be conducted =SimNum');
output('Esimated total time duration =estimate minutes');
input(stop, 'Continue with simulations (y=0/n=1)?');
if(stop){
    output('Simulation aborted by user');
    exit();
}

!-----
!-----START OF WHILE LOOPING-----
!-----

oStepOut_C:dline=L_St0_min;
while(oStepOut_C:dline<=L_St0_max){

    oSupA_C:dline=L_SupA_min;
    while(oSupA_C:dline<=L_SupA_max){

        oSupB_C:dline=L_SupB_min;
        while(oSupB_C:dline<=L_SupB_max){

            oLd1_C:dline=L_Ld12_min;
            oLd2_C:dline=L_Ld12_min;
            while(oLd1_C:dline<=L_Ld12_max){

                oLd3_C:dline=L_Ld34_min;
                oLd4_C:dline=L_Ld34_min;
                while(oLd3_C:dline<=L_Ld34_max){

                    nRow = SCTT_ResMat.NRow();
                    nRow+=1;
                    SCTT_ResMat.Resize(nRow, 22);

                    ! Run a load-flow simulation
                    Ldf = GetCaseObject('ComLdf');
                    LoadFlow = 1;
                    while(LoadFlow){
                        LoadFlow = Ldf.Execute();
                        if(LoadFlow){
                            oLd3_C:dline+=0.0005; !Increase cable length slightly if load flow not converging
                            oLd4_C:dline+=0.0005; !Increase cable length slightly if load flow not converging
                        }
                    }

                    ! Extract LDF results
                    v_TS_main = oTS_Main:m:u1;
                    v_TS_HV = oTS_HV:m:u1;
                    v_SwA = oSwA:m:u1;
                    v_SwB = oSwB:m:u1;
                    v_Ld1_t = oLd1_t:m:u1;
                    v_Ld2_t = oLd2_t:m:u1;
                    v_Ld3_t = oLd3_t:m:u1;
                    v_Ld4_t = oLd4_t:m:u1;
                    v_T5term = oT5term:m:u1;

```

```

!Computing voltage drop
vDrop=((v_TS_HV-v_T6term)/v_TS_HV)*100;

! Run a Harmonic Load Flow
HrmLdf = GetCaseObject('ComHldf');
HrmLdf.Execute();
!Extract HrmLDF results
THD_TS_main = oTS_Main:m:THD;
THD_TS_HV = oTS_HV:m:THD;
THD_SwA = oSwA:m:THD;
THD_SwB = oSwB:m:THD;

!Run Short-Circuit Simulation on Switchboard A

SC_Sim = GetCaseObject('ComShc');
SC_Sim:shcobj=oSwA;
SC_Sim:iopt_asc=0;
SC_1 = SC_Sim.Execute();
!Extract SC results from Switchboard A
if(SC_1){
    ip_SwA = 0;          !Skipping SC caclulation if not successful
}else{
    ip_SwA = oSwA:m:ip;
}
!Extract SC results from Switchboard A

!Run Short-Circuit Simulation on Switchboard B
SC_Sim:shcobj=oSwB;
SC_Sim:iopt_asc=0;
SC_2 = SC_Sim.Execute();
!Extract SC results from Switchboard B
if (SC_2){
    ip_SwB = 0;
}else{
    ip_SwB = oSwB:m:ip;
}
! Writing to result matrix
SCTT_ResMat.Set(nRow, 1, oStepOut_C:dline);
SCTT_ResMat.Set(nRow, 2, oSupA_C:dline);
SCTT_ResMat.Set(nRow, 3, oSupB_C:dline);
SCTT_ResMat.Set(nRow, 4, oLd1_C:dline);
SCTT_ResMat.Set(nRow, 5, oLd3_C:dline);
SCTT_ResMat.Set(nRow, 6, THD_TS_main);
SCTT_ResMat.Set(nRow, 7, THD_TS_HV);
SCTT_ResMat.Set(nRow, 8, THD_SwA);
SCTT_ResMat.Set(nRow, 9, THD_SwB);
SCTT_ResMat.Set(nRow, 10, oT5:c:nntap);
SCTT_ResMat.Set(nRow, 11, v_TS_main);
SCTT_ResMat.Set(nRow, 12, v_TS_HV);
SCTT_ResMat.Set(nRow, 13, v_T6term);
SCTT_ResMat.Set(nRow, 14, vDrop);
SCTT_ResMat.Set(nRow, 15, v_SwA);
SCTT_ResMat.Set(nRow, 16, v_SwB);
SCTT_ResMat.Set(nRow, 17, v_Ld1_t);
SCTT_ResMat.Set(nRow, 18, v_Ld2_t);

```

```

SCTT_ResMat.Set(nRow, 19, v_Ld3_t);
SCTT_ResMat.Set(nRow, 20, v_Ld4_t);
SCTT_ResMat.Set(nRow, 21, ip_SwA);
SCTT_ResMat.Set(nRow, 22, ip_SwB);

completed=(nRow/SimNum)*100;
output('Simulation =completed % completed');

oLd3_C:dline+=L_Ld34_incr;
oLd4_C:dline+=L_Ld34_incr;
}
oLd1_C:dline+=L_Ld12_incr;
oLd2_C:dline+=L_Ld12_incr;
}
oSupB_C:dline+=L_SupB_incr;
}
oSupA_C:dline+=L_SupA_incr;
}
oStepOut_C:dline+=L_St0_incr;
}
!-----
!-----END OF WHILE LOOPING-----
!-----
EchoOn();

!END OF SCRIPT

```

D.2 Short Step-out DPL Script

```
!SUBSEA PUMP SYSTEM TOPOLOGY, Simulation script !
!
!Oeyvind Garvik !
!Master thesis, Energy and Environmental Engineering, Electrical Power Engineering !
!NTNU, spring 2015 !
!
! Script functions !
! Load Flow !
! Harmonic Load Flow !
! Short Circuit !
!-----!

! Variable declarations
set sAllObjs;
object Ldf,HrmLdf, SC_Sim,oStepOut_C, oSup_C,
    oLd1_C, oLd2_C, oLd3_C, oLd4_C,
    oTS_Main, oTS_HV,
    oSwA, oSwB,oLd1_t,oLd2_t,
    oLd3_t, oLd4_t, oT6;
int nRow, completed, stop, n1, n2 ,n3, n4, n5 , n6, SimNum, LoadFlow,
    SC_1, SC_2;
double THD_TS_main, THD_TS_HV,
    THD_SwA, THD_SwB,v_TS_main,
    v_TS_HV, v_SwA, v_SwB, v_T5_HV,
    v_Ld1_t, v_Ld2_t, v_Ld3_t,v_Ld4_t,
    ip_SwA, ip_SwB, estimate, vDrop;

ClearOutput();
EchoOff(); ! suppress output windows and graphics updates

! Get the set of all objects
sAllObjs = AllRelevant();

!=====Identifying all network components needed=====
! Finding Step-out cable
oStepOut_C = sAllObjs.FirstFilt('SPST_Step-out Cable.ElmLne');
if (oStepOut_C)
    Info('Step-out Cable found: \ce%s',oStepOut_C:loc_name);
else {
    Error('No Step-out Cable found');
    exit();
}

! Finding Supply Cable
oSup_C = sAllObjs.FirstFilt('SPST_Supply Cable.ElmLne');
if (oSup_C)
    Info('Supply Cable found: \ce%s',oSup_C:loc_name);
else {
    Error('No Supply Cable cable found');
    exit();
}

! Finding Load Cable 1
oLd1_C = sAllObjs.FirstFilt('SPST_Load Cable 1.ElmLne');
if (oLd1_C)
```

```

    Info('Load Cable 1 found: \ce%s',oLd1_C:loc_name);
else {
    Error('No Load Cable 1 cable found');
    exit();
}

! Finding Load Cable 2
oLd2_C = sAll0bjs.FirstFilt('SPST_Load Cable 2.ElmLne');
if (oLd2_C)
    Info('Load Cable 2 found: \ce%s',oLd2_C:loc_name);
else {
    Error('No Load Cable 2 cable found');
    exit();
}

! Finding Load Cable 3
oLd3_C = sAll0bjs.FirstFilt('SPST_Load Cable 3.ElmLne');
if (oLd3_C)
    Info('Load Cable 3 found: \ce%s',oLd3_C:loc_name);
else {
    Error('No Load Cable 3 cable found');
    exit();
}

! Finding Load Cable 4
oLd4_C = sAll0bjs.FirstFilt('SPST_Load Cable 4.ElmLne');
if (oLd4_C)
    Info('Load Cable 4 found: \ce%s',oLd4_C:loc_name);
else {
    Error('No Load Cable 4 cable found');
    exit();
}

! Finding Load 1 terminal
oLd1_t = sAll0bjs.FirstFilt('SPST_SS_T1term_HV.ElmTerm');
if (oLd1_t)
    Info('Load 1 T1 terminal found: \ce%s',oLd1_t:loc_name);
else {
    Error('No Load 1 T1 terminal found');
    exit();
}

! Finding Load 2 terminal
oLd2_t = sAll0bjs.FirstFilt('SPST_SS_T2term_HV.ElmTerm');
if (oLd2_t)
    Info('Load 2 T2 terminal found: \ce%s',oLd2_t:loc_name);
else {
    Error('No Load 2 T2 terminal found');
    exit();
}

! Finding Load 3 terminal
oLd3_t = sAll0bjs.FirstFilt('SPST_SS_T3term_HV.ElmTerm');
if (oLd3_t)
    Info('Load 3 T3 terminal found: \ce%s',oLd3_t:loc_name);
else {

```



```

    Error('No Load 3 T3 terminal found');
    exit();
}

! Finding Load 4 terminal
oLd4_t = sAllObjs.FirstFilt('SPST_SS_T4term_HV.ElmTerm');
if (oLd4_t)
    Info('Load 4 T4 terminal found: \ce%s',oLd4_t:loc_name);
else {
    Error('No Load 4 T4 terminal found');
    exit();
}

! Finding Switchboard A
oSwA = sAllObjs.FirstFilt('SPST_SS_Switchboard A.ElmTerm');
if (oSwA)
    Info('Switchboard A found: \ce%s',oSwA:loc_name);
else {
    Error('No Switchboard A found');
    exit();
}

! Finding Switchboard B
oSwB = sAllObjs.FirstFilt('SPST_SS_Switchboard B.ElmTerm');
if (oSwB)
    Info('Switchboard B found: \ce%s',oSwB:loc_name);
else {
    Error('No Switchboard B found');
    exit();
}

! Finding Topside Main switchboard
oTS_Main = sAllObjs.FirstFilt('SPST_TS_Main.ElmTerm');
if (oTS_Main)
    Info('TS Main found: \ce%s',oTS_Main:loc_name);
else {
    Error('No TS Main found');
    exit();
}

! Finding Topside HV switchboard
oTS_HV = sAllObjs.FirstFilt('SPST_TS_HV.ElmTerm');
if (oTS_HV)
    Info('TS HV found: \ce%s',oTS_HV:loc_name);
else {
    Error('No TS HV found');
    exit();
}

! T6
oT6 = sAllObjs.FirstFilt('SPST_TS_T6_step-up.ElmTr2');
if (oT6)
    Info('T6 found: \ce%s',oT6:loc_name);
else {
    Error('No T6 found');
    exit();
}

```

!=====

```
! initialize result matrix
SPST_ResMat.Init(0,22,0);
SPST_ResMat.ColLbl('Stp-o C [km]',1);
SPST_ResMat.ColLbl('Sup C [km]',2);
SPST_ResMat.ColLbl('Ld1 C [km]',3);
SPST_ResMat.ColLbl('Ld2 C [km]',4);
SPST_ResMat.ColLbl('Ld3 C [km]',5);
SPST_ResMat.ColLbl('Ld4 C [km]',6);
SPST_ResMat.ColLbl('THD_TS_main [%]',7);
SPST_ResMat.ColLbl('THD_TS_HV [%]',8);
SPST_ResMat.ColLbl('THD_SwA [%]',9);
SPST_ResMat.ColLbl('THD_SwB [%]',10);
SPST_ResMat.ColLbl('T6 tap',11);
SPST_ResMat.ColLbl('Volt_TS_main [pu]',12);
SPST_ResMat.ColLbl('Volt_TS_HV [pu]',13);
SPST_ResMat.ColLbl('Volt_SwA [pu]',14);
SPST_ResMat.ColLbl('Step-out vDrop [%]',15);
SPST_ResMat.ColLbl('Volt_SwB [pu]',16);
SPST_ResMat.ColLbl('Volt_Ld1 [pu]',17);
SPST_ResMat.ColLbl('Volt_Ld2 [pu]',18);
SPST_ResMat.ColLbl('Volt_Ld3 [pu]',19);
SPST_ResMat.ColLbl('Volt_Ld4 [pu]',20);
SPST_ResMat.ColLbl('Ip Sw A [kA]',21);
SPST_ResMat.ColLbl('Ip Sw B [kA]',22);

!Computes estimated duration
n1 = (floor((L_St0_max-L_St0_min)/L_St0_incr)+1);
n2 = (floor((L_Sup_max-L_Sup_min)/L_Sup_incr)+1);
n3 = (floor((L_Ld1_max-L_Ld1_min)/L_Ld1_incr)+1);
n4 = (floor((L_Ld2_max-L_Ld2_min)/L_Ld2_incr)+1);
n5 = (floor((L_Ld3_max-L_Ld3_min)/L_Ld3_incr)+1);
n6 = (floor((L_Ld4_max-L_Ld4_min)/L_Ld4_incr)+1);
SimNum = n1*n2*n3*n4*n5*n6;
estimate = (SimNum*0.154)/60;
output('Number of simulations to be conducted =SimNum');
output('Esimated total time duration =estimate minutes');
input(stop, 'Continue with simulations (y=0/n=1)?');
if(stop){
    output('Simulation aborted by user');
    exit();
}

!-----
!-----START OF WHILE LOOPING-----
!-----

oStepOut_C:dline=L_St0_min;
while(oStepOut_C:dline<=L_St0_max){

    oSup_C:dline=L_Sup_min;
    while(oSup_C:dline<=L_Sup_max){

        oLd1_C:dline=L_Ld1_min;
```

```

while(oLd1_C:dline<=L_Ld1_max){

oLd2_C:dline=L_Ld2_min;
while(oLd2_C:dline<=L_Ld2_max){

oLd3_C:dline=L_Ld3_min;
while(oLd3_C:dline<=L_Ld3_max){

oLd4_C:dline=L_Ld4_min;
while(oLd4_C:dline<=L_Ld4_max){

nRow = SPST_ResMat.NRow();
nRow+=1;
SPST_ResMat.Resize(nRow, 22);

! Run a load-flow simulation
Ldf = GetCaseObject('ComLdf');
LoadFlow=1;
while(LoadFlow){
LoadFlow=Ldf.Execute();
if(LoadFlow){
oLd4_C:dline+=0.0005; !Increasing cable length slightly if loadflow not converging
}
}
! Extract LDF results
v_TS_main = oTS_Main:m:u1;
v_TS_HV = oTS_HV:m:u1;
v_SwA = oSwA:m:u1;
v_SwB = oSwB:m:u1;
v_Ld1_t = oLd1_t:m:u1;
v_Ld2_t = oLd2_t:m:u1;
v_Ld3_t = oLd3_t:m:u1;
v_Ld4_t = oLd4_t:m:u1;

vDrop = ((v_TS_HV-v_SwA)/v_TS_HV)*100;

! Run a Harmonic Load Flow
HrmLdf = GetCaseObject('ComHldf');
HrmLdf.Execute();
!Extract HrmLDF results
THD_TS_main = oTS_Main:m:THD;
THD_TS_HV = oTS_HV:m:THD;
THD_SwA = oSwA:m:THD;
THD_SwB = oSwB:m:THD;

!Run Short-Circuit Simulation on Switchboard A
SC_Sim = GetCaseObject('ComShc');
SC_Sim:shcobj = oSwA;
SC_Sim:iopt_asc = 0;
SC_1=SC_Sim.Execute();
!Extract SC results from Switchboard A
if(SC_1){
ip_SwA = 0; !Skipping SC caclulation if not successful
}else{
ip_SwA = oSwA:m:ip;
}
}
}
}
}

```

```

!Run Short-Circuit Simulation on Switchboard B
SC_Sim:shcobj = oSwB;
SC_Sim:iopt_asc = 0;
SC_2=SC_Sim.Execute();
!Extract SC results from Switchboard B
if (SC_2){
    ip_SwB = 0;
}else{
    ip_SwB = oSwB:m:ip;
}

! Writing to result matrix
SPST_ResMat.Set(nRow, 1, oStepOut_C:dline);
SPST_ResMat.Set(nRow, 2, oSup_C:dline);
SPST_ResMat.Set(nRow, 3, oLd1_C:dline);
SPST_ResMat.Set(nRow, 4, oLd2_C:dline);
SPST_ResMat.Set(nRow, 5, oLd3_C:dline);
SPST_ResMat.Set(nRow, 6, oLd4_C:dline);
SPST_ResMat.Set(nRow, 7, THD_TS_main);
SPST_ResMat.Set(nRow, 8, THD_TS_HV);
SPST_ResMat.Set(nRow, 9, THD_SwA);
SPST_ResMat.Set(nRow, 10, THD_SwB);
SPST_ResMat.Set(nRow, 11, oT6:c:nntap);
SPST_ResMat.Set(nRow, 12, v_TS_main);
SPST_ResMat.Set(nRow, 13, v_TS_HV);
SPST_ResMat.Set(nRow, 14, v_SwA);
SPST_ResMat.Set(nRow, 15, vDrop);
SPST_ResMat.Set(nRow, 16, v_SwB);
SPST_ResMat.Set(nRow, 17, v_Ld1_t);
SPST_ResMat.Set(nRow, 18, v_Ld2_t);
SPST_ResMat.Set(nRow, 19, v_Ld3_t);
SPST_ResMat.Set(nRow, 20, v_Ld4_t);
SPST_ResMat.Set(nRow, 21, ip_SwA);
SPST_ResMat.Set(nRow, 22, ip_SwB);

completed=(nRow/SimNum)*100;
output('Simulation =completed % completed');

    oLd4_C:dline+=L_Ld4_incr;
}
oLd3_C:dline+=L_Ld3_incr;
}
oLd2_C:dline+=L_Ld2_incr;
}
oLd1_C:dline+=L_Ld1_incr;
}
oSup_C:dline+=L_Sup_incr;
}
oStepOut_C:dline+=L_St0_incr;
}
!-----
!-----END OF WHILE LOOPING-----
!-----

EchoOn();

!END OF SCRIPT

```